学位論文（要約）

A climate modeling study on the mechanism of Antarctic ice sheet changes in the past and future
（過去と将来の南極氷床変動メカニズムの理解に向けた気候モデリング研究）

平成 29 年 12 月博士（理学）申請

東京大学大学院理学系研究科
地球惑星科学専攻

小長谷　貴志

Doctoral Dissertation

A climate modeling study on the mechanism of Antarctic ice sheet changes in the past and future

by

Takashi Obase

Department of Earth and Planetary Science
Graduate School of Science
The University of Tokyo

December 2017

Abstract

Understanding the nature of the Antarctic ice sheet is important for projecting future sea level change, which has a significant impact on human activities. Combined ice sheet and climate modeling studies are conducted to project future climate change and associated responses of the Antarctic ice sheet. Paleoclimate is used to validate numerical models used for future projections, and it is indicated the Antarctic ice sheet retreated in the past such as the Last Interglacial (LIG, about 130,000 years ago). However, there are two significant problems in understandings the climate and Antarctic ice sheet. The first problem is the relationship between the forcing and the responses of Antarctic ice sheet during the LIG. Climate model simulations did not reproduce warm climate in the Antarctic region, when the boundary conditions of insolation and greenhouse gas concentrations at the LIG are used. This means that the retreatment of Antarctic ice sheet during the LIG can be explained by warmer Antarctic climate, but the ultimate cause is unknown. The second problem is in the processes of the retreatment of Antarctic ice sheet to climate change. Basal melting of the Antarctic ice shelves, determined by the heat delivered by the ocean, is an important factor in the response of the Antarctic ice sheet to climate change. However, change in basal melting rate is simply parameterized without considering ocean temperature and circulation changes in the Antarctic shelf seas. The objective of this study is to understand the mechanisms and physical processes of Antarctic climate and Antarctic ice sheet changes in the past and future.

In Chapter 2, I investigate the cause of the warm Antarctic climate during the LIG compared to the present interglacial (PIG), as a probable reason of different Antarctic ice sheet retreatments between the last two interglacials. I focus on the time series of reconstructed Atlantic Meridional Overturning Circulation (AMOC) and the speed of Northern Hemisphere ice sheet melting during deglaciation before the early LIG. A transient simulation from the glacial to the interglacial is conducted using an atmosphere-ocean coupled general circulation model, considering uncertainties in

glacial meltwater flux. The different time series in the AMOC during the deglaciations were simulated, and the magnitude of simulated temperature differences in the Antarctic regions were shown to be close to reconstructions of the LIG and the PIG. The results suggest that the difference in Antarctic climate between the last two interglacials was caused by the speed of Northern Hemisphere ice sheet melting, through the "bipolar seesaw" mechanism derived from ocean circulations driven in the North Atlantic.

In Chapter 3, the responses of basal mass balance of Antarctic ice shelves to climate changes are investigated. The climatic outputs of an atmosphere–ocean general circulation model of a doubling of CO_2 and Last Glacial Maximum conditions are used to force a circumpolar ocean model that resolves ice shelf cavity circulation. It is found that the basal melting rate change due to warming is much greater than due to cooling. This is mainly because the intrusion of warm water onto the continental shelves, linked to sea ice production and climate change, is crucial in determining the basal melt rate of many ice shelves. The results indicate the water mass formation associated with sea ice production and brine rejection in the Antarctic coast by the atmospheric processes, combined with the subsurface ocean temperature change, are important to basal melting of Antarctic ice shelves.

In Chapter 4, based on the results of the Chapter 2 and 3, I discuss how the different climates between the early LIG and the early PIG could constrain the future retreatment of Antarctic ice sheet. The climate of the LIG is compared with future projection based on CO_2 emission scenarios of RCP 4.5 and 8.5. Although the mechanisms of Antarctic warming are different, the early LIG and the future climate change exhibit warmer winter surface air temperature and subsurface ocean temperature in the Antarctic region. The time series of future projection indicate the extent of Antarctic warming would reach the LIG within ~300 years even in a stabilized CO_2. According to the results of the climate model, the global warming may reach the threshold of a several meters of sea level rise due to the retreatment of Antarctic Ice Sheet in near future, even under a reduced emission and stabilized atmospheric CO_2 concentrations.

Acknowledgment

I am deeply grateful to Prof. Ayako Abe-Ouchi whose critical advices and discussions improved this study. Her encouragements and patientness helped me a lot. I would like to express my gratitude to Profs. Akira Oka, Masahiro Watanabe, Ryuji Tada and Kay I. Ohshima for their striking comments and warm encouragements. Comments and advices given by Prof. Hiroyasu Hasumi, Dr. Kazuya Kusahara, Dr. Fuyuki Saito contributed a lot to this study. I also appreciate the discussions and activities with research fellows, Prof. Masakazu Yoshimori, Drs. Sam Sherriff-Tadano, Akitomo Yamamoto, Ryota O'ishi, Wing-Lee Chan, Takanori Kodama, Shun Tsutaki, Shota Katsura, Takahito Mitsui, Kazumi Ozaki, Takashi Sakamoto, Takao Kawasaki, Hiroyasu Kubokawa, Rumi Ohgaito, Kunio Takahashi, Mika Ichino, Hidetaka Kobayashi, and Ms. Kanon Kino, Mr. Yasuto Watanabe, Mr. Keita Uehara. Thanks are also extended to all of the current and former members in the Division of Climate System Research, the Earth and Planetary System Science Group, and participants of the activities at scientific meetings. The numerical model simulations were performed on the Earth Simulator at the Japan Agency for Marine-Earth Science and Technology (JAMSTEC) and the Oakleaf-FX at the University of Tokyo. The figures were generated by Genetic Mapping Tool (GMT). Last, but not least, I would like to thank my family Makoto, Rumi, Tomoya and Tadashi for their support and encouragements.

Contents

Chapter 1

General Introduction

Understanding the nature of the Antarctic ice sheet is important for projecting future sea level change, which has a significant impact on human activities (IPCC AR5 chapter 13; Clark et al. 2016). Today, Antarctic continent is covered with a continental ice. Ice sheet is a grounded ice mass of continental size with typical thickness of ~3,000 meters. The volume of Antarctic ice sheet is 27 million km^3, which is 58 meters sea level equivalent (Fretwell et al. 2013). Recent observations have elucidated significant mass loss of the Antarctic ice sheet in these decades (Pritchard et al. 2009; Velicogna 2009; Rignot et al. 2011; Pritchard et al. 2012; Shepherd et al. 2012). It is concluded that the average rate of ice loss from Antarctica was 0.20 to 0.61 mm (sea level equivalent) per year during the period of 2002−2011 by the IPCC AR5 (IPCC AR5 chapter 4).

One unique characteristic of Antarctic ice sheet is the bedrock topography beneath the ice. The elevation of Antarctic continent is below sea level especially in the western part of Antarctica (Fig. 1.1, 1.2). Since the bedrock topography is below the sea level in many regions, the ends of Antarctic ice sheet exists as ice shelves, floating tongues of ice on the ocean. The spatial extent of ice shelves in the present-day is indicated as grey area in Fig. 1.1. Ice shelves constitute 12% of Antarctic continent in the areal extent (Fretwell et al. 2013), and nearly half of the coastline of Antarctica is fringed by ice shelves (Swithinbank 1988). The shape and volume of ice sheet is determined by mass balance of ice and the flow of ice. The mass balance of Antarctic ice sheet and related processes are schematically described in Fig. 1.3. The main source of Antarctic ice sheet is accumulation due to snowfall, and the ice is lost from Antarctica mainly by cutoff of iceberg (calving) and melting of ice shelves. Today, surface melting due to atmospheric processes is very small in Antarctica (Krinner et al. 2006; Cuffey and Paterson 2010). Instead, calving of icebergs and basal melting account for most of ablation processes in Antarctica, and these processes operate primarily on ice shelves.

The estimated accumulation rate on the whole Antarctic continent is 2144−2295 Gt/yr (Jacobs et al. 1992; Wild et al. 2003; Krinner et al. 2006), and estimated ablation rates due to basal melting of ice shelves and iceberg calving are 1325−1454 Gt/yr and 1089−1321 Gt/yr, respectively (Depoorter et al. 2013; Rignot et al. 2013).

As ice shelves exerts backward stresses (buttressing effect) to inland ice sheets, thinning or loss of ice shelves leads to an acceleration of the ice flow, and to an increased runoff of the ice sheet (Dupont and Alley 2005). In addition, grounding lines are unstable on the reversed-bed (downward towards the inland) slopes, which are commonly found in Antarctic continent (Fig. 1.2). When the ice sheet rests on a bed that deepens toward the inland, the ice outflow to the ocean will increase in general as the grounding line retreats (Weertman 1974; Schoof 2007). Therefore, in case of a retreat, this increased outflow leads to a further retreatment of Antarctic ice sheet until a region of shallower bedrock is reached. Ice sheet modeling studies applied a changing mass balance of Antarctic ice sheet including basal melt rate of ice shelves, and showed that the thinning of ice shelves played an essential role in the retreatment of the Antarctic Ice Sheet in the future, for specific ice sheet catchments (Joughin et al. 2010; Joughin et al. 2014; Favier et al. 2014; Pittard et al. 2017) and whole Antarctica (Sato and Greve 2012; Bindschadler et al. 2013). The essential role of basal melt rate change is important to variations of Antarctic ice sheet not only in the future, but also glacial cycles in the past (Pollard and Deconto 2009; Golledge et al. 2012; Golledge et al. 2014).

While accumulation of Antarctic ice sheet is determined by atmospheric processes of snowfall, ablation is mainly determined by ocean processes. Basal melting of ice shelf is a result of the heat delivered by the ocean (Jacobs 1992). Iceberg calving involves many different processes, such as melting at the ice shelf front by buoyancy by seawater, and crevasses (Greve and Blatter 2010). According to current glaciological estimates, the average rate of basal melting in total Antarctic ice shelf is ~1 meters per year, but a very high rate of basal melting (>10 meter per year) is observed in some ice shelves, such as Pine Island Glacier in the Amundsen Sea (Jacobs et al. 2011; Rignot et

al. 2013; Depoorter et al. 2013). Oceanographic observations indicate the cause of very high basal melt rate is the ocean circulations in the Antarctic shelf seas. A warm water of ~1 °C originating from the Southern Ocean is the cause of greater basal melting in the Pine Island Glacier and other ice shelves (Jenkins and Jacobs 2008; Jacobs et al. 2011; Rintoul et al. 2016). On the other hand, seawater temperature above the continental shelf is close to the freezing point (~ −1.9 °C) where basal melt rate is small, typically for the Filchner-Ronne and the Ross ice shelves (Jacobs 1985; Nicholls et al. 2009). The cold and saline seawater is formed by brine rejection from sea surface water associated with the formation of sea ice (Jacobs 1992, Morales Maqueda 2004). There is limited monitoring in recent ocean temperature change near Antarctic ice shelves, but one study estimated that a higher ocean temperature observed in increased the basal melting of the Pine Island Glacier by about 50% in 2009 compared to 1994 (Jacobs et al. 2011). This indicates that the retreatment of Antarctic ice sheet occurs through changes in ocean temperature and basal mass balance of ice shelves.

While climate model simulations indicate both accumulation and surface melting of Antarctic ice sheet would be changing due to global warming (Ohmura et al. 1996; IPCC AR5 chap. 13), ocean models combined with climate model indicate that a drastic increase in basal melting of ice shelves would occur (Hellmer et al. 2012; Timmermann and Hellmer 2013). Hellmer et al. (2012) utilized a regional ocean model, forced by an output of atmosphere-ocean general circulation model (AOGCM) through 22nd century. In the beginning of the 21st century, the simulated basal melt rate of the Filchner-Ronne ice shelf is small since the ocean temperature beneath ice shelf is cold as observed in the present-day. However, in the late 21st century, the basal melt rate increased drastically, as warm water at subsurface depth in the Southern Ocean started to flow onto the continental shelf and the ice shelf cavity. In order to project future climate change and the associated response of the Antarctic ice sheet, it is necessary to take basal melting of ice shelves into account (Holland and Holland 2015; Kusahara 2016). In the most recent study, ice sheet models are utilized with climate models,

especially for AOGCMs, to project future change in Antarctic ice sheet. Some studies conducted future projection of Antarctic ice sheet change using time series of mass balances of Antarctic ice sheet derived from simulation of climate models and ocean models resolving Antarctic ice shelf cavities for the next ~ 200 years (Gong et al. 2014; Mengel and Levermann 2014; Mengel et al. 2015; Cornford et al. 2015). For example, Cornford et al. (2015) conducted future projections of Antarctic ice sheet using output of a climate model up to 2200 AD. As for basal melting of ice shelves, they used outputs of ocean models which resolve Antarctic ice shelves (BRIOS and FESOM models), assuming basal mass balance of ice shelves increases approximately 16 meters per 1 °C in ocean temperature anomalies at 200 to 800 m depth. They found that the major retreatment of WAIS did not occur until 2100 AD (Antarctic ice sheet volume change was less than 10 cm sea level equivalent), as the simulated ocean warmings were insufficient to cause significant melting of ice shelves.

In contrast, as for long-term simulations including paleoclimate studies, basal melt rate changes are simply parameterized with ocean temperature derived from AOGCMs (Winkelmann et al. 2015; Golledge et al. 2015; Sutter et al. 2016; Deconto and Pollard 2016), since ocean models resolving Antarctic ice shelf cavities are computationally expensive. In these studies, subsurface ocean temperature near ice shelves from AOGCMs is used to consider basal melt change. For example, Golledge et al. (2015) conducted future projections of Antarctic ice sheet using output of a climate model up to 5000 AD forced by extended Representative Concentration Pathway (RCP). They found that the major retreatment of WAIS occurred in RCP 4.5, and the simulated Antarctic ice sheet volume change reached 2.77 meters sea level equivalent in 5000 AD. As for basal melting of ice shelves, they used Antarctic sea surface temperature of from a climate model (GENESIS ver. 3), assuming basal mass balance of ice shelves increases approximately 10 meters per 1 °C. The horizontal resolution of climate model was about ~80 km, and the model does not resolve Antarctic ice shelves. It means that the methods of simulating Antarctic ice sheet changes are divided between the

near-future projections and the paleoclimates from the point of the treatments on basal melting of ice shelves.

In the fifth assessment report of Intergovernmental Panel on Climate Change (IPCC), a multi-millennial commitment of sea level rise was presented based on Levermann et al. (2013). They present a relationship between global mean temperature and Antarctic ice sheet volume changes using sea level reconstructions in the past and an ice sheet modeling study. As for the Greenland Ice Sheet, surface melting of ice sheets due to the atmospheric warming is a main driver of the ice sheet retreatment. A climatic threshold of near-complete melting of ice sheet is shown to exist between global mean temperature change of 1 to 3 °C, due to a positive feedback between ice sheet and climate. As an ice sheet begins to melt, the local surface temperature rises due to a decreased surface elevation, and a decrease in ice sheet area additionally contributes to warming through a reduction in the surface and planetary albedo, which brings further melting (Robinson et al. 2012). For the Antarctic ice sheet, there is not only the atmosphere-ice sheet feedback but also the melting and dynamics of ice shelves (Weertman 1974; Schoof 2007). but they discussed the climatic threshold of the retreatment of Antarctic ice sheet was uncertain due to the uncertainties in forcing data and models (Levermann et al. 2013).

Paleoclimate reconstruction is one of means to validate numerical models used for future projections. Geological surveys have elucidated variations of the Antarctic ice sheet in the past, and the volume of Antarctic ice sheet was less in a warm climate. The Last Interglacial (LIG, about 130 ka: ka is 1000 years before present) was an interglacial of the current glacial cycles, and is a most recent warm period before the present interglacial (Fig. 1.4). Sea level reconstructions indicate that the global mean sea level during the LIG was higher than the present-day (Kopp et al. 2009; Dutton and Lambeck 2012; O'Leary et al. 2013), and IPCC AR5 concluded that the sea level was at least 5 meters higher than the present-day with very high confidence (IPCC AR5). Although direct evidences of the retreatment of Antarctic ice sheet were not found so far (Bradley

et al. 2012), the high sea level indicates the West Antarctic Ice Sheet (WAIS) was retreated, as the estimated volume of Greenland ice sheet is insufficient to account for the reconstructed sea level (Dutton et al. 2015). This indicates the climate during the LIG was above the climatic threshold of the retreatment of WAIS. The retreatment of Antarctic ice sheet is indicated from sea level reconstructions during other interglacial of MIS 11 (about 400 ka, Raymo and Mitrovica 2012). During the Pliocene (about 3 million years ago), marine sediments in the Antarctic Ocean indicate Antarctic ice sheet retreated in the Wilkes Land (Cook et al. 2013) while the ice sheet was thicker in the Dronning Maud Land (Suganuma et al. 2014; Yamane et al. 2015). As for a cold period of the Last Glacial Maximum (LGM, about 21 ka), the Antarctic ice sheet expanded to Antarctic continental shelf edges and the volume of Antarctic ice sheet was larger than the present-day (Bentley et al. 2014; Clark and Tarasov 2014). Therefore, it is indicated that the volume of Antarctic ice sheet was large during glacials and was small during interglacials, but the volume differed between each interglacials.

The LIG is the main focus of the present study as for the past. Climate reconstructions during the LIG indicate that the surface temperature was higher than the present-day especially in high latitudes including Antarctica (Turney and Jones 2010). The global mean sea surface temperature was estimated to be higher by about 1 °C compared to the present-day (Hoffman et al. 2017). However, climate model simulation could not reproduce warm climate in the Antarctic region, when the boundary conditions of insolation and greenhouse gas concentrations at the LIG is used (Lunt et al. 2013). Due to this problem, integrated climate and ice sheet modeling studies could not reproduce the retreatment of WAIS, when the model is forced with the boundary condition at the LIG. For example, Sutter et al. (2016) used the output of climate model simulation of the LIG to drive an Antarctic ice sheet model. As for basal melting of ice shelves, they used Antarctic ocean temperature at 400 m depth from a climate model (COSMOS), assuming basal mass balance of ice shelves increases approximately 0.2 meters per 1 °C, following Beckmann and Goosse (2003). However, the climate model

did not exhibit significant warming in the Antarctic region when the model was forced by the boundary condition of the LIG. They investigated the threshold of the retreatment of WAIS by additional sensitivity experiments, and found that an additional ocean temperature change of 2 to 3 °C, which was close to reconstructed surface ocean temperature in the Southern Ocean, was needed to reproduce the retreatment of WAIS. For the same reason, Deconto and Pollard 2016 drove an ice sheet model with reconstructed air and ocean temperature to reproduce the retreatment of Antarctic ice sheet at the LIG. These results indicate that the retreat of WAIS during the LIG can be explained by warmer Antarctic climate during the LIG, but the ultimate cause is unknown. The recent studies based on the time series of sea surface temperature reconstructions indicate the Atlantic Meridional Overturning Circulation (AMOC) was weak during the transition from the preceding glacial to the LIG (Capron et al. 2014). As the weakening in AMOC produces a warming in the Southern Hemisphere by a reduced meridional heat transport known as a "bipolar seesaw" mechanism (Broecker 1998; Stocker 1998), previous climate modeling studies incorporate the mechanism of Antarctic warming associated with a weakening in AMOC (Holden et al. 2010; Stone et al. 2016). These studies applied meltwater input in the North Atlantic to weaken AMOC at LIG, but the simulated temperature change in the Southern Ocean is still smaller than reconstructions. In addition, the cause of the difference between the LIG and the present interglacial was not addressed, as the meltwater input to the ocean due to melting of Northern Hemisphere ice sheet was a common event between the transition from glacial to interglacial, for both the LIG and the present interglacial.

Therefore, in the present study, I investigate the mechanisms and physical processes of Antarctic ice sheet changes in the past and future to help understanding climatic thresholds of Antarctic ice sheets. In chapter 2, I focus on the LIG, which is the most recent period when the retreatment of WAIS is thought to occur. As for the LIG, the retreatment of WAIS can be explained by the increased basal melting of ice shelves due to a warmer Antarctic climate (Sutter et al. 2016; Deconto and Pollard 2016), but

climate model simulations could not reproduce such warmer climate in the Antarctic region. This gives a serious concern on the future retreatment of the Antarctic ice sheet. I conducted a transient climate model simulation from the glacial to interglacial, and investigated the role of glacial meltwater due to the melting of Northern Hemisphere ice sheet as a probable factor in determining the climate of Antarctica. In chapter 3, the process of Antarctic Ocean circulation changes and basal mass balance of Antarctic ice shelves were investigated. As for future projection, ocean circulation changes in the Antarctic Ocean are recently adopted, but not for paleoclimate as well as long-term future projections. I utilized a regional ocean model resolving ocean circulations beneath ice shelves to understand the mechanism and responsible processes of basal melting of Antarctic ice shelves. In chapter 4, I analyzed climate model simulations of the past and the future climate projections, and discussed the relation between the past and the future on the climatic thresholds for Antarctic ice sheet retreat.

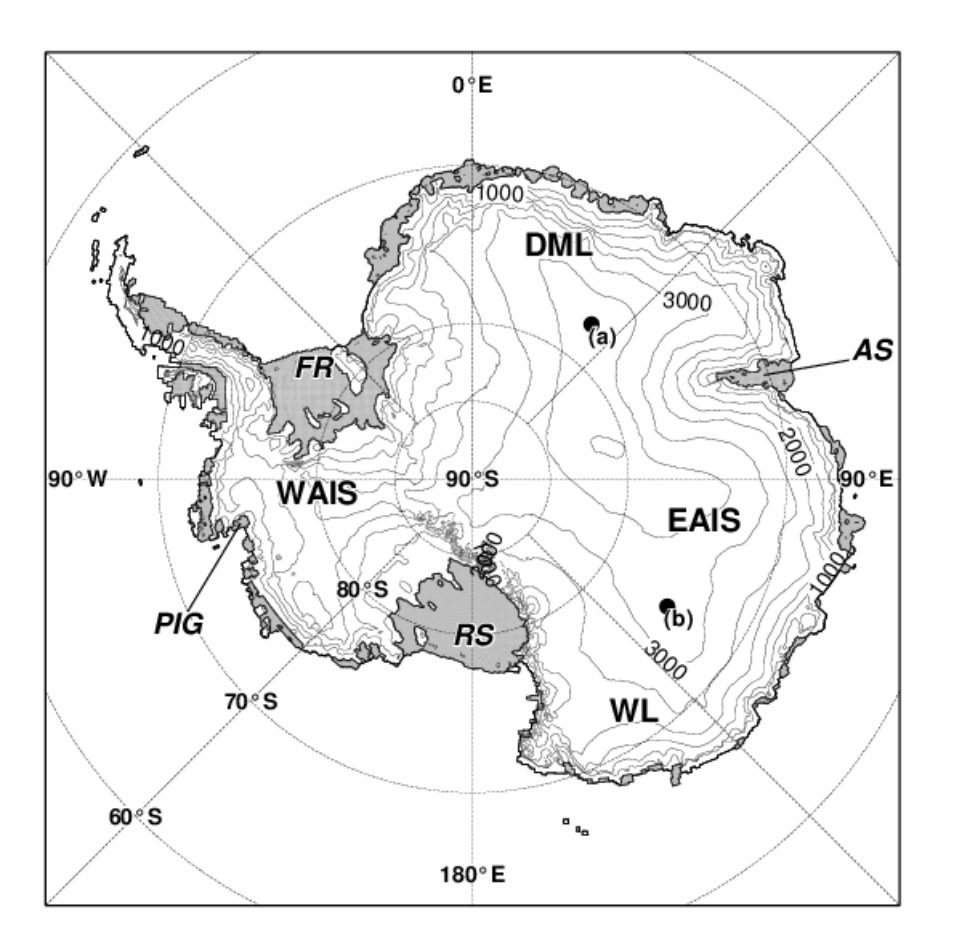

Fig. 1.1 Map of Antarctica. Shaded area indicates ice shelves, contour indicates surface elevation of ice sheet. Dots indicates the locations of representative deep ice cores: (a) Dome Fuji, (b) Dome C, respectively. Bold letters indicate the names of locations: DML indicates Dronning Maud Land, WAIS (West Antarctic Ice Sheet), EAIS (East Antarctic Ice Sheet), WL (Wilkes Land), respectively. Italic letters indicate the names of notable ice shelves: FR (Filchner-Ronne Ice Shelf), RS (Ross Ice Shelf), AS (Amery Ice Shelf) and PIG (Pine Island Glacier), respectively.

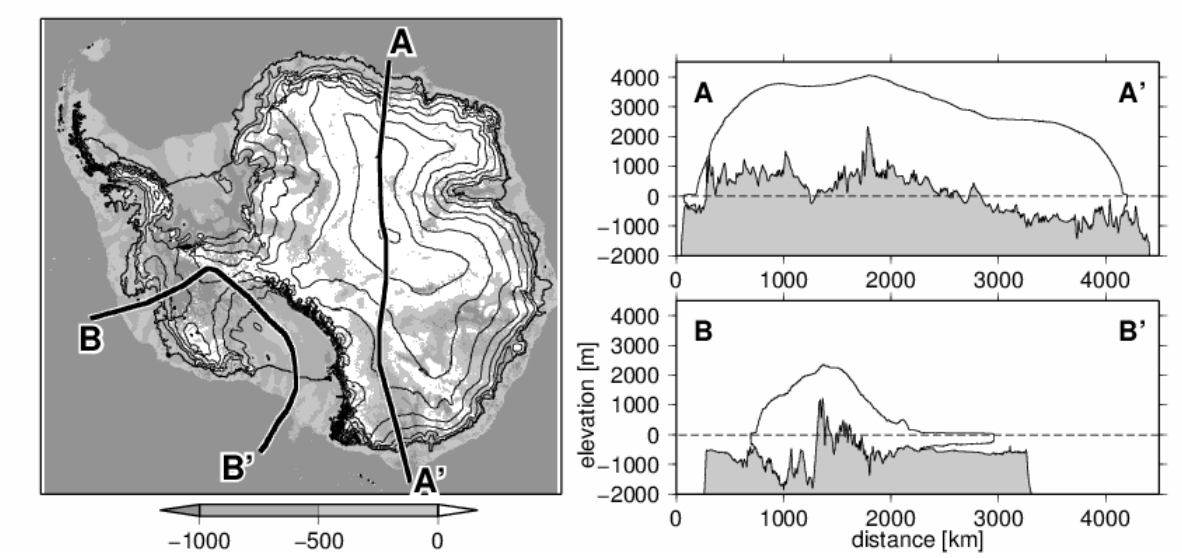

Fig. 1.2 (Left) Bedrock (gray shading) and surface (contour lines) topography of the Antarctic ice sheet at present-day. (Right) Bedrock and surface topography from the two transects across Antarctic continent shown in the left panel. The data is derived from BEDMAP2 (Fretwell et al. 2013)

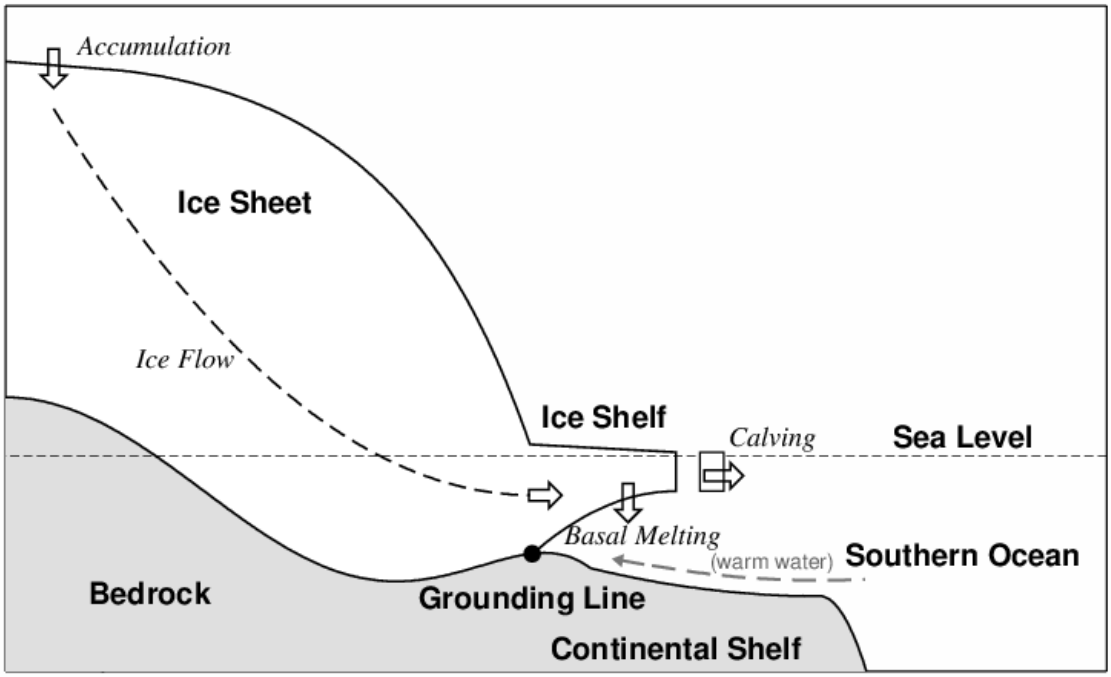

Fig. 1.3 Schematic figure of Antarctic ice sheet mass balance and related processes among climate system components.

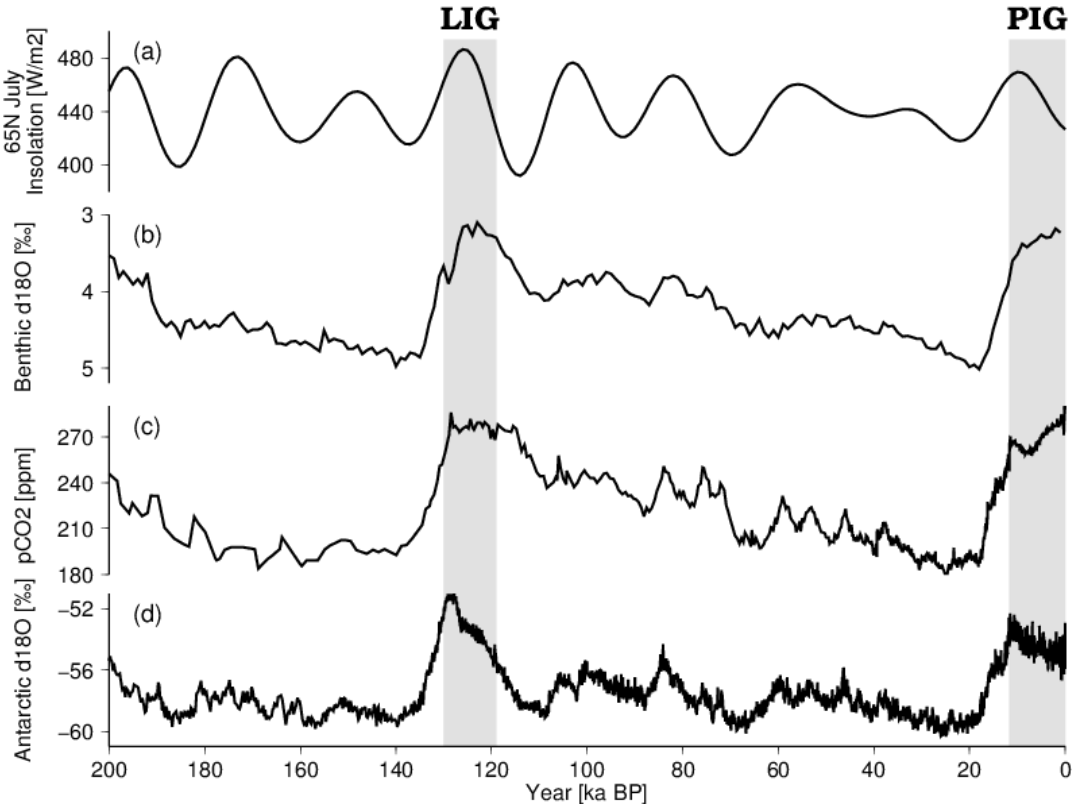

Fig. 1.4 Reconstructions of the past 200,000 years for (a) July insolation at 65°N (Berger and Loutre 1991), (b) Global benthic stack of oxygen isotope (Lisiecki and Raymo 2005). (c) Atmospheric carbon dioxide concentrations (Bereiter et al. 2015), (d) Antarctic oxygen isotope (Kawamura et al. 2017). The shaded area indicates the present-day interglacial (PIG) and the last interglacial (LIG).

Chapter 2

The role of glacial meltwater derived from the Northern Hemisphere on the Antarctic climate during deglaciation and interglacial

本章については、5 年以内に雑誌などで刊行予定のため、非公開。

Chapter 3:

Responses of basal melting of Antarctic ice shelves to the climatic forcing of the Last Glacial Maximum and CO_2 doubling

ABSTRACT

Basal melting of the Antarctic ice shelves is an important factor in determining the response of the Antarctic ice sheet to climate changes. In this study, the responses of Antarctic ice shelf melting to a doubling of CO_2 and Last Glacial Maximum conditions are investigated. The climatic output of an atmosphere–ocean general circulation model is used to force a circumpolar ocean model that resolves ice shelf cavity circulation. Sensitivity experiments are conducted to investigate the respective roles atmosphere and ocean processes. It is found that the basal melting rate change due to climate warming is much greater (by an order of magnitude) than due to cooling. This is mainly because the intrusion of warm water onto the continental shelves, linked to sea ice production and climate change, is crucial in determining the basal melt rate of many ice shelves. Sensitivity experiments showed that changes in atmospheric heat flux strongly affected the production of sea ice and high-density water, preventing warmer water approaching the ice shelves under a colder climate. The results indicate the water mass formation associated with sea ice production in the Antarctic coast by the atmospheric processes, combined with the subsurface ocean temperature change, are important to basal melting of Antarctic ice shelves.

3.1 Introduction

Understanding the nature and stability of the Antarctic ice sheet is important when projecting future rises in sea level (Church et al. 2013; Clark et al. 2016). Climate can affect the ice sheet directly via changes in atmospheric temperature and precipitation, but the primary mechanism is through local ocean temperature change near the ice shelves. Numerical ice sheet models have been used to reconstruct the shapes of ice sheets, and to investigate their responses to variations in climate forcing. In Antarctica, basal ice shelf melting is one of the two important processes that determine the mass balance of the ice sheet besides calving of icebergs (Depoorter et al. 2013; Rignot et al. 2013). Studies modeling the Antarctic ice sheet have shown that an increase in basal melting plays an essential role in the retreat of the marine ice sheet (Pollard and DeConto 2009; Golledge et al. 2012; Sato and Greve 2012; Bindschadler et al. 2013; de Boer et al. 2013; Golledge et al. 2014). This is because the loss of the ice shelves reduces ice-shelf buttressing, which affects the flow of the continental ice sheet (Dupont and Alley 2005; Schoof 2006; Walker et al. 2008; Gagliardini et al. 2010).

Modeling of the Antarctic ice sheet requires the basal melt rates of the ice shelves as boundary conditions. Physically, basal melting occurs because of heat delivered from the ocean beneath the ice shelves (Hellmer and Olbers 1989). According to glaciological estimates, it is indicated that high rates of basal melting occur in the western part of Antarctica, and is concentrated on the grounding lines (Rignot and Jacobs 2002; Rignot et al. 2013). The observed differences in basal melt rates among various regions are shown to reflect the differences in the basal melting mode, which depends on ocean temperature of the Antarctic shelf seas (Jacobs et al. 1992). The first mode is characterized by a low rate of basal melting, driven by the thermohaline circulation due to sea ice production and the formation of high-salinity shelf water (whose temperature of approx. –1.9 °C) (Jacobs et al. 1985; Nicholls et al. 2009). In contrast, the second mode of basal melting is characterized by a very high rate of melting (Talbot 1988; Jacobs et al. 1996; Jenkins and Jacobs 2008) due to the flow onto

the continental shelves of warm (approx. 1 °C) and saline circumpolar deep water (CDW) originating from the Southern Ocean. Generally, the steep topography at the continental shelf break limits the inflow of CDW onto the continental shelves; however, eddies generated by the seafloor topography (St-Laurent et al. 2012), tides (Dinniman et al. 2011), and winds around the continental shelf break (Thoma et al. 2008) are proposed mechanisms for the transport of warm water onto the continental shelves. The third mode of basal melting is characterized by summertime melting in the frontal area of the ice shelf because of the formation of seasonal warm water (Jacobs et al. 1985), as observed in the Ross Sea. An another mode has been proposed, which is characterized by low basal melting due to easterly winds and the subduction of cold surface water along the Antarctic coast, which prevents warm subsurface water from flowing into ice shelf cavities (Whitworth et al. 1998; Nøst et al. 2011; Hattermann et al. 2012)

Ocean models with an ice shelf cavity component are used to investigate the response of ice shelf melting to changes in boundary conditions (Hellmer 2004, Losch 2008, Galton-Fenzi et al. 2012; Miller et al. 2012; Timmermann et al. 2012; Dinniman et al. 2015; Kusahara et al. 2015). The response of ice shelf melting to subsurface ocean warming in front of the ice shelf has been investigated in previous studies (Hellmer et al. 1998; Williams et al. 1998; Holland et al. 2008). However, it is shown that the response to climate change is affected not only by subsurface ocean temperature but also by sea-surface-driven water mass formation of High Salinity Shelf Water in the Antarctic shelf seas. It is shown that sea ice production and the formation of cold and dense water masses in the Antarctic shelf seas affect the intrusion of warm water onto the Antarctic continental shelves (Petty et al. 2013; Timmermann and Hellmer 2013). Kusahara and Hasumi (2013) systematically applied air temperature anomalies of 1–6 °C and discussed the changing properties of the water masses flowing into the ice shelf cavities. Hellmer et al. (2012) and Timmermann and Hellmer (2013) used atmosphere–ocean general circulation models (AOGCMs) with CO_2 emission scenarios of the Intergovernmental Panel on Climate Change to force an ocean model to project the

basal melt rates of Antarctic ice shelves in the 21st and 22nd centuries. They showed that drastic increases in both the seawater temperature of the shelf seas and the basal melt rate of the ice shelves occur because a reduction in the extent of sea ice and convection lead to the flow of warm water onto the continental shelves and into the ice shelf cavities.

To project future climate change and the associated response of the Antarctic ice sheet, it is necessary to couple an ice sheet model and an AOGCM (Holland and Holland 2015; Kusahara 2016). Future projections have indicated the importance to the basal melt rate of ice sheets of resolving water mass formation in the shelf seas (Hellmer et al. 2012; Timmermann et al. 2013). However, one of the most recent ice sheet modeling studies have used an ocean model to project the future loss of Antarctic ice sheet (Gong et al. 2014; Mengel and Levermann 2014; Mengel et al. 2015). They used an ocean model, which resolves Antarctic ice shelf cavity circulations over the next two centuries, forced by and AOGCM (Timmermann and Hellmer 2013). These generated data were then used as inputs for the basal mass balance of the ice shelves in ice sheet models. Since the sea level and global mean temperature will decline slowly due to the inertia in the climate and carbon cycle systems (Levermann et al. 2013; Clark et al. 2016), a long-term (millennial to multi-millennial) perspective is required. However, Antarctic subsurface ocean temperatures derived from an AOGCM is frequently used to parameterize the basal mass balance beneath the ice shelves (Beckmann and Goosse 2003; de Boer et al. 2015; Golledge et al. 2015; Sutter et al. 2016; Deconto and Pollard 2016). One important limitation of AOGCMs is they do not have ice shelf component and sufficient horizontal resolution to resolve water mass formation in the Antarctic continental shelf seas.

The objective of this paper is to understand the important processes that determine the long-term responses of ocean temperature in the Antarctic shelf seas and basal melt rate of the Antarctic ice shelves. I use a circumpolar ocean model that resolves ice shelf cavity circulations, combined with an AOGCM, to investigate the

response of the basal melt rate of the Antarctic ice shelf. I simulate the climates of the LGM and a quasi-equilibrium CO_2 doubling ($2xCO_2$) as representatives of extreme colder and warmer conditions, respectively, which are often referred to as benchmarks among paleoclimate modeling studies and future projections (Braconnot et al. 2007; Yoshimori et al. 2009). A challenge in simulating Antarctic Ice Sheet at the LGM is that both the climatic conditions and the Antarctic ice shelf configuration affect the basal melt rate (Kusahara et al. 2015). In this study, I focus on the response of basal melt rate to changing climate by keeping the same configuration of Antarctic ice shelf as present-day. In order to investigate the mechanisms that determine the responses of basal melting, we additionally conduct sensitivity experiments by applying individual atmospheric and oceanic boundary conditions derived from the AOGCM individually. I analyze the responses of multiple ice shelves from West to East Antarctica to the climatic conditions and discuss their determining mechanism of changing basal mass balance for different locations.

3.2 Model Description and Experimental Design

a. Model description of the Circumpolar Ocean Model

I used a circumpolar ocean model to resolve the Antarctic ice shelf cavities (Kusahara and Hasumi 2013, 2014) based on the COCO model (Hasumi 2006), which includes dynamic and thermodynamic sea ice. The model domain encompassed the Southern Hemisphere and an artificial northern boundary was set near 35°S (lower-left inset of Fig. 3.1). The model does not calculate ocean circulation northern than the boundary. Horizontal resolution was about 10–20 km along the Antarctic coast. The heat and freshwater fluxes at the ice-shelf–ocean interface were computed using a three-equation scheme (Hellmer and Olbers 1989; Holland and Jenkins 1999). This scheme diagnoses the heat and freshwater fluxes at the ice–ocean interface using temperature and salinity below the ice shelf prescribed from ocean model grids. By introducing an ice–ocean interface boundary layer between the ice shelf and the ocean,

the upward heat flux Q_M^T and salt flux Q_M^S from the ocean to the boundary layer can be parameterized with a bulk formulation:

$$Q_M^T = -\rho c_p \gamma_t (T_b - T_m) \quad (1)$$

$$Q_M^S = \rho \gamma_s (S_b - S_m) \quad (2)$$

where ρ is the density of seawater (1028 $kg\,m^{-3}$), c_p is the specific heat capacity of seawater (4200 $J\,kg^{-1}K^{-1}$), $\gamma_t = 1.0 \times 10^{-4}$ m/s and $\gamma_s = 5.05 \times 10^{-7}$ m/s are constant thermal and salinity exchange velocities, respectively, T_b and S_b are the temperature and salinity at the ice–ocean interface boundary layer, respectively, and T_M and S_M are the temperature and salinity of the ocean model grid beneath the ice shelf base, respectively. Q_I^T is the conductive heat flux through the ice shelf (upward is positive). Therefore, $Q_I^T - Q_M^T$ represents the heat used in ice shelf melting, such that:

$$Q_I^T - Q_M^T = -\rho w_b L \quad (3)$$

$$Q_I^S - Q_M^S = -\rho w_b S_b \quad (4)$$

where w_b is the meltwater flux due to ice shelf melting and L is the latent heat of fusion (3.34×10^5 J/kg). The value of Q_I^T is estimated by assuming a constant vertical advection and diffusion (Holland and Jenkins 1999). The value of $Q_I^S = 0$ because no salinity flux exists within the ice shelf. Temperature at the ice shelf–ocean interface (T_b) is maintained at the freezing point of seawater. We use a linearized version of the equation of freezing point of seawater, which depends on salinity and ocean depth (Mellor and Kantha 1989). Freshwater flux due to ice shelf melting or seawater freezing w_b can be computed using simultaneous equations on T_b, S_b, and w_b. Basal melt rate w_b is determined largely by the term representing the temperature gradient between the seawater and the ice shelf ($T_b - T_M$). The model does not calculate dynamic and thermodynamic change in ice shelves.

b. Description of the AOGCM experiments

I used the MIROC 4m AOGCM, the same model used in the Chapter 2. In the

CTL experiment, pre-industrial boundary conditions were prescribed such as atmospheric CO_2 concentration of 285 ppm. LGM experiment followed the protocol of PMIP2 (Braconnot et al. 2007), in which greenhouse gas concentrations (atmospheric CO_2 concentration of 185 ppm) and global LGM ice sheet topography were prescribed. In the $2xCO_2$ experiment, we increased the atmospheric CO_2 concentration by 1% compound per year from the pre-industrial value until it doubled (571ppm, at 70th years) and the value was held constant thereafter. Based on the Representative Concentration Pathway (RCP), CO_2 concentration reaches the value of 571 ppm around 2100 and mid-2050 for RCP 4.5 and RCP 8.5, respectively. The model was integrated for thousands of model years (3800 years for CTL, 2300 years for LGM) to reach respective quasi-steady states. The climatology of the AOGCM experiments were taken for 100-years from quasi-equilibrium states for the analysis and used for boundary conditions of the circumpolar ocean model experiments. In case of the $2xCO_2$, we took the climatology from the years 791–890, when the sea surface and subsurface ocean temperatures in the Southern Ocean reached quasi-equilibrium as shown in Fig. 3.2a. While more than 70% of global mean surface air temperature increase is accomplished within 200 years, surface and ocean temperature increase in the Southern Ocean have not even reached half of the final change in the same periods (Fig. 3.2a). This is because of the thermal inertia of the Southern Ocean (Manabe et al. 1991). The increase of sea surface temperature around years 700–800 is related to the recovery of deep convection in the Weddell Sea (Yamamoto et al. 2015).

The climatic fields simulated by the AOGCM experiments are displayed in Figs. 3.3 and 3.4. The simulated global mean annual 2-m air temperature anomaly to CTL for the LGM (–5.7 °C) is consistent with previous reconstructions and other climate model results (Braconnot et al. 2012, Abe-Ouchi et al. 2015). The air temperature and ocean temperature from the surface to the bottom decrease in the Antarctic region (Fig. 3.3a) for the LGM conditions. The 2-m air temperature anomaly depends on the season, winter air temperature anomaly is larger than that in summer.

Sea ice extent during the LGM experiment (Fig. 3.4) is consistent with previous reconstructions (Gersonde et al. 2005; MARGO Project Members 2009), as analyzed in Roche et al. (2012). Decreased precipitation over the Antarctic region (Fig. 3.3e) during LGM is consistent with other reconstructions (Parrenin et al. 2007). The katabatic winds from the Antarctic continent is intensified in the LGM experiment (Fig. 3.3c). The Southern Westerly exhibits a very little change in the LGM experiment, and precipitation in the Southern Ocean has shifted as in most of the AOGCMs (Rojas et al. 2009).

The simulated global annual mean 2-m air temperature anomaly in the $2xCO_2$ experiment is 4.2 °C (Fig. 3.3b), but in comparison, the LGM experiment exhibits larger amplitudes of temperature change in the air and ocean temperature anomalies. As indicated by Fig. 3.4, the area of sea ice shrinks and sea ice cover in summer almost disappears. In the $2xCO_2$ experiment, the westerly in the Southern Ocean shifts southward and weakens the easterly wind along the Antarctic coast (Fig. 3.3d). Net precipitation over the Southern Ocean and Antarctica increases (Fig. 3.3f).

Focusing on the air and ocean temperatures in the Antarctic region, the 2-m air temperature anomaly averaged over the marine area of 65–90°S is –8.1 °C for the LGM and 6.7 °C for the $2xCO_2$ experiments. In contrast, the amplitude of sea surface temperature in the Antarctic region is smaller than the subsurface because of sea ice cover. For the CTL experiment, the Antarctic surface and subsurface (200−1000m depth average) ocean temperature are −1.2°C and 1.7°C, respectively. Note that the subsurface ocean temperature (1.7°C) is warmer by 0.6°C than the observation. In the LGM experiment, surface and subsurface ocean temperature drops by 0.6°C and 2.8°C, while in the 2xCO2 experiment, they increases by 1.5°C and 0.9°C, respectively (Fig, 3.3g−h). showing that the subsurface seawater temperature anomaly is much higher in the LGM experiment compared with the $2xCO_2$ experiment. The smaller subsurface ocean temperature anomaly in the $2xCO_2$ experiment is likely a result of the stronger deep convection in the Southern Ocean (Yamamoto et al. 2015)

c. Experimental Design of the circumpolar ocean model

The settings of the present-day (CTL) experiment for the circumpolar ocean model were the same as in Kusahara and Hasumi (2013). The daily atmospheric fields derived from the ERA-15 reanalysis (Röske 2006) were used as sea surface boundary conditions. Ocean temperature and salinity columns in the northernmost six grid cells were restored to the monthly Polar Science Center Hydrographic Climatology (PHC, Steele et al. 2001) with a damping scale of 10 days. The ocean temperature and salinity fields were initialized with the PHC and ocean velocities as zero. The atmospheric and oceanic boundary conditions were modified in the LGM and $2xCO_2$ experiments based on the results of AOGCM experiments. The monthly mean anomalies of the LGM and $2xCO_2$ experiments from the CTL simulation of the AOGCM were superimposed on the present-day atmospheric and oceanic boundary conditions used in the CTL experiment. This procedure was applied to minimize the biases of the AOGCM. The identical present-day Antarctic ice sheet configuration is used in all experiments to study the role of climate on basal melt rate. I initiated the LGM and $2xCO_2$ experiments by applying two different initial ocean fields to both to investigate their dependence on the initial conditions and the required time to reach quasi-steady states. One experiment was initialized with ocean temperature and salinity fields from the PHC, and the other was initialized with the LGM or $2xCO_2$ derived from the AOGCM. After the 60-years' integration, the simulated basal melt rate and ocean temperature reached similar quasi-steady states (Fig. 3.2b). As the simulated basal melt rate exhibited spatial interannual variability, the final 20-year averaged climatology was analyzed in all experiments.

d. Design of sensitivity experiments for individual climatic forcing

I conducted sensitivity experiments to separate the factors contributing to the changes in basal melt rate for the LGM and $2xCO_2$ experiments (Table 3.1). The forcing

of the ocean model constituted the sea surface atmospheric boundary conditions and the ocean temperature and salinity forcing of the lateral boundary. Atmospheric boundary conditions comprised heat flux (sensible heat, latent heat, and radiative fluxes), sea surface momentum flux, and sea surface freshwater flux due to net precipitation. I named the sensitivity experiments using the terms "ATM," "OCN," "ATMHEAT," "ATMWIND," and "ATMPRCP" combined with LGM and $2xCO_2$. The terms "LGM_OCN" and "$2xCO_2$_OCN" denote that the ocean temperature and salinity at the lateral boundary were set to LGM or $2xCO_2$, while other boundary conditions were set to CTL. Similarly, "LGM_ATM" and "$2xCO_2$_ATM" denote that the atmospheric boundary conditions were set to LGM or $2xCO_2$, while the ocean temperature and salinity at the lateral boundary were set to CTL. The terms "ATMHEAT," "ATMWIND," and "ATMPRCP" denote branches of the "ATM" experiments. The term "ATMHEAT" denotes that only atmospheric heat flux was set to LGM or $2xCO_2$, while the other atmospheric boundary conditions as well as the oceanic boundary conditions were set to CTL. Similarly, "ATMWIND" denotes that sea surface momentum flux and "ATMPRCP" denotes that sea surface freshwater flux due to net precipitation were set to LGM or $2xCO_2$.

3.3 Results

3.3.1 Results of the CTL experiment

This section presents the results of the CTL experiments to compare the basal melting and oceanic structures with observations. The model in this study is shown to be able to roughly reproduce the total melting amount and the spatial distribution of basal melt rate under the present-day climate (Kusahara and Hasumi 2013). However, one remark is that basal melt rate of ice shelves in the Amundsen Sea are much smaller than observations, as the warm water intrusion onto Amundsen Sea continental shelf is too weakly simulated (Figs. 3.5 and 3.6). Stronger sea ice production (Timmermann and Hellmer 2013), insufficient horizontal resolution of the ocean model (Nakayama et al.

2014a) and atmospheric boundary conditions (Dinniman et al. 2015) has been proposed as possible causes. The total rate of basal melting in Antarctica (830 Gt/yr) is less than the glaciological estimates of 1325 ± 235 Gt/yr by Rignot et al. (2013) and 1454 ± 174 Gt/yr by Depoorter et al. (2013). The model exhibits a Southern Ocean temperature that is colder by about 0.5°C (Fig. 3.5) compared with observations in many but not all regions. Sea ice extent (Fig. 3.7) and the spatial distribution of sea ice production rate (Fig. 3.8) reproduces the observed characteristics of active sea ice production in the polynya areas along the Antarctic coast (Tamura et al. 2008).

Simulated basal melt rate, sea ice production, ocean temperature, and density structure from fourteen transects around Antarctica are displayed in Fig. 3.9. The first basal melting mode, characterized by cold and dense shelf water above the continental shelf (Jacobs et al. 1992), is reproduced in the Ross, Filchner-Ronne, and Amery ice shelves (Fig. 3.9a, g, k). The Ross Ice Shelf also has the characteristics of the third basal melting mode as well as those of the first mode (Fig. 3.9a), associated with a sea ice retreat during summer (Fig. 3.7). The second basal melting mode, characterized by the intrusion of warm CDW onto the continental shelves, is reproduced in the Bellingshausen Sea (Fig. 3.9e), whereas it is absent in the Amundsen Sea (Fig. 3.9c, d). The simulated water mass properties of the Amundsen Sea continental shelf resemble those of the first mode of basal melting. The features of a low basal melt rate and thermocline deepened toward the Antarctic coast are reproduced in the eastern Weddell Sea and in East Antarctica (Fig. 3.9h, i). The observed high melt rate in the Shackleton and Totten ice shelves (Rignot et al. 2013) suggests the intrusion of warm water, but the simulated intrusion of warm water is weak and the basal melt rate is small (Fig. 3.9l, m). Intrusion of warm subsurface water across the continental shelf break is simulated in the Totten Ice Shelf; however, a ridge in front of the ice appears to protect the ice shelf from warm water intrusion (Fig. 3.9m). Sea ice production near the Mertz glacier tongue is active but seasonal influences of warm subsurface water are simulated here (Fig. 3.9n). Cold ice shelf water originating from the Filchner-Ronne Ice Shelf flows near the

Larsen C Ice Shelf causing low basal melting (Fig. 3.9f). To summarize, the vertical oceanic structure and basal melt rate in the CTL experiment are reproduced well, although there are some discrepancies at specific locations. The comparison with observed climatology of World Ocean Atlas 13 (Locarnini e tal. 2013) aand AOGCM are presented in Fig. 3A.1 for five ice shelf transects.

3.3.2 Results of the LGM and 2xCO_2 experiments

Sea ice distribution shows a northward shift in the LGM experiment (Fig. 3.7), which is consistent with reconstructions (Gersonde et al. 2005; MARGO Project Members 2009). The circumpolar ocean model exhibits a complex pattern in summer sea ice extent, which is a side effect of the method of driving the model by AOGCM due to the bias of the present-day as discussed in Roche et al. (2012). However, it reproduces the expansion of sea ice extent better than the AOGCM. The large sea ice loss in the 2xCO_2 experiment is consistent with the results of the AOGCM (Fig. 3.4 and 3.7). The simulated total basal melt rates are 556 Gt/yr in the LGM and 2746 Gt/yr in the 2xCO_2 experiments. Hence, the total basal melt rate is reduced by 30% in the LGM experiment and increased by 230% in the 2xCO_2 experiment compared with the CTL. Spatial distributions of the basal melt rate (Fig. 3.6) indicate that its response depends on the region, but high rates of basal melting at the grounding lines and ice shelf fronts, and low rates of basal melting in the interior parts of the ice shelves are common features among all the experiments. In the LGM experiment, basal melting rates in the Bellingshausen seas decline in comparison with the CTL, as the intrusion of warm water onto the continental shelf reduced in the LGM (Fig. 3.9c). Basal melting rates in the Amundsen Sea also decline, as summertime warm water formation in the Antarctic coast is reduced in the LGM (Fig. 3.9c−d). On the other hand, strong basal melting at the grounding line of the Filchner-Ronne and Amery ice shelves remains, as ocean temperature near ice shelf is already close to freezing point in the CTL experiment. In the 2xCO_2 experiment, many ice shelves experience drastic increases in basal melt rate

in comparison with the CTL, but some ice shelves such as Ross Ice Shelves do not (Fig. 3.9a). Summertime basal melting (January–March) constitutes 29%, 35%, and 40% of the annual basal melting in the LGM, CTL, and 2xCO_2 experiments, respectively, which indicates that the seasonality in basal melting is intensified under a warmer climate (Fig. 3.10). As changes in the atmospheric fields influence heat loss at the sea surface, sea ice production increases in the LGM experiment and decreases in the 2xCO_2 compared to the CTL (Fig. 3.6). Ocean temperature in the Southern Ocean offshore of the continental shelf break is reduced at the LGM, but the reduction in ocean temperature along the continental shelf is small in most regions as it is already close to freezing point in the CTL (Fig. 3.6). This is a consistent feature that is found in the continental shelf seas of the AOGCM and the circumpolar ocean model (Fig. 3.11). In the 2xCO_2 experiment, ocean temperature above the continental shelves of the Amundsen and Bellingshausen seas increases in comparison with the CTL, where the basal melt rate increases drastically. In contrast, ocean temperature on the continental shelf does not increase in the Ross Sea for the circumpolar ocean model.

Figure 3.9 indicates that the vertical oceanic structures in the shelf seas depend on climatic conditions. In the LGM experiment, the basal melt rate decreases in comparison with the CTL in the Bellingshausen Sea continental shelf area where cold shelf water is formed (Fig. 3.9e). Due to the increase in sea ice cover during summer, the reduced s surface warm water by the summer insolation reduces the basal melt rate at the ice shelf front of the Ross Ice Shelf in the LGM experiment (Fig. 3.9a). In the 2xCO_2 experiment, the cold and dense shelf water on the continental shelf is replaced with warm water, and the basal melt rate is increased in comparison with the CTL (Fig. 3.9c–d, k). The increase in subsurface water temperature leads to an increase in the basal melt rate in the Bellingshausen Sea where warm water intrusion already occurs in the CTL (Fig. 3.9e). The disappearance of sea ice cover during summer also contributes to the higher sea surface temperature and higher basal melt rate (Fig. 3.9f and 3.9i). In contrast, active sea ice production limits the intrusion of warm subsurface water in the

Ross Ice Shelf and at the Mertz glacier tongue (Fig. 3.9a, n).

3.3.3 Results of the sensitivity experiments under individual climatic forcing

The simulated total basal melt rates of the sensitivity experiments are summarized in Fig. 3.12. It can be seen that nearly half of the change in basal melting can be attributed to the change in atmospheric boundary conditions (ATM) and one-third can be attributed to far-field oceanic boundary condition (OCN), that is mimicked by changes in the restoring at the northern boundary. The sum of the basal melt rate change in the "OCN" and "ATM" sensitivity experiments is displayed in Fig. 3.12 under the heading "SUM," indicating that the simulated basal melting change is explained by the combination of oceanic and atmospheric boundary conditions. With regard to the atmospheric boundary conditions, the majority of basal melt rate change can be attributed to heat flux change. The contributions from wind and net precipitation changes are minor, with the exception of the opposite sign of the LGM wind. The increased basal melting in the LGM_ATMWIND experiment occurs because of enhanced northward sea ice transport and sea ice decay during summer due to stronger offshore winds along the Antarctic coast, which increases sea surface temperature and thus, enhances basal melting. On the other hand, in the LGM_ATM case, extensive sea ice remains along the Antarctic coast during summer due to colder air temperature (Fig. 3.7). This means the effect of stronger wind on basal melt rate depends on the thermal condition, and it is why the sum of LGM_ATMWIND and LGM_ATMHEAT is different from LGM_ATM. The impact of the $2xCO_2$ wind change is relatively minor ($2xCO_2$_ATMWIND), but it does increase area-mean basal melting of the ice shelves of Dronning Maud Land where the easterly wind along the coast is weakened. The simulated changes in basal melt rate, subsurface ocean temperature, and sea ice production rate for the $2xCO_2$ sensitivity experiments, due to the modification of the atmospheric heat flux ($2xCO_2$_ATMHEAT) and oceanic boundary conditions ($2xCO_2$_OCN), are displayed in Fig. 3.13. The contribution from net precipitation

change is small. For sea ice production rate in the Antarctic shelf seas, sea surface thermal forcing (91%, Table 3.1 and Fig. 3.13) is the most important factor and the contribution from ocean forcing is minor (23%). The stronger offshore winds along the Antarctic Coast in the LGM experiment contribute to increased sea ice production via enhanced sea ice transport and the maintenance of coastal polynyas.

The ocean transects from the sensitivity experiments are displayed in Fig. 3.14. While the change in atmospheric heat flux has small impact on the subsurface ocean temperature directly, it reduces sea ice production and promotes warm water intrusion onto the continental shelves in the Amundsen Sea (Fig. 3.14b–d). Warming in the far-field ocean temperature is insufficient to change the water mass properties in this region. The change in atmospheric heat flux reduces the sea ice extent and increases the sea surface temperature along the Antarctic coast during summer, and increases the area-mean basal melt rate in Dronning Maud Land and East Antarctica. This result indicates that changes in sea ice production and shelf water formation can affect the intrusion of warm water across the continental shelf break without any change in the ocean temperature offshore of the continental shelf break.

3.4 Discussion

I investigated the response of the basal melt rate of the Antarctic ice shelves to LGM and CO_2 doubling to understand the long-term climatic changes, using a circumpolar ocean model forced by the output of a coupled climate model. In the CTL experiment, the temperature of the Antarctic shelf seas is close to the freezing point of seawater; nevertheless, warm water exists off the continental shelf break. This characteristic of ocean temperature difference across the continental shelf break is widely observed, and is shown to be generated by active sea ice production and the formation of cold and dense shelf water (Petty et al. 2013). The basal melting mode changes drastically in the $2xCO_2$, where warm water intrusion onto continental shelves occurs in many places. This result is consistent with future projections (Hellmer et al.

2012; Timmermann and Hellmer 2013) that find warm water more able to intrude onto the continental shelves in a warmer climate. Hence, it is important for the response of basal melting, that the responses of seawater temperature between the shelf sea and outside the continental shelf break are different. In addition, the basal melting mode characterized by the presence of thermocline deepening toward the continental shelf break disappears in the $2xCO_2$ climate, as summer sea ice almost disappears. The stronger seasonality in basal melt rate (Fig. 3.10) reflects the higher summer sea surface temperature in the $2xCO_2$ experiment, where summer sea ice cover vanishes along almost all the Antarctic coast (Fig. 3.7), while most of the Antarctic coast remains covered with sea ice in summer in the CTL experiment.

The subsurface ocean temperature is often used to parameterize basal mass balance beneath ice shelves for ice sheet models (de Boer et al. 2015; Golledge et al. 2015; Sutter et al. 2016; Deconto and Pollard 2016). In the present study, the circumpolar ocean model is forced by an output of AOGCM output, that subsurface ocean temperature (1.7°C for the CTL) decreases by –2.8 °C for the LGM and increases by 0.9 °C for the $2xCO_2$. Nevertheless, the change in basal melting due to climate warming is much greater (by an order of magnitude) than due to cooling. The results suggest that a change in basal melt rate is highly nonlinear in relation to the extent of changes in ocean temperature, and the water mass formation in the Antarctic shelf seas, associated with sea ice production and cold and dense shelf water formation, can be critical to the responses of basal melt rate to climate changes.

One remark is that warm water intrusion onto the Amundsen Sea continental shelf is simulated weakly in the CTL experiment. Although this is a common problem for ocean models (Timmermann and Hellmer 2013), too weak intrusion of warm water onto the Amundsen Sea continental shelf and too strong sea ice production of ~20 m/yr in the Amundsen Sea do not match with observations. These have to be improved in our model in future by using higher horizontal resolution of the ocean model (Nakayama et al. 2014a) and atmospheric boundary conditions (Dinniman et al. 2015). In the

Appendix C1, I conducted additional experiments to modify the bedrock topography of the Antarctic continental shelves. The results suggest that the representation in the Amundsen Sea continental shelf bathymetry (due to a less fine horizontal resolution) might have contributed to the model bias of weaker warm water intrusion onto the continental shelves and smaller basal melt rate of ice shelves.

The sensitivity experiments that changed individual boundary conditions of the LGM or $2xCO_2$ experiments were performed to investigate the mechanism of the response of basal melt rate to climate change. The results show that the majority of basal melt rate change can be explained by the thermal conditions of the atmosphere and the ocean, and that the impact of atmospheric heat flux is larger than that of subsurface ocean temperature change. The change in atmospheric heat flux plays a primary role in the intrusion of warm water onto the continental shelves by changing the sea ice production. The changes in ocean structure, therefore, imply that climate influences the mode of basal melting proposed by Jacobs et al. (1992) and others. Although the far-field oceanic boundary condition changes the subsurface ocean temperature near the continental shelf break, it alone is insufficient to change sea ice production or the basal melting mode.

As a long-term perspective, one essential difference between the transient future projection for the next few centuries (Hellmer et al. 2012; Timmermann and Hellmer 2013) and the quasi-equilibrium $2xCO_2$ comes from the fact that the response of subsurface and deep ocean temperature in the Southern Ocean is very slow. The response of the deep Southern Ocean is delayed due to thermal inertia and deep convection, while the responses of the sea surface and sea ice are relatively fast (Yamamoto et al. 2015). Around years 700–800 in the $2xCO_2$ AOGCM experiment (Fig. 3.2), the recovery of deep convection transports additional heat to the surface, increasing the temperatures of the sea surface and air, while cooling the subsurface ocean. As subsurface ocean temperature and sea surface atmospheric conditions affect the basal melt rate, the temporal evolutions of the atmosphere and ocean could produce

a complicated temporal evolution of the basal melt rate under future climate change.

The results of the sensitivity experiments indicate that wind affects the basal melt rate via the several processes of sea ice and ocean currents, whose relative effectiveness depends on the thermal climatic conditions. In the LGM experiment, a stronger offshore katabatic winds enhances sea ice production and reduces the basal melt rate. On the other hand, the winds of the LGM under the present-day warm climate increases the basal melt rate. This increase in basal melting occurs because of enhanced northward winds along the Antarctic coast that transport sea ice, which in turn increases the sea surface temperature during summer. Under a warmer climate as in the $2xCO_2$ experiment, the wind has little impact on basal melt. However, it does affect the basal melt rate along Dronning Maud Land, where the thermocline shoals toward the continental shelf, which is consistent with previous studies (Smedsruds et al. 2006; Hattermann et al. 2014; Spence et al. 2014).

My study does not consider the effect of glacial meltwater and iceberg discharge into the Southern Ocean, which could warm subsurface ocean by inducing stronger stratification and reducing vertical convection in the Southern Ocean (Stouffer et al. 2007). An additional ice shelf and ice sheet meltwater input can lead to increased basal melting because the Antarctic ice shelf is exposed to the warm ocean at such subsurface depths (Menviel et al. 2011; Nakayama et al. 2014b; Fogwill et al. 2015) while an increased sea ice extent is also expected (Bintanja et al. 2013, 2015; Pauling et al. 2016). Studies modeling ice sheets have shown that this subsurface warming could lead to a rapid retreat of the Antarctic ice sheet (Golledge et al. 2014). Thus, the interactions between the Antarctic ice sheet and the Southern Ocean could amplify the response of ice shelf melting to warmer climates.

We assumed a fixed configuration of the ice shelves in all of the experiments in order to focus our scope to understand the role of climatic forcing determining the basal melt of ice shelves. In reality, however, the changing basal mass balance modifies ice shelf thickness and the positions of grounding lines, that will further impact the sea ice

and the ocean around ice shelves, which in turn impact the basal melting. With regard to the LGM experiments, reconstructions indicate that the grounding lines of the Antarctic ice sheet advanced to near the continental shelf break during the LGM (Bentley et al. 2014, Abe-Ouchi et al, 2015). Kusahara et al. (2015) used an enlarged LGM ice sheet extent and showed that basal melting during the LGM was greater than the present-day climate. It is because of the greater exposure of the ice shelves to the warmer subsurface water of the Southern Ocean, as the grounding lines advanced toward the continental shelf breaks. The result is consistent with that of Abe-Ouchi et al. (2013) in the point that the advance of Laurentide ice sheet to lower latitudes leads to negative mass balance for ice sheet and was essential to explain the ice age cycles. While the present study demonstrates the response of ice shelf melting to long-term climate changes, the development of ice sheet-ocean coupling will be required to understand the Antarctic ice sheet change (Kusahara 2016). Whether the topographical change of Antarctic ice shelf has a greater impact on the rate of ice sheet melting than the climate change could depend on the background climate, colder or warmer than present-day. Coupling studies of ice sheet, and climate are therefore needed in future for investigating both glacial climate and future climate change.

In summary, our results derived from the LGM and CO_2 doubling experiments show the importance of atmosphere-driven water mass formation on the basal melt rate, which generates a nonlinear response of the basal melt rate to subsurface ocean temperature in the Antarctic region. The cold and dense water mass formation in the Antarctic shelf seas due to sea ice production influences the intrusion of warm water onto the continental shelves, and reduced summer sea ice extent contributes to higher sea surface temperature during summer. Our results demonstrate the importance of combining AOGCMs and ocean models that can resolve ice shelf cavity circulations to enhance our understanding of the response of the Antarctic ice sheet to climate change.

Name	Atmospheric Heat flux	Wind stress	Net precipitation	Ocean Restoring	Total Basal melt rate [Gt/yr]	Sea ice production rate [1000 Gt/yr]
CTL	CTL	CTL	CTL	CTL	830	6.77
LGM	LGM	LGM	LGM	LGM	556	10.97
$2xCO_2$	$2xCO_2$	$2xCO_2$	$2xCO_2$	$2xCO_2$	2746	3.96
LGM_ATM	LGM	LGM	LGM	CTL	662 (61%)	10.27 (83%)
LGM_OCN	CTL	CTL	CTL	LGM	724 (39%)	7.03 (6%)
LGM_ATMHEAT	LGM	CTL	CTL	CTL	700 (47%)	8.54 (12%)
LGM_ATMWIND	CTL	LGM	CTL	CTL	1028 (-72%)	7.54 (18%)
LGM_ATMPRCP	CTL	CTL	LGM	CTL	850 (-7%)	6.81 (1%)
$2xCO_2$_ATM	$2xCO_2$	$2xCO_2$	$2xCO_2$	CTL	1864 (54%)	4.25 (90%)
$2xCO_2$_OCN	CTL	CTL	CTL	$2xCO_2$	1449 (32%)	6.13 (23%)
$2xCO_2$_ATMHEAT	$2xCO_2$	CTL	CTL	CTL	1819 (52%)	4.20 (91%)
$2xCO_2$_ATMWIND	CTL	$2xCO_2$	CTL	CTL	962 (7%)	6.64 (5%)
$2xCO_2$_ATMPRCP	CTL	CTL	$2xCO_2$	CTL	816 (-1%)	6.64 (5%)

Table 3.1 List of the circumpolar ocean model experiments. The names of the experiments are listed in the first column. The second to fifth columns denote the combinations of atmosphere and ocean boundary conditions used in each of the experiments. The simulated basal melting amount of all Antarctic ice shelves and sea ice production amount within the Antarctic shelf seas (defined by the 1000-m isobath) are displayed in the last two columns. The parenthetical values in the sensitivity experiments indicate the contributions of each forcing, calculated from the ratio of the anomaly from the CTL (e.g. ($2xCO_2$ATM - CTL) / ($2xCO_2$ - CTL)).

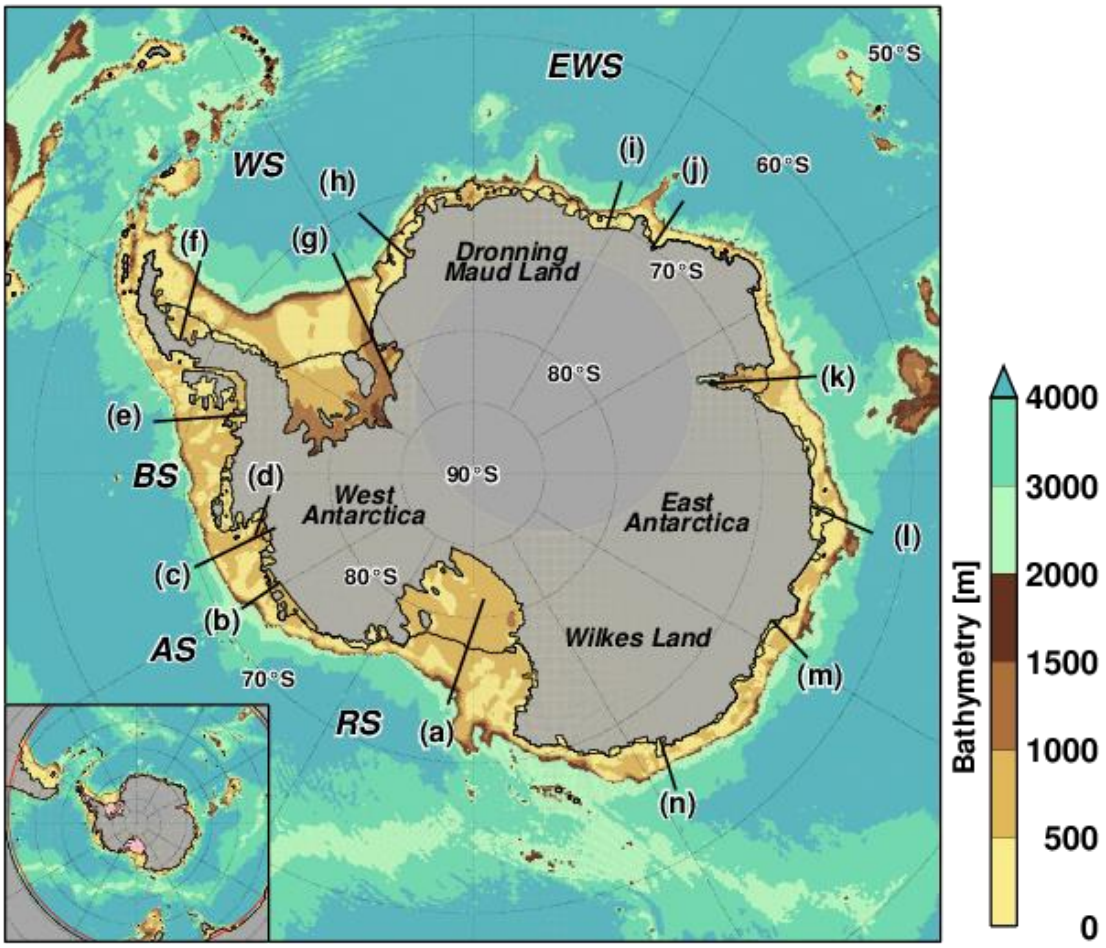

Fig. 3.1 Bottom topography used in the circumpolar ocean model. The model domain is indicated by the red line in the lower-left inset. Ocean temperature and salinity are restored to monthly climatology in the area north of the red line. Solid black lines show the locations along which the cross sections of the ocean profiles displayed in Figs. 3.9 and 3.14. WS indicates the Weddell Sea, EWS the Eastern Weddell Sea, RS the Ross Sea, AS the Amundsen Sea, and BS the Bellingshausen Sea. ©American Meteorological Society. Used with permission.

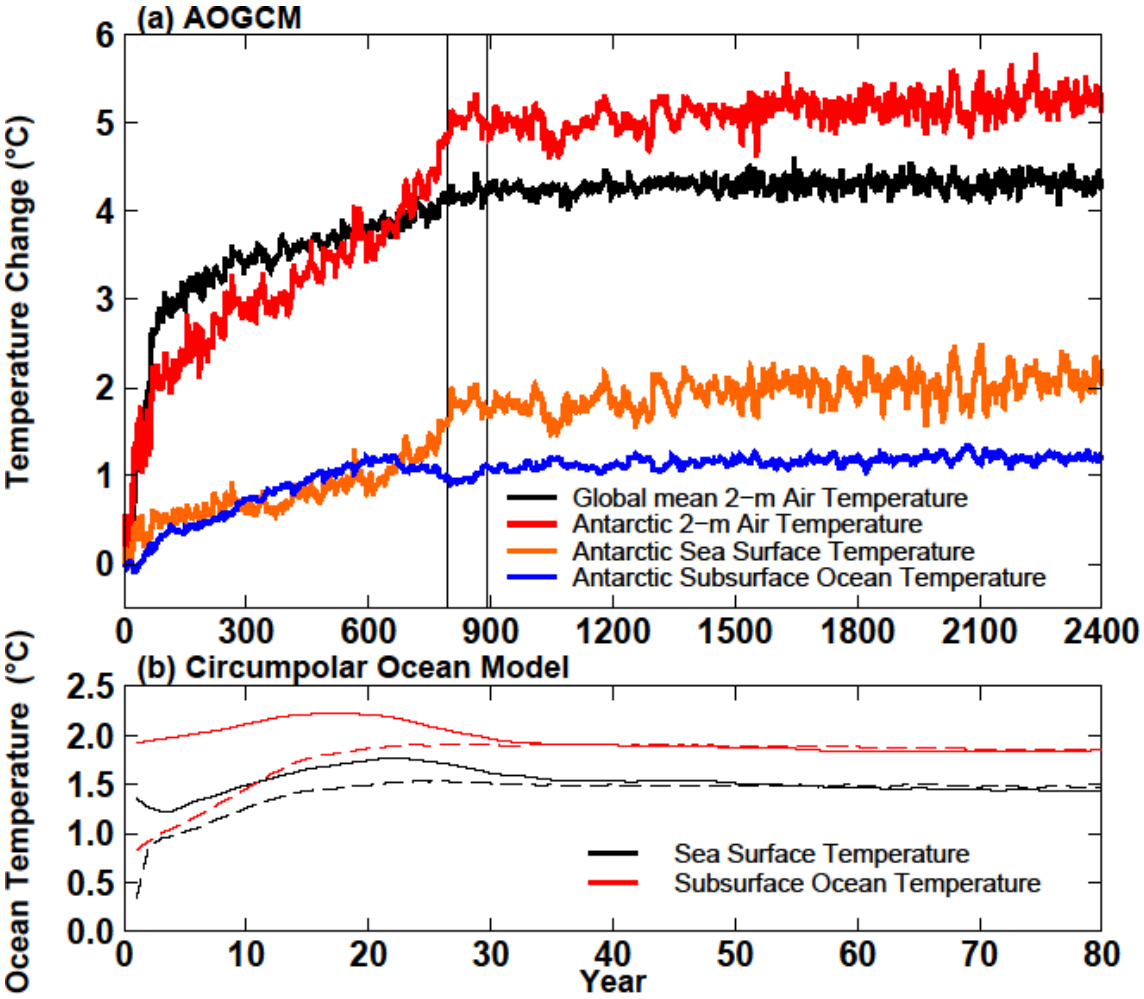

Fig. 3.2 Time series of the $2xCO_2$ AOGCM (top panel) and circumpolar ocean model (bottom panel) experiments. (Top panel) The anomalies (from CTL) global mean 2-m air temperature, Antarctic 2-m air temperature (50°S to 65°S), Antarctic sea surface and subsurface ocean temperature (south of 65°S, averaged for 200-1000 m depth) are displayed. The climatology of years 791–890 (indicated by two thin vertical black lines) is analyzed and used. (Bottom panel) Annual mean sea surface and subsurface (averaged for south of 60°S, 200-1000 m depth) temperature for the circumpolar ocean model. The dashed line is initialized with present-day ocean temperature and salinity fields, and the solid lines are initialized with $2xCO_2$ ocean temperature and salinity fields derived from the AOGCM experiments.

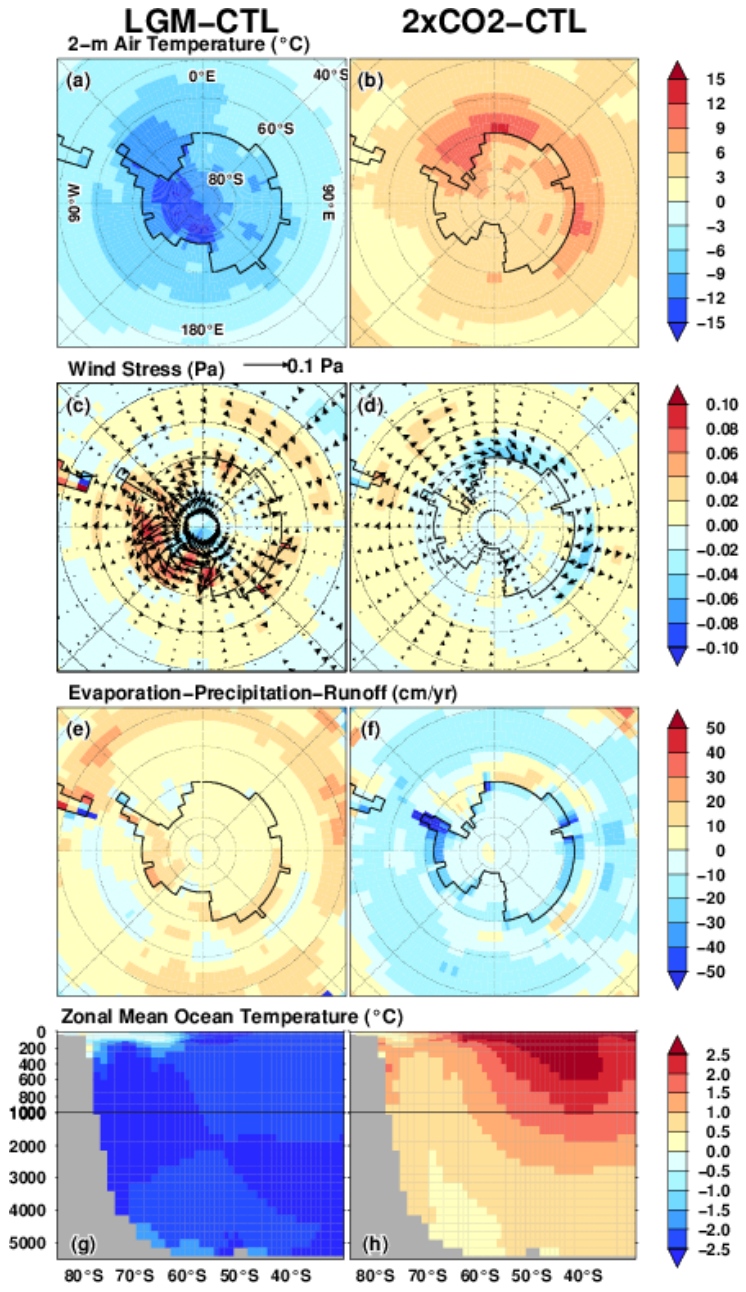

Fig. 3.3 Simulated climatic fields for (left) LGM and (right) 2xCO_2 in the AOGCM experiments (anomaly from the CTL experiment). (a, b) 2-m air temperature, (c, d) surface wind stress (positive value indicates stronger wind stress), (e, f) sea surface freshwater flux due to evaporation, precipitation and river runoff (positive value indicates net precipitation increase), and (g, h) zonal mean ocean temperature in the Southern Hemisphere. Note that 2xCO_2 experiments are taken from the climatology years 791-890 in Fig. 3.2. ©American Meteorological Society. Used with permission.

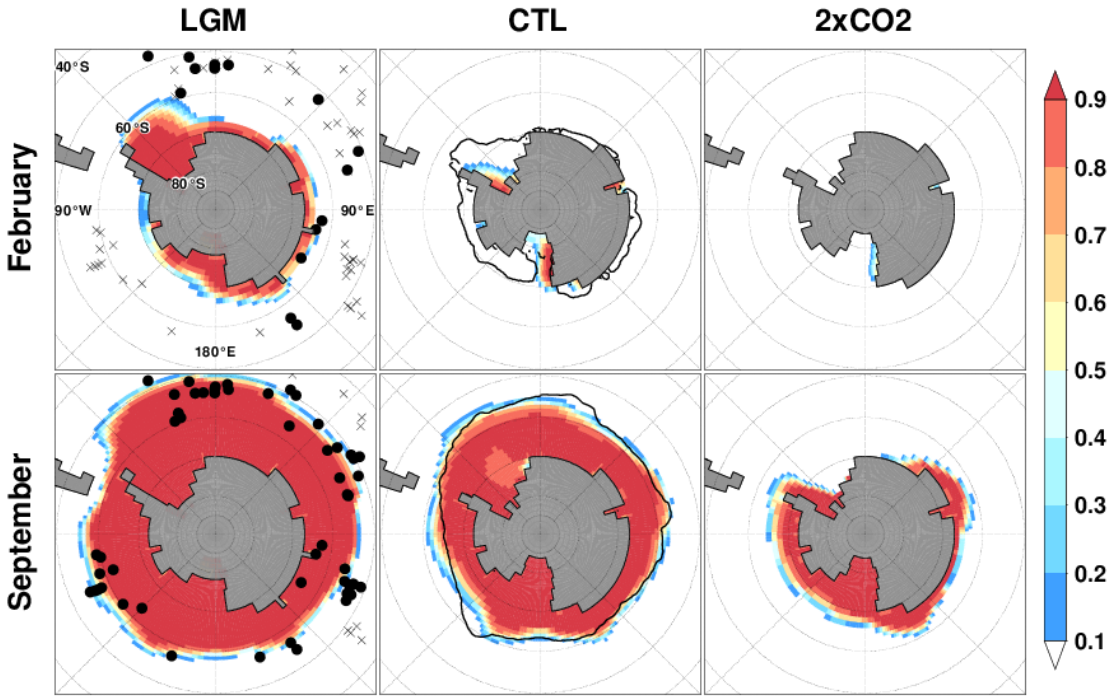

Fig. 3.4 Simulated sea ice concentration from the AOGCM experiments for LGM, CTL, and 2xCO_2 (left to right). Black dots (presence of sea ice) and crosses (sea ice-free areas) on the panels of LGM experiments denote the reconstructions (Gersonde et al. 2005; MARGO Project Members 2009). Black lines in the CTL experiments indicate the observed present-day sea ice edge, which is defined by a sea ice concentration of 15%, averaged for the period 1982-2011 (Reynolds et al. 2002). ©American Meteorological Society. Used with permission.

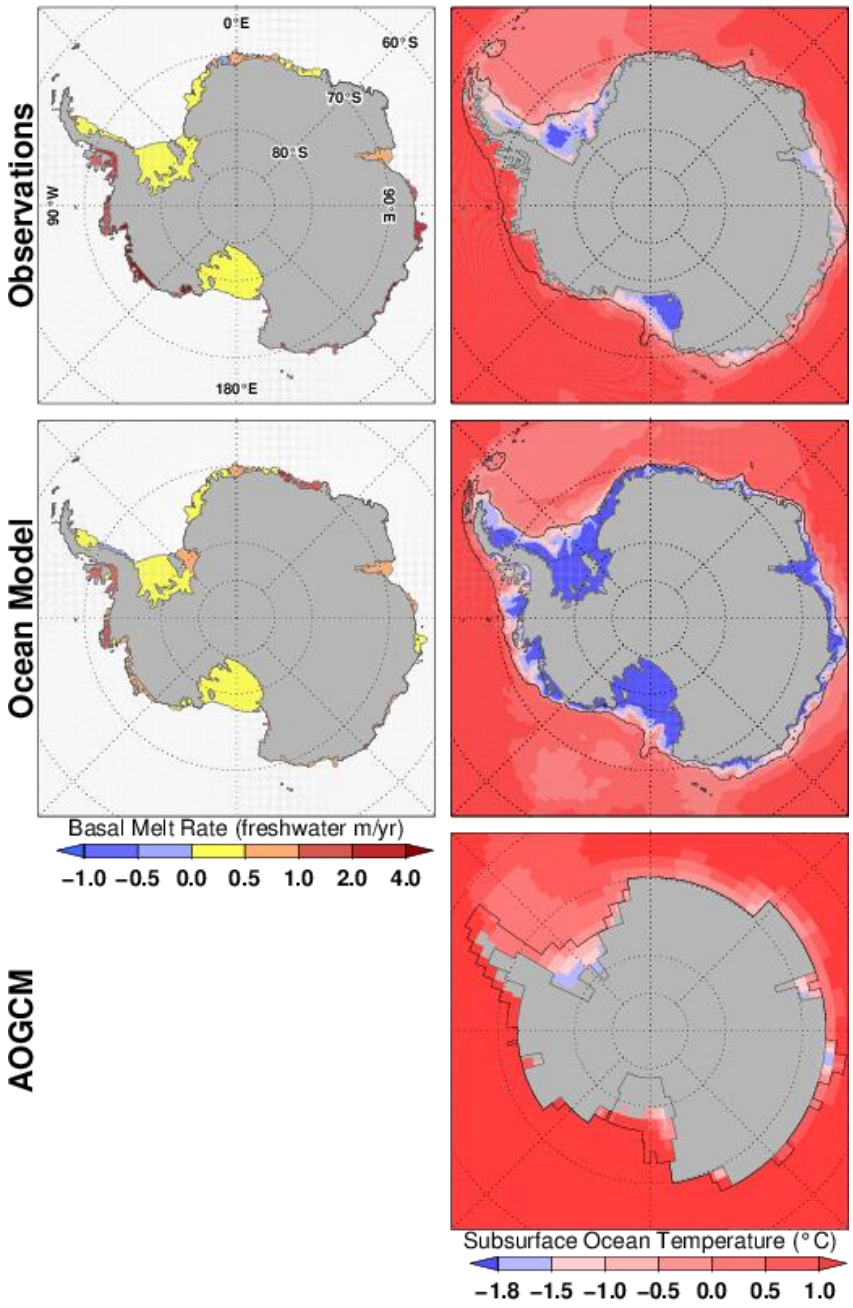

Fig. 3.5 (Left panel) Comparison of observed and simulated basal melt rate of ice shelves in the circumpolar ocean model for the CTL experiment. Observed basal melting rate is derived from Rignot et al. (2013). Basal melt rate is averaged within each ice shelves. (Right panel) Observed and simulated annual mean subsurface ocean temperature (averaged for 200-1000 m depth) in the circumpolar ocean model (middle) and AOGCM (bottom). Black lines indicate the 1000-m isobath. ©American Meteorological Society. Used with permission.

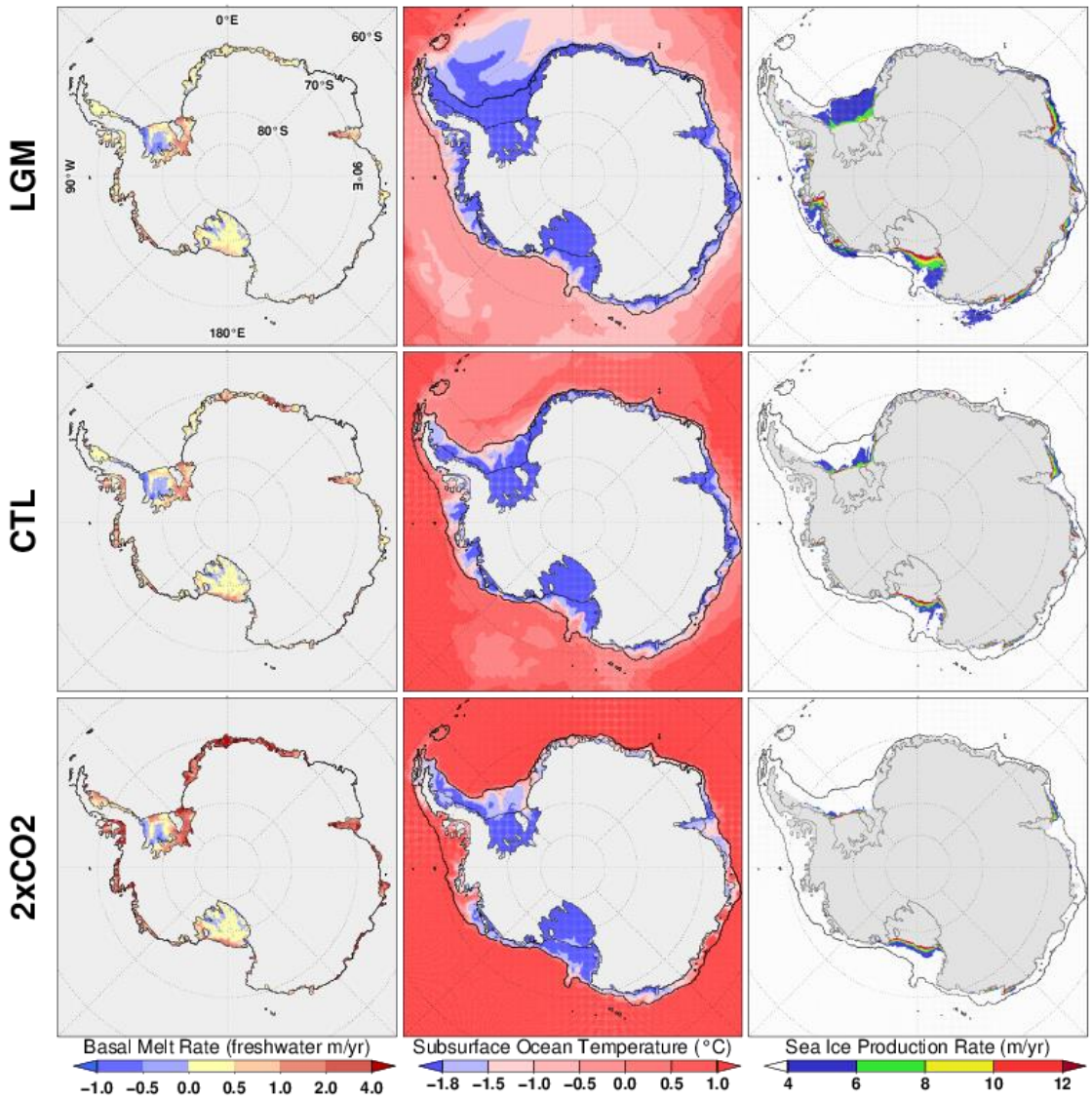

Fig. 3.6 (Left panel) Simulated annual mean basal melt rate distribution (freshwater m/yr), subsurface (averaged for 200-1000 m depth) ocean temperature for the LGM, CTL and 2xCO_2 experiments. (Right panel) Simulated sea ice production rate, whose color bar follows Tamura et al. (2008), displaying the values above 4 m/yr. Black lines indicate the 1000-m isobath. ©American Meteorological Society. Used with permission.

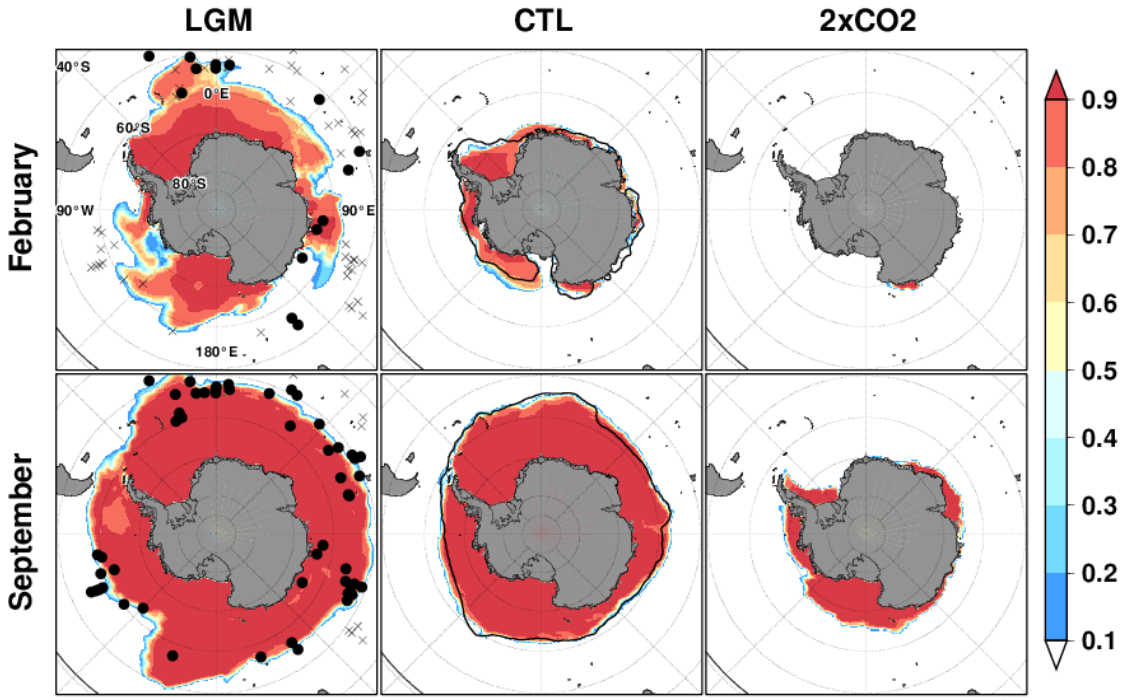

Fig. 3.7 Same as Fig. 3.4, but the circumpolar ocean model experiments. ©American Meteorological Society. Used with permission.

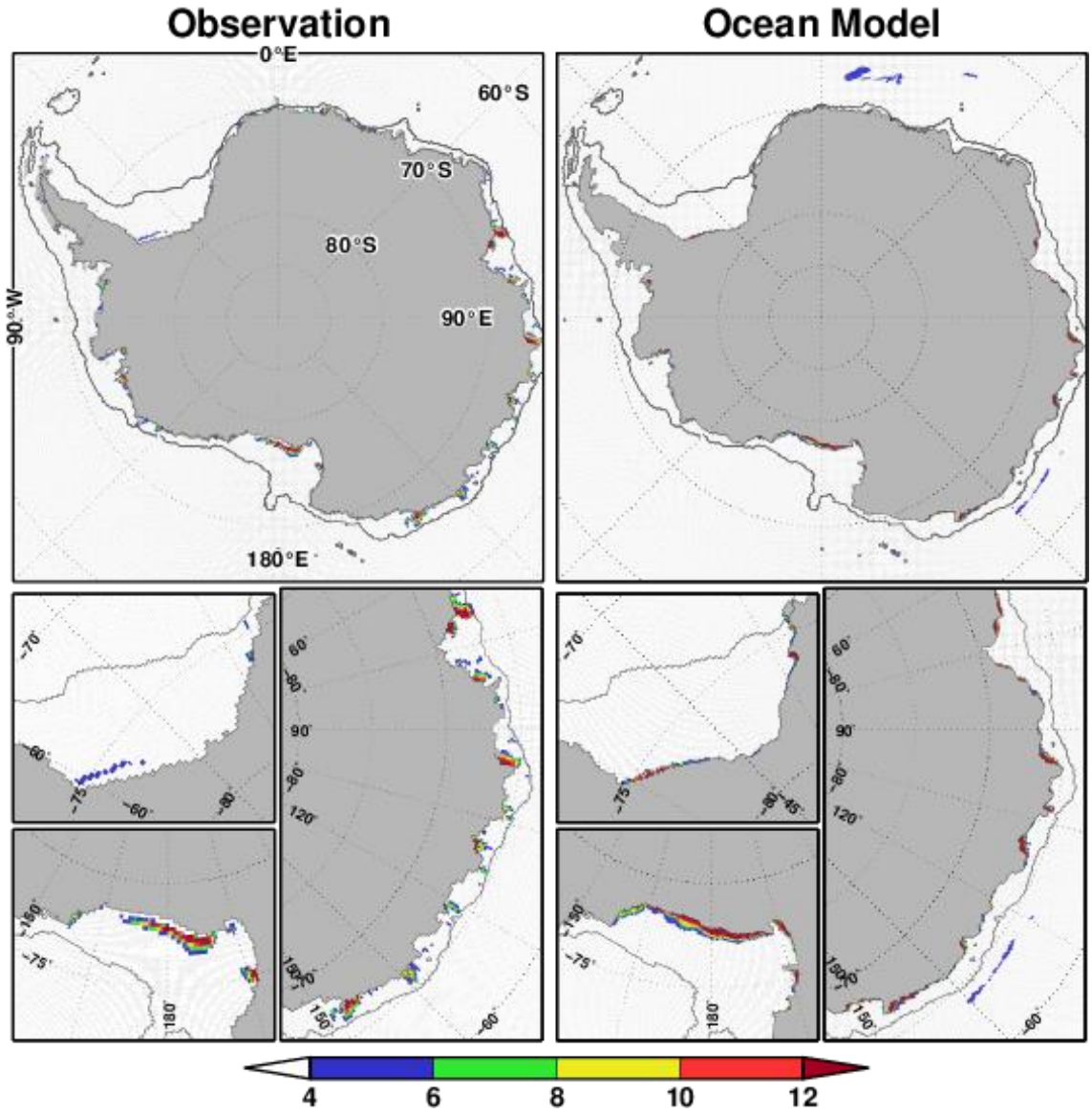

Fig. 3.8 (Left panels) Observed sea ice production rate [sea ice m/yr] derived from Tamura et al. (2008). (Right Panels) Simulated sea ice production rate in the CTL experiment as in Fig. 3.6 using the same color bar. Black contours indicate the 1000-m isobath. Bottom panels focus on sea ice production in three major polynya regions of the Weddell Sea, Ross Sea and in East Antarctica. ©American Meteorological Society. Used with permission.

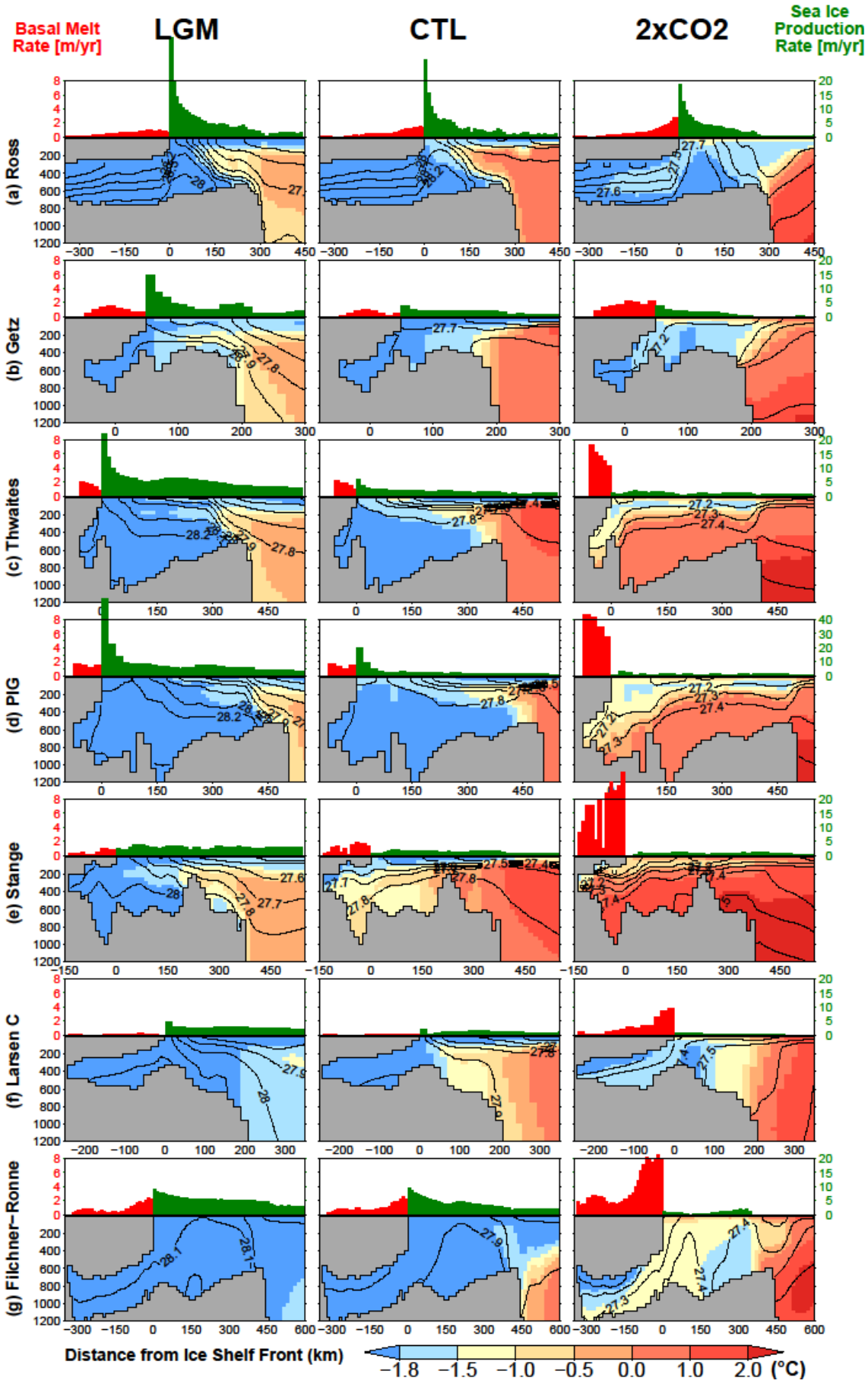
Basal Melt Rate [m/yr]
LGM
CTL
2xCO2
Sea Ice Production Rate [m/yr]
(a) Ross
(b) Getz
(c) Thwaites
(d) PIG
(e) Stange
(f) Larsen C
(g) Filchner–Ronne
Distance from Ice Shelf Front (km)
−1.8 −1.5 −1.0 −0.5 0.0 1.0 2.0 (°C)

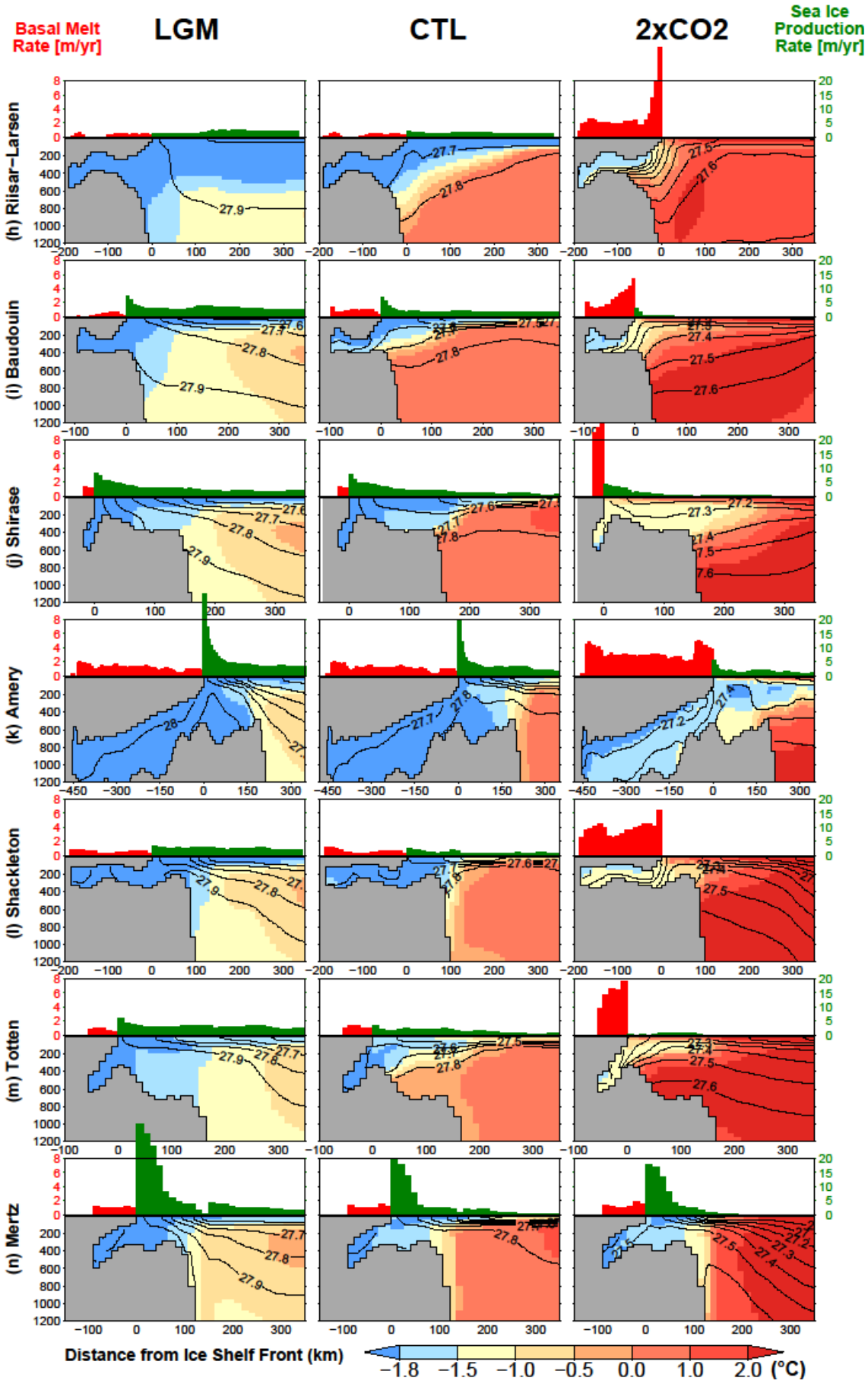
Basal Melt Rate [m/yr]
LGM
CTL
2xCO2
Sea Ice Production Rate [m/yr]
(h) Riiser–Larsen
(i) Baudouin
(j) Shirase
(k) Amery
(l) Shackleton
(m) Totten
(n) Mertz
Distance from Ice Shelf Front (km)
−1.8 −1.5 −1.0 −0.5 0.0 1.0 2.0 (°C)

Fig. 3.9 Ocean transects from fourteen ice shelves around Antarctica in the LGM, CTL and $2xCO_2$ experiments are displayed. The lines denote the neutral density of seawater, and the colors denote the ocean temperature. Basal melt rate (red bars above ice shelves) and sea ice production rate (green bars above open ocean) are displayed in the upper panels. The vertical axis denotes ocean depth and the horizontal axis denotes the distance from the ice shelf front. The locations of the transects are given in Fig. 3.1.

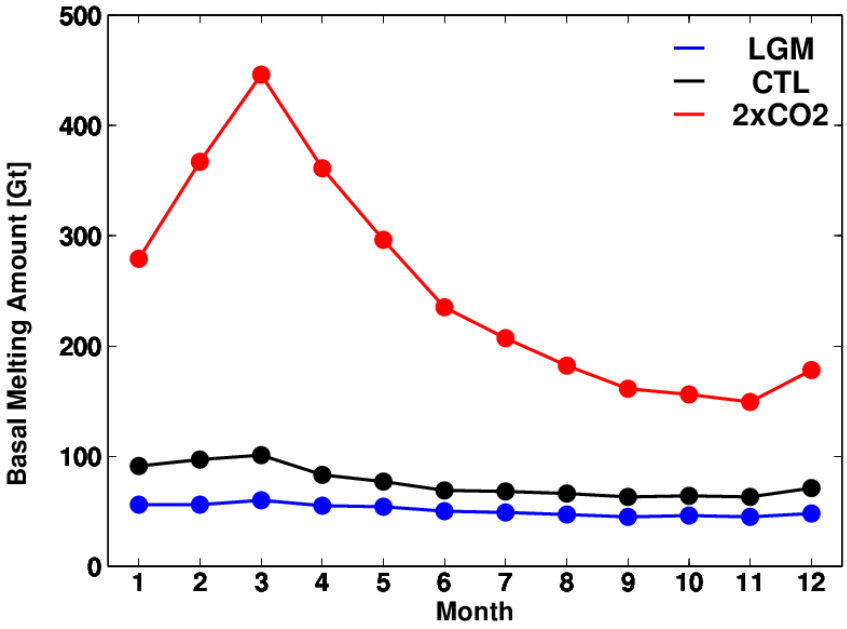

Fig. 3.10 Simulated basal mass loss of all Antarctic ice shelves for each month of the year. ©American Meteorological Society. Used with permission.

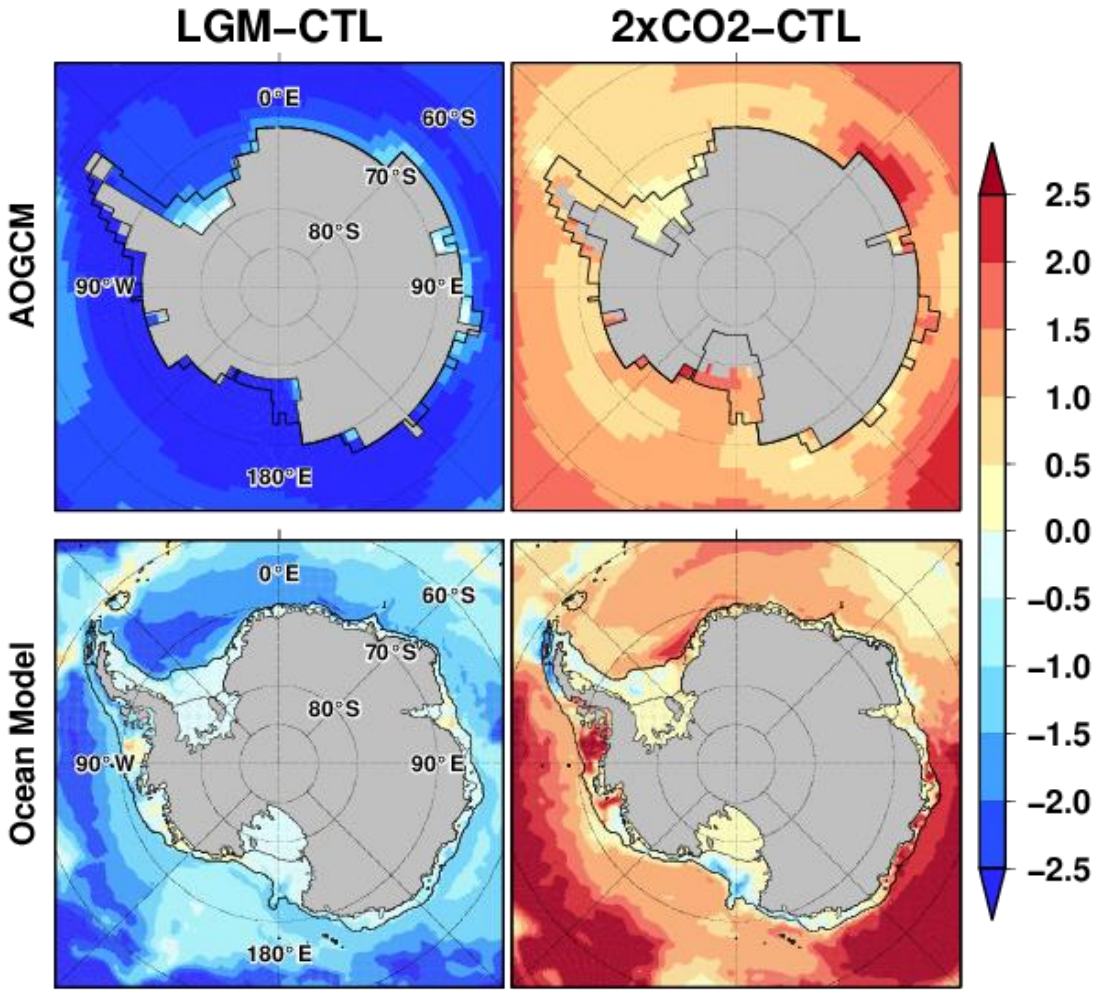

Fig. 3.11 Spatial distribution of annual mean subsurface ocean temperature (averaged for 200-1000 m) anomaly (from the CTL) for the AOGCM and circumpolar ocean model experiments for LGM and 2xCO_2. Black lines indicate the 1000-m isobath of the AOGCM and the ocean model. ©American Meteorological Society. Used with permission.

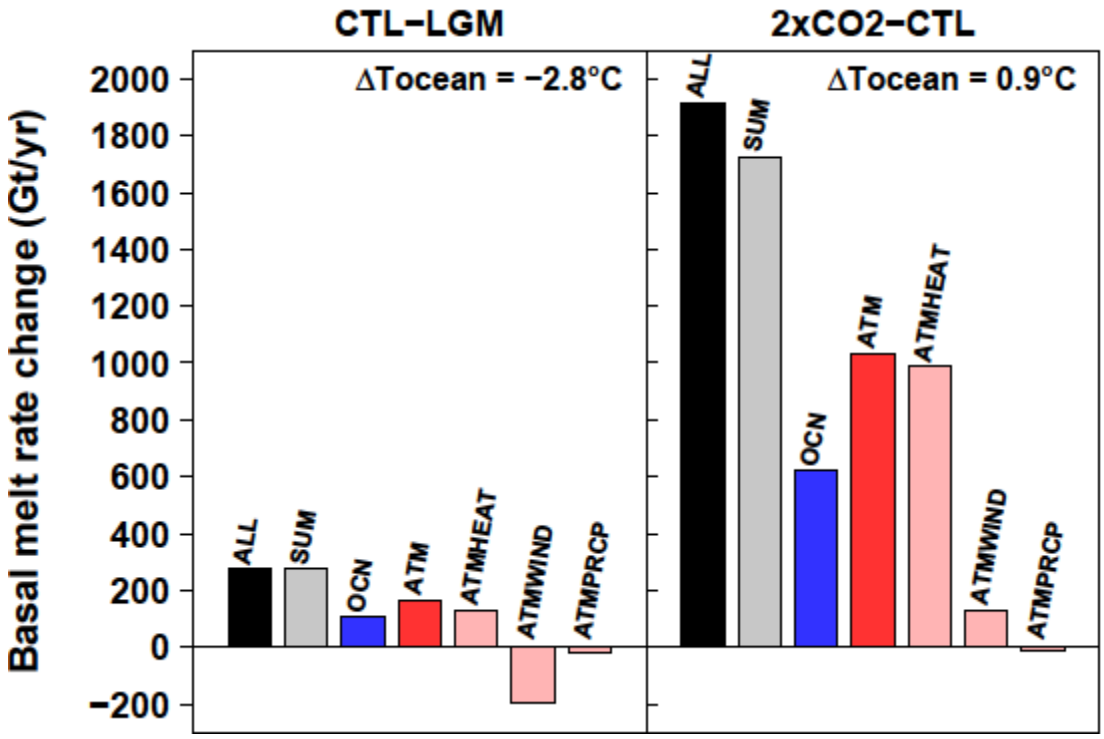

Fig. 3.12 The results of sensitivity experiments in Table 3.1 showing the response of total basal melt rate to the individual boundary conditions, CTL-LGM in the left hand side and $2xCO_2$ - CTL in the righ hand side. "ALL" denotes the LGM and $2xCO_2$ experiments. "SUM" denotes the sum of two sensitivity experiments of "OCN" and "ATM". "OCN" denotes the contributions from far-field ocean boundary conditions, and "ATM" denotes the contributions from atmospheric boundary conditions. The right three columns are three components of atmospheric boundary conditions, that denotes the contributions from atmospheric heat flux (ATMHEAT), sea surface momentum flux (ATMWIND), and net precipitation (ATMPRCP). ΔTocean denotes the subsurface ocean temperature anomaly in the Antarctic region simulated by the AOGCM experiments.

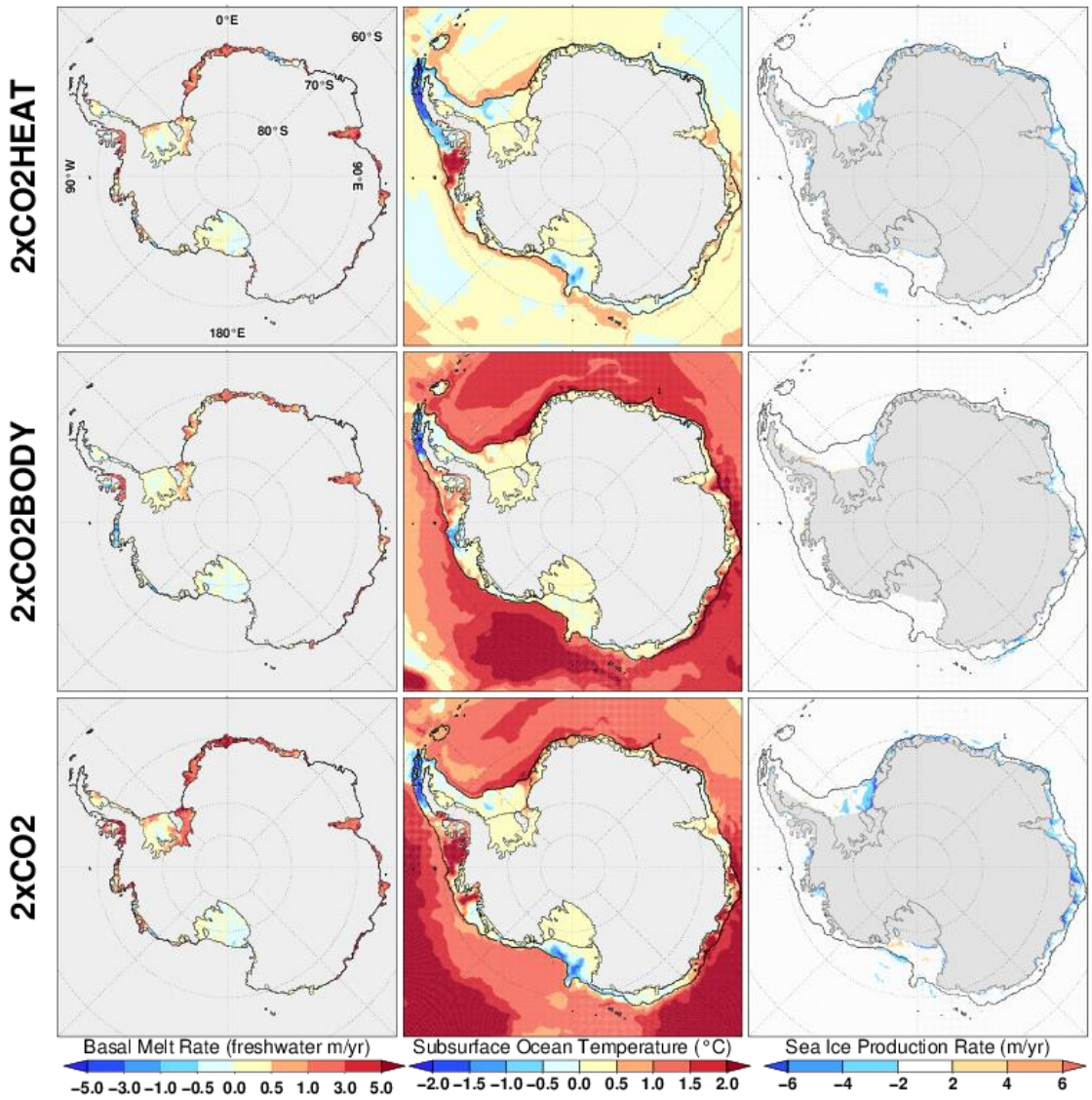

Fig. 3.13 Results of the 2xCO_2_ATMHEAT, 2xCO_2_OCN together with 2xCO_2 experiments. (Left panel) Simulated annual mean basal melt rate anomaly (freshwater m/yr, difference from CTL), (middle column) subsurface (averaged for 200-1000 m depth) ocean temperature anomaly, (Right panel) Simulated sea ice production rate anomaly. Black lines indicate the 1000-m isobath. ©American Meteorological Society. Used with permission.

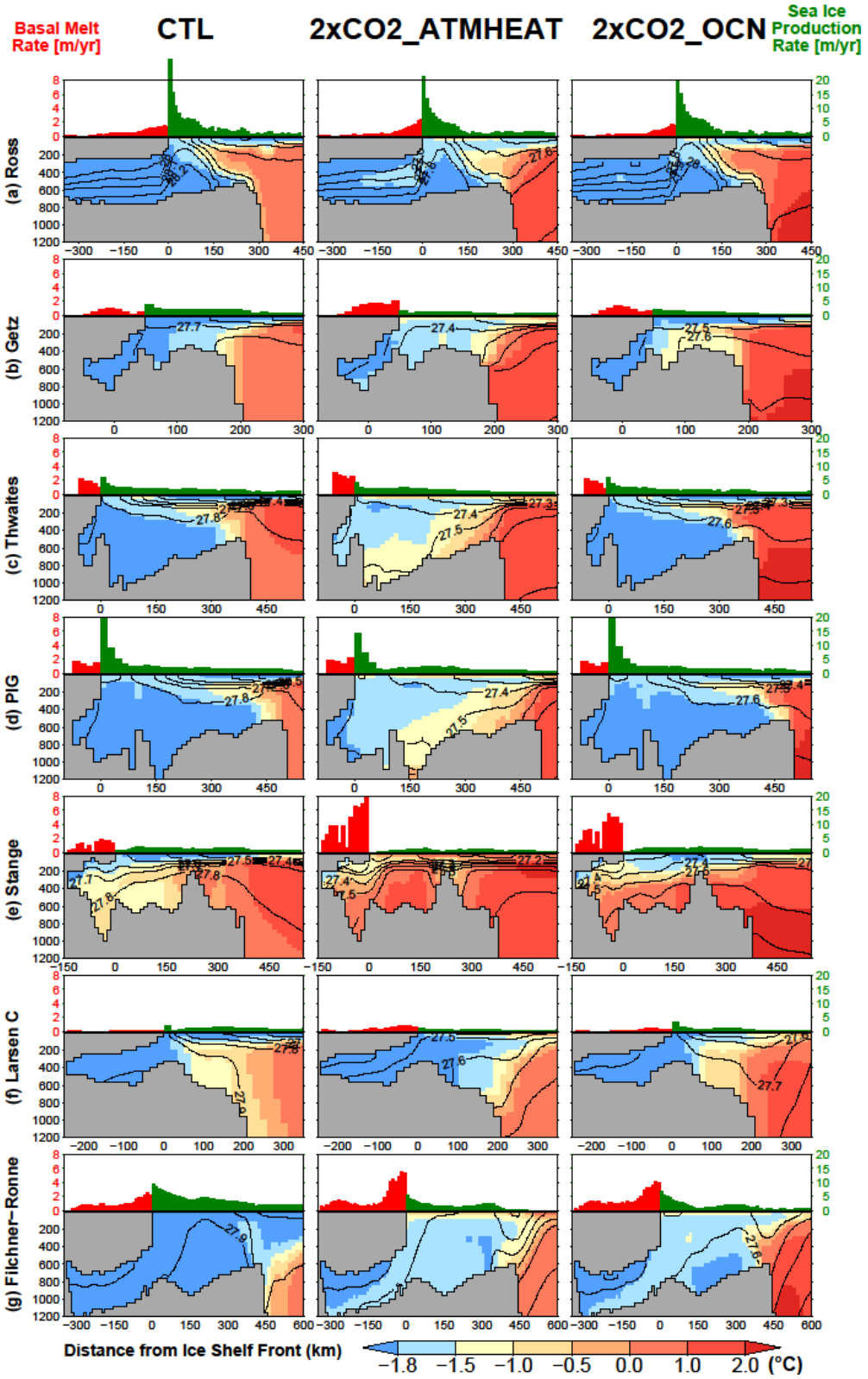
Basal Melt Rate [m/yr]
CTL
2xCO2_ATMHEAT
2xCO2_OCN
Sea Ice Production Rate [m/yr]
(a) Ross
(b) Getz
(c) Thwaites
(d) PIG
(e) Stange
(f) Larsen C
(g) Filchner−Ronne
Distance from Ice Shelf Front (km)
−1.8 −1.5 −1.0 −0.5 0.0 1.0 2.0 (°C)

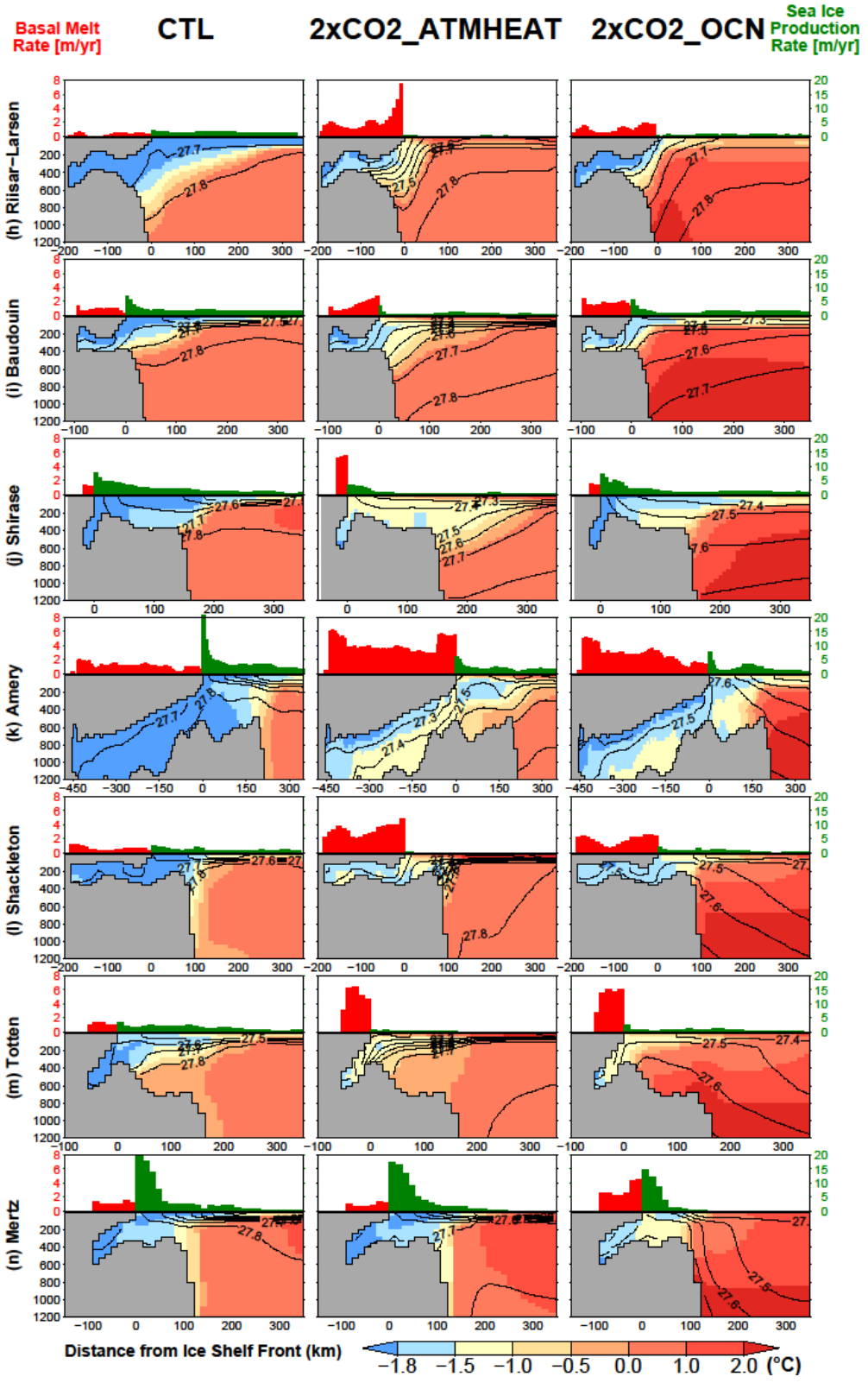

Fig. 3.14 Same as Fig. 3.9 but for CTL, 2xCO_2_ATMHEAT and 2xCO_2_OCN experiments. ©American Meteorological Society. Used with permission.

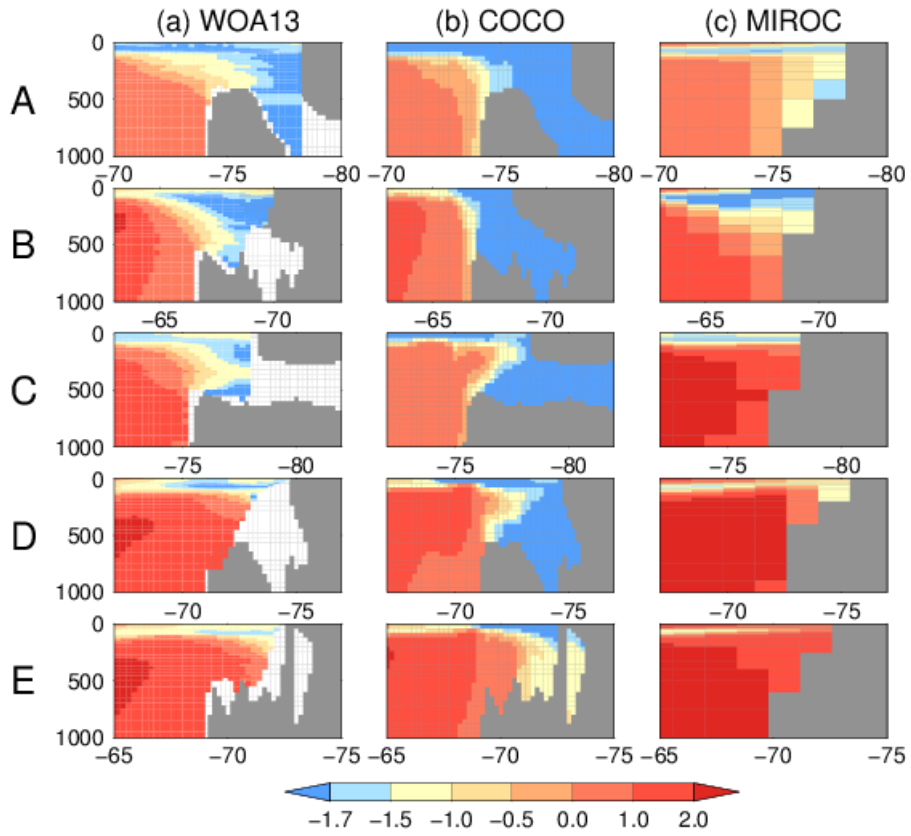

Fig. 3.A1 North-South transects of ocean temperature at five ice shelves, for (a) climatology based on observations (World Ocean Atlas 2013, (Locarnini et al. 2013)), (b) COCO for CTL experiment (This study), (c) MIROC 4m for preindustrial experiment (This study). The transects are from (A) 282°E, (B) 254°E, (C) 185°E, (D) 72°E, (E) 320°E.

Chapter 4

Discussion on Antarctic ice sheet in the past, present, and the future

4.1 Backgrounds

The relationship between the climate change and the response of Antarctic ice sheet has been discussed using present-day observations, numerical models and paleoclimate reconstructions. Levermann et al. (2013) acquired a sea level change of 1.2 meters per degree of global mean temperature change based on a model simulation of the past five million years (Pollard and Deconto 2009). Levermann et al. (2013) compared the total sea level change from each climate system components with reconstructed sea level changes in the past including the LIG, and showed that the sea level commitment was consistent with sea level reconstructions. They discussed that there are significant uncertainty that came from the forcing data, representations in ice sheet physics, and the time-dependent nature of the simulation. As for the LIG, previous climate model simulations did not reproduce reconstructed warm Antarctic climate and the retreatment of Antarctic ice sheet, when the models were forced by the boundary conditions of the LIG (Sutter et al. 2016; Deconto and Pollard 2016). However, the direct forcing of Antarctic ice sheet is the mass balance, not the global mean temperature anomaly. It is required to understand the relationship between the climate forcing and the responses of Antarctic ice sheet, as reconstructions of mass balance of Antarctic ice sheet in the past would be virtually impossible.

4.2 Comparison of past and future

In Chapter 2, I proposed a mechanism of warmer Antarctic climate during the LIG compared to the present interglacial, as the weak AMOC during the transition from the glacial to interglacial and bipolar seesaw mechanism. In contrast, the future Antarctic warming is driven by global radiative imbalance due to increasing greenhouse gas concentrations. In order to compare Antarctic climate changes during the LIG and in the future, I analyzed climate model simulations of future projection. The model used in this analysis is almost identical with that used in Chapter 2 and 3: only one difference is the coefficient of the isopycnal layer thickness diffusivity of the ocean, which was 7.0 ×

10^6 cm^2/s for the LIG experiment but 3.0×10^6 cm^2/s for the RCP experiment. I analyze the results of historical run and Representative Concentration Pathway (RCP) scenario runs from phase 5 of the Coupled Model Intercomparison Project (CMIP5) (Taylor et al. 2012; Bakker et al. 2016). Four scenarios (RCP 2.6, 4.5, 6.0, 8.5) were presented in the CMIP5, and the results of RCP 4.5 and 8.5 experiments were analyzed here. In the RCP experiments, the climate model was spun up with the boundary conditions of the pre-industrial of 1850 AD, and was forced by observed atmospheric greenhouse gas concentrations and insolation until 2005. The concentration of atmospheric CO_2 is 379 ppm at 2005. After 2005 and until 2300, the greenhouse gas concentrations were changed following the time series of RCP 4.5 and 8.5, respectively (Fig. 4.1a). Note that the atmospheric CO_2 concentration at 2300 AD of RCP 4.5 is 543 ppm, which is close to that of CO_2 doubling (571 ppm) in Chapter 3.

The time series of simulated surface air temperature and subsurface ocean temperature in the Antarctic region are shown in Fig. 4.1. The Antarctic air temperature and ocean temperature gradually increased, and surface air temperature anomaly at 2300 in the Antarctic region (60−90°S) reached 3 °C and 8 °C for the RCP 4.5 and 8.5 experiments, respectively. The Antarctic climate of the LIG (difference of T2-like and T1-like experiment at 13 ka) based on the Chapter 2 is indicated with the dashed lines in Fig. 4.1. The results indicate that the atmosphere and ocean temperature anomalies in the Antarctic region at 2300 for RCP 4.5 experiment are comparable to the LIG. The global map of surface air temperature change is shown in Fig. 4.2. The LIG is characterized with warming in the Southern Hemisphere and cooling in the Northern Hemisphere, due to a weakened AMOC and northward heat transport. In the RCP experiment, the surface air temperature increased globally due to increased greenhouse gas concentrations. One important thing is that simulated Antarctic surface air temperatures at 21st and 23rd century were significantly different. This comes from the large response time of the Southern Ocean, due to the large thermal inertia derived from the deep convection of the ocean (Manabe et al. 1991). The Antarctic winter surface air

temperature and zonal mean ocean temperature in the West Antarctic region are displayed in the Fig. 4.3, indicating that the magnitude and spatial distribution of temperature anomaly are similar between the LIG and the future. The warmer Antarctic surface air temperature reduced sea ice production rate in the Antarctic coast (Fig. 4.4b−d, f). The largest surface air temperature change in the Antarctic coast is a similarity between the LIG and the future, likely due to the retreatments of sea ice. Note that there are some dissimilarities between the LIG and the future, one point is a subsurface ocean temperature in the Southern Ocean, indicating there is a cooling in the LIG but not for the future (Fig. 4.3). The responses of subsurface ocean likely reflect changes in vertical convection in the Southern Ocean. As indicated by Fig. 4.5a−b, wintertime mixed layer depth in the Southern Ocean deepened in the T2-like experiments, which represents the LIG. The stronger vertical convection cools subsurface ocean since the Southern Ocean is characterized with the stratification, formed by fresh and cold surface water and saline and warm subsurface water. In contrast, the vertical convection in the Southern Ocean already occurs in the pre-industrial (Fig. 4.5c). The convection significantly weakened in the future (Fig. 4.5d), likely due to the stronger stratification results from atmospheric warming and melting of sea ice (Yamamoto et al. 2015).

In order to discuss the threshold of the retreatment of WAIS by comparing the LIG and future, I utilize some assumptions based on previous studies. (1) A higher sea level at the LIG was a result of the retreatment of WAIS (Dutton et al. 2015), indicating the LIG was warmer than the threshold of the WAIS retreatment, (2) An increased basal melting was a major cause of the retreatment of WAIS (Sutter et al. 2016; Deconto and Pollard 2016), (3) Basal melting is determined by atmosphere and ocean conditions in the Antarctic region (Chapter 3), (4) The LIG was warmer than the present interglacial, and the cause of warmer Antarctic climate is a bipolar seesaw mechanism, as indicated by Chapter 2, (5) The duration of the LIG warmth was about several thousand years (Fig. 2.1).

Based on the present analysis, it is shown that the atmospheric and oceanic temperature in the Antarctic region reaches the level of the LIG within several hundred years (Fig. 4.1), indicating it may reach the threshold of the retreatment of WAIS in the future even in RCP 4.5 (relatively stabilized CO_2). The proposed threshold of the retreatment of WAIS is consistent with previous two studies with different approaches (Winkelmann et al. 2015; Deconto and Pollard 2016), in that the threshold of the retreatment of WAIS lies below RCP 4.5. Although mass balances and the shapes of Antarctic ice sheet were not investigated in the present study, a greater basal melting of Antarctic ice shelves and retreatment of ice sheet is expected in the future as well as the LIG. The same analysis was applied to the CO_2 doubling experiment used in Chapter 3, which extends to 2000 years from the Pre-Industrial. The time series of Antarctic climate highlights the response time of the Southern Ocean, that it takes about 1,000 years to reach the quasi steady-states, and equilibrium Antarctic temperature was significantly larger than AD 2300 of RCP 4.5 (Fig. 4.6, 4.7). These results indicate an increasing greenhouse gas concentrations could exert a long-term impact on Antarctic climate and ice sheets.

Here I examine the validity and uncertainties in the assumptions used in the previous discussion. Although the direct evidence of the retreatment of WAIS during the LIG is lacking (Bradley et al. 2012), it is frequently discussed that the retreatment of WAIS is required to account for the higher sea level during LIG (Dutton et al. 2015). The basal melting rate of Antarctic ice shelves were not quantified in the present study, although it is shown to be a major cause of the retreatment of WAIS (Sutter et al. 2016; Deconto and Pollard 2016). As the cause of warmer Antarctic climate during LIG, I simply substituted the result of Chapter 2, using the time series of greenhouse gas concentrations and insolation of Termination 1. These parameters should be set to that of the LIG to conduct direct comparisons. An identical climate model is used to minimize biases of the climate model, but the climate model exhibits a large bias in sea surface temperature in the Southern Ocean (Abe-Ouchi et al. in prep.), which would

affect the response of Southern Ocean to climate changes. As the time series of Antarctic ocean temperature and surface air temperature depends on the processes in the Southern Ocean involving sea ice retreatment and deep ocean convections (Yamamoto et al. 2015), improvements on climate model representations are required to reduce model uncertainties. Although the treatment of basal mass balance differs between models, ice sheet models of Golledge et al. (2015) and Deconto and Pollard (2016) exhibits significant retreat of WAIS (>2 m sea level equivalent) occurs within several hundreds of years in RCP 4.5. These results indicate it is possible that the retreatment of the WAIS occurred within the LIG warmth, although there are still significant uncertainties in the response of Antarctic Ice Sheet at certain forcings (Bindschadler et al. 2013). In addition, it is proposed that the melting of Antarctic Ice Sheet in turn melt ice shelves and cause further retreat, by changing subsurface ocean temperature by strengthening stratification in the Southern Ocean (Golledge et al. 2014; Fogwill et al. 2015). I conducted preliminary model experiments to investigate the impact of glacial meltwater in the Southern Ocean using a climate model and a regional ocean model used in the present study, and found that the glacial meltwater could cause significant increase in basal melting (Appendix C2). Such interactions between Antarctic Ice Sheet and atmosphere-ocean system could play a role in the retreatment of Antarctic Ice Sheet in the past and the future.

4.3 Factors determining the relationship between climate and Antarctic Ice Sheet

Recent studies suggest that there is regional dependency in the response of Antarctic ice sheet to climate change. Golledge et al. (2017) used an ice sheet model and investigated the responses of respective Antarctic ice sheet catchments to systematic changes in surface and basal mass balance of ice shelves. They found that the climatic threshold of the retreatment of Antarctic ice sheet significantly differs between Antarctic ice sheet catchments: atmospheric surface mass balance was effective in EAIS in contrast the ocean warming was effective in WAIS. They discussed the different

responses of respective Antarctic ice sheet catchments came from topographic features of Antarctic continent. Geological reconstructions also indicate there is regional dependency in the response of Antarctic ice sheet in the past. Marine sediments suggest that the Antarctic Ice Sheet retreated in the West Antarctica and Wilkes Land during the Pliocene (Cook et al. 2013; McKay et al. 2016), despite the exposure ages of Antarctic mountain rocks suggests the ice sheet was thicker in Dronning Maud Land (Suganuma et al. 2014; Yamane et al. 2015).

Not only there is regional dependency in the responses of Antarctic ice sheet to climate change (Golledge et al. 2017), the results of Chapter 3 indicates there is a regional dependence of climatic threshold in ocean-induced basal melting of ice shelves through changes in sea ice production. The increase in basal melting rate due to the intrusion of warm water onto continental shelves exhibits a threshold-like response to climate change associated with sea ice production, and the thresholds of warm water intrusion differ between regions (Fig. 3.9). In the Amundsen and Bellingshausen Seas where basal melting is already active, the global warming would induce steadily increase basal melting rate, and would cause retreatment of ice sheet as simulated by Joughin et al. (2014). In the Weddell Sea and Wilkes Land, where basal melting rate is small in the present-day, but the reduced sea ice production would promote the intrusion of warm water, as simulated Chapter 3 and Hellmer et al. (2012), and would cause the retreatment of ice sheet such as Mengel et al. (2015). In contrast, the increase in basal melt in the Dronning Maud Land was ineffective to the retreatment of ice sheet (Golledge et al. 2017) although model predicted significant increase in basal melting rate (Chapter 3), as the most of ice sheet lies Antarctic continent much higher than the sea level. It is also discussed that the present-day sea ice production in the Antarctic coast is affected by topography of Antarctica (Morales Maqueda 2004), and the intrusion of warm water onto the Antarctic continental shelves is affected by topography of continental shelf (de Rydt et al. 2014; Rintoul et al. 2016).

Preliminary ice sheet modeling results indicate that the drastic retreatment of

Antarctic ice sheet could occur in response to changes in basal melting rate, and their thresholds of retreatments are sensitive to the topography of Antarctic continents (Appendix D). Therefore, I discuss that the topography of Antarctic continent is a responsible factor determining the relationship between the climate and Antarctic ice sheet, in the point it would determine the responses of Antarctic ice sheet to change in mass balance of ice shelves, and the responses of mass balances to climate.

4.4 What is the state of the present-day Antarctic ice sheet?

The discussion on the LIG highlights the state of the Antarctic ice sheet at the present-day interglacial. Sea level reconstructions indicate the WAIS retreated during the LIG. Today, WAIS is remained and the resulting global mean sea level is relatively lower than the LIG. The Antarctic ice sheet actually retreated during the last deglaciation, and recent ice sheet reconstructions suggest that the retreatment of the Antarctic ice sheet occurred during early Holocene. Geological records indicate that the thickness of ice sheet upstream of Pine Island Glacier occurred during 8−6 ka (Johnson et al. 2014), possibly due to the occurrence of the warm water intrusion onto the continental shelves (Hillenbrand et al. 2017). The retreat of grounding lines occurred in the Ross Sea during late Holocene (Conway et al. 1999: Yokoyama et al. 2016). Mercer (1968) wrote: “What is the likelihood that the West Antarctic Ice Sheet will disintegrate during the present interglacial, as during the Sangamon (note: the Sangamon corresponds to LIG)?”. The West Antarctic Ice Sheet might have failed to melt during the last deglaciation due to a cold event of Antarctic Cold Reversal which lasted about ~2,000 years associated with an abrupt recovery of the AMOC. As the Antarctic climate during the LIG is proposed to be close to that projected in the future of a stabilizing concentration of greenhouse gas concentrations, the global warming may help the WAIS to melt during the present interglacial.

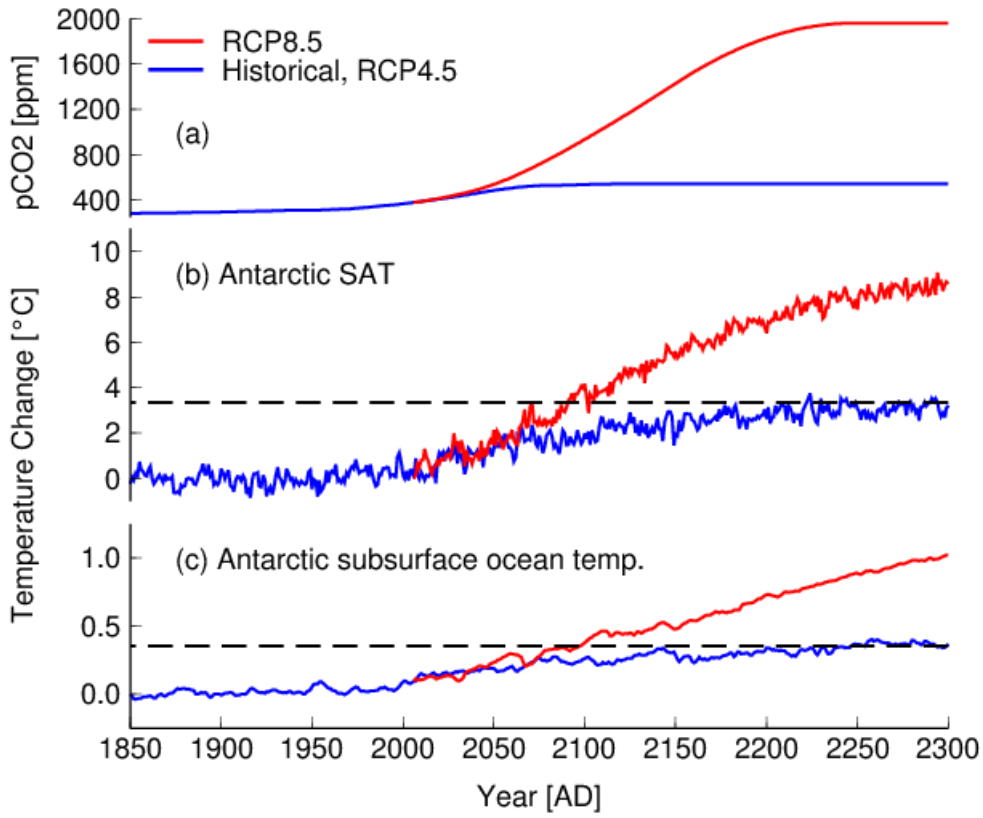

Fig. 4.1 Results of RCP experiments using MIROC4m. The blue and red lines indicate historical run (before 2005 AD), RCP 4.5 and 8.5 experiments, respectively. (a) Atmospheric CO_2 concentration as experimental settings. (b) Annual-mean Antarctic surface air temperature (60−90°S) and (c) annual-mean Antarctic subsurface ocean temperature (500−m depth, 60−90°S), anomaly from the period of AD 1850−1899. The dashed lines indicate the difference between Termination 1 and Termination 2 at 13 ka derived from the results of chapter 2.

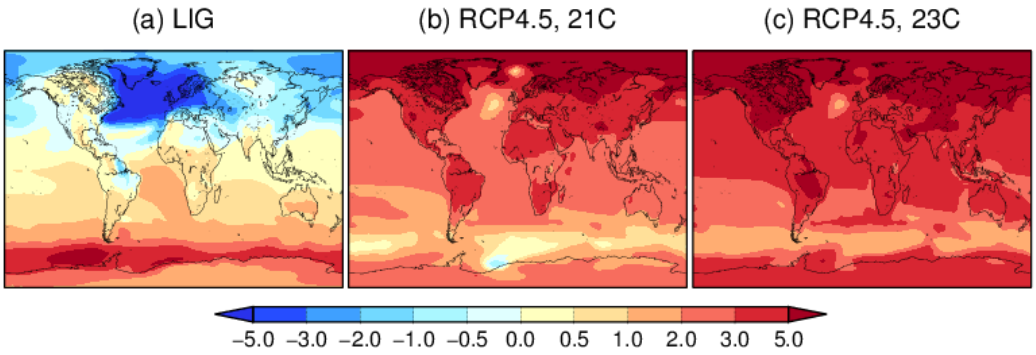

Fig. 4.2 Results of MIROC experiments. annual-mean surface air temperature anomaly of (a) the LIG from the chapter 2 (Fig. 2.15), (b−c) RCP 4.5 experiments at the 21st century (AD 2051−2100) and 23rd century (AD 2251−2300) (anomaly from AD 1850−1899).

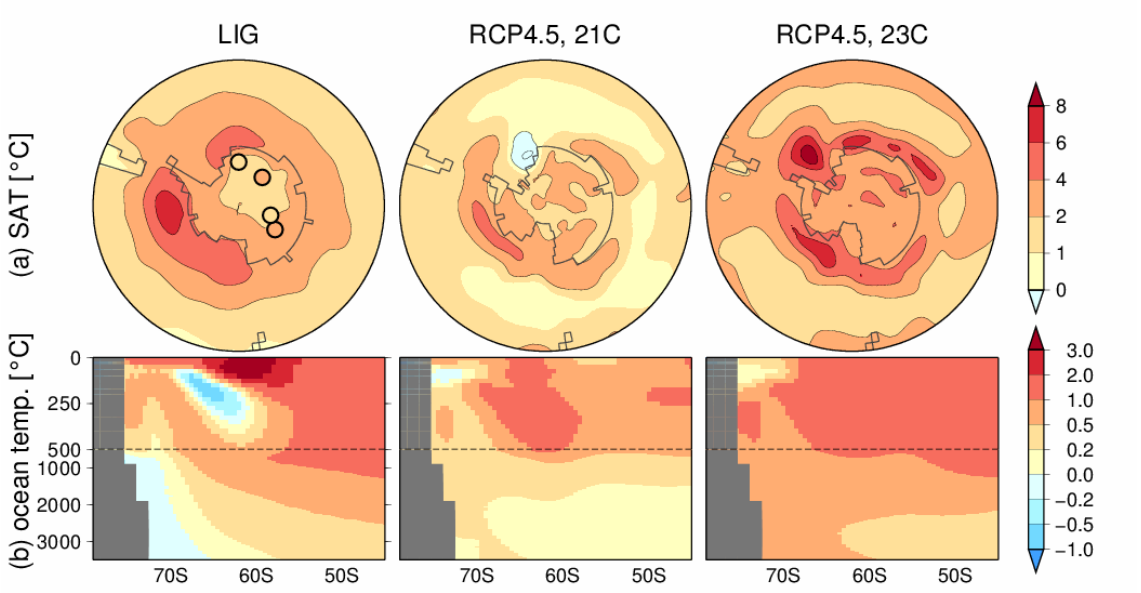

Fig. 4.3 Results of MIROC experiments. (a) Surface air temperature during austral winter (June−August), (b) zonal mean ocean temperature in the West Antarctica (225−270°E). (Left) LIG, based on the difference between Termination 2 and Termination 1 experiments of the Chapter 2. The circles indicate surface temperature reconstructions at 130 ka (Capron et al. 2014). (Center and Right) RCP experiments at the 21st century (2051−2100AD) and 23rd century (2251−2300AD) (anomaly from 1850−1899AD).

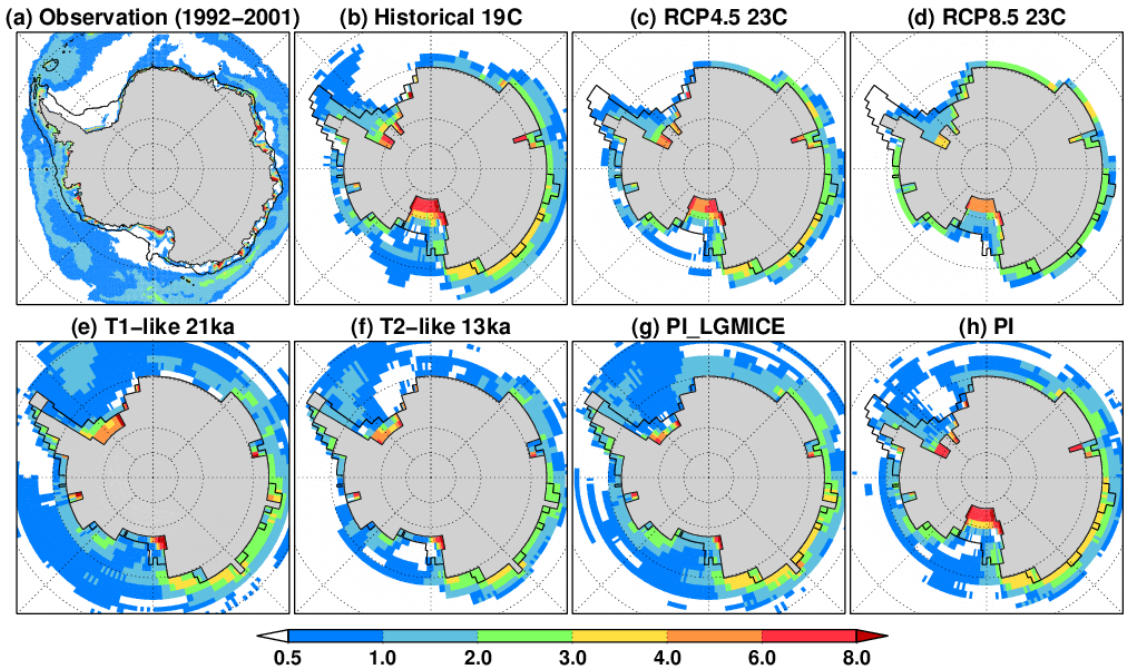

Fig. 4.4 Map of sea ice production. (a) An observational estimate derived from Tamura et al. (2008) (ERA-40, 1992−2001AD), and (b−h) climate model results estimated by monthly sea surface salt flux. (b−d) Historical and RCP experiments of Chapter 4, (e) T1-like experiment at 21 ka (LGM), (f) T2-like experiment at 13 ka as a representative of the LIG, (g) Present-day insolation and greenhouse gases but LGM ice sheet derived from Appendix B, (h) present-day experiment. The unit is sea ice m/yr.

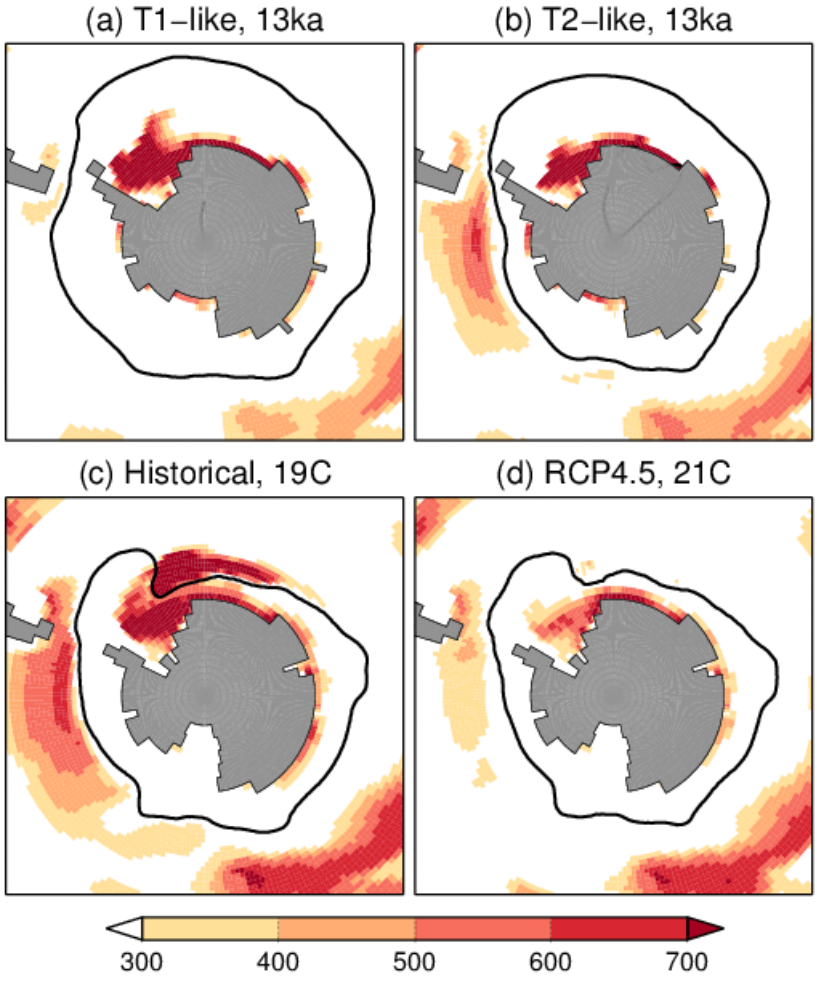

Fig. 4.5 Results of MIROC experiments for deglaciation experiments (upper panels, Chapter 2) and RCP experiments at the 19th (1851−2000AD) and 21st century (2051−2100AD) (lower panels). Bold lines indicate winter sea ice edge (sea ice concentration > 0.15). The color indicates mixed layer depth during Austral winter [m], defined by the depth where density anomaly is less than 0.03 g/cm3 compared to the sea surface. All model variables are 100-year mean climatology of the Austral winter (September)

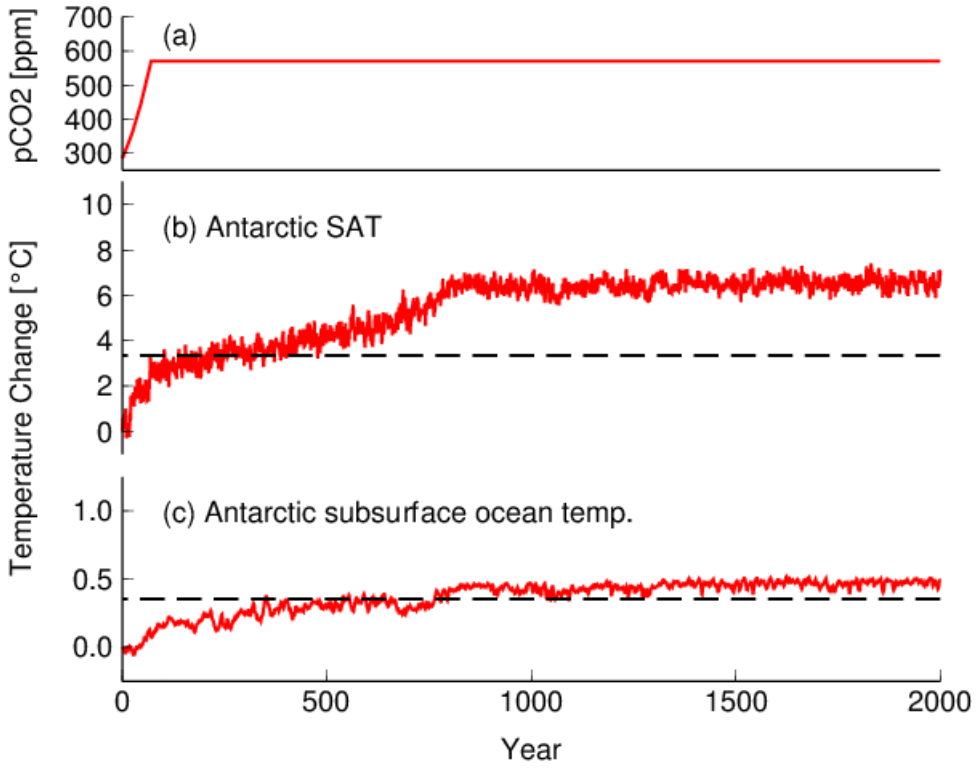

Fig. 4.6 Same as Fig. 4.1, but for the CO_2 doubling experiment.

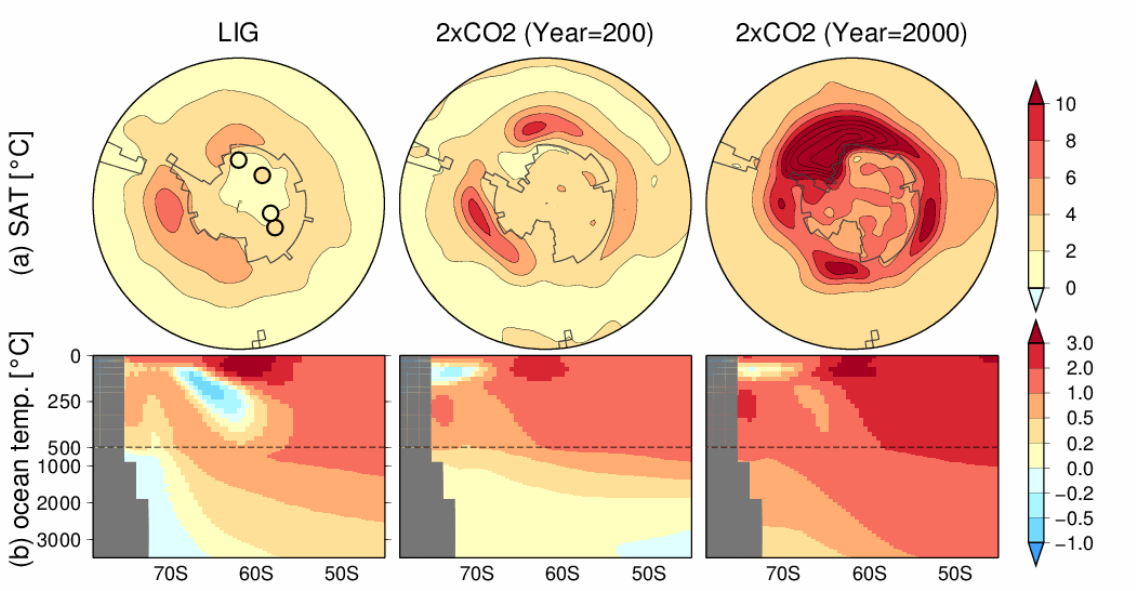

Fig. 4.7 Same as Fig. 4.3, but for the CO_2 doubling experiment.

Chapter 5

Conclusion

In the present study, I investigated the mechanisms and physical processes of Antarctic ice sheet changes in the past and future to help understanding climatic thresholds of Antarctic ice sheets.

In Chapter 2, transient simulations from the glacial to interglacial were conducted to investigate the cause of a warmer Antarctic climate during the Last Interglacial compared to the present interglacial. It is shown that a recovery of AMOC could occur during the last deglaciation under a continuous glacial meltwater flux in the North Atlantic. The fluctuations in AMOC well explained the time series in Antarctic surface air temperature during Termination 1 and 2, by the bipolar seesaw mechanism of ocean heat transport. The peak in Antarctic temperature was large in case the AMOC was weak throughout the deglaciation, and the amplitude is comparable to reconstructions of the LIG. The results suggested that the speed of ice sheet melting in the Northern Hemisphere influenced the Antarctic climate during deglaciations through change in the AMOC.

In Chapter 3, I utilized a regional ocean model which resolves ocean circulation in the Antarctic region including beneath ice shelf cavities, to understand the mechanism and responsible processes of basal melting change to long-term climate change. The responses of basal melting change in a warmer climate was larger than that in a colder climate, as the responses of ocean temperatures between the Southern Ocean outside the continental shelf break and Antarctic shelf seas are different. The sea ice production forms a cold and dense water mass on continental shelves by brine rejection, turned out to influence the intrusion of warm water onto continental shelves. The results imply basal melting is determined by warm water intrusion due to change in atmospheric conditions, combined with subsurface ocean temperature change.

The Chapter 3 presents general relationship between climate change and mass balance of Antarctic ice shelves, and Chapter 2 presents LIG as one probable application to understand variations in Antarctic ice sheet in the past. Therefore In Chapter 4, based on the results of climate model simulations, I discussed the characteristics and

determining factors of climatic thresholds for Antarctic ice sheet retreat, and implications for the Antarctic ice sheet in the present day, and in the future climate change. The warmer Antarctic air temperature, reduced sea ice production, and subsurface ocean temperatures are common between the Last Interglacial and the future. Based on climate model simulations, Antarctic climate reaches the threshold of the retreatment of WAIS inferred by the LIG within several hundred years even with a stabilized atmospheric CO_2 concentration, suggesting the vulnerability of WAIS in the future.

In future, the quantification of mass balances of Antarctic ice sheet and the response of Antarctic ice sheet at certain periods of time (or transient evolutions) will further understand the relation between climatic forcings and the response of Antarctic ice sheet. Such integrated climate and ice sheet model will enable direct model-data comparisons. I expect further paleoclimate reconstructions, such as responsible factors of mass balance of ice sheets (accumulation, ocean temperature at depth), time series of sea level rise during glacial terminations, will contribute to improve our understanding on the Antarctic ice sheet.

References

Abe-Ouchi, A., R. Ohgaito, W-L. Chan, S. Sherriff-Tadano, M. Yoshimori, A. Oka and J. C. Hargreaves (to be submitted), Glacial Atlantic overturning in CMIP/PMIP models controlled by Southern and Northern high latitude changes, at PMIP4 meeting, September, 2017.

Abe-Ouchi, A., F. Saito, K. Kawamura, M. E. Raymo, J. Okuno, K. Takahashi, and H. Blatter (2013), Insolation-driven 100,000-year glacial cycles and hysteresis of ice-sheet volume. Nature, 500, 190-193, doi:10.1038/nature12374.

Abe-Ouchi, A., et al. (2015), Ice-sheet configuration in the CMIP5/PMIP3 Last Glacial Maximum experiments. Geoscientific Model Development, 8 (11), 3621-3637, doi:10.5194/gmd-8-3621-2015.

Anderson, R. F., S. Ali, L. I. Bradtmiller, S. H. H. Nielsen, M. Q. Fleisher, B. E. Anderson and L. H. Burckle (2009), Wind-Driven upwelling in the Southern Ocean and the deglacial rise in atmospheric CO2, Science, 323(5920), 1443-1448, doi:10.1126/science.1167441.

Bakker, P. et al. (2013), Last Interglacial temperature evolution - a model inter-comparison, Climate of the Past, 9, 605-619, doi:10.5194/cp-9-605-2013

Bakker, P. et a. (2016), Fate of the Atlantic Meridional Overturning Circulation: Strong decline under continued warming and Greenland melting, Geophysical Research Letters, 43, 12,252-12,260, doi:10.1002/2016GL070457.

Beckmann, A., and H. Goosse (2003), A parameterization of ice shelf-ocean interaction for climate models. Ocean Modelling, 5, 157-170, doi:10.1016/S1463-5003(02)00019-7.

Bentley, M. J., et al. (2014), A community-based geological reconstruction of Antarctic Ice Sheet deglaciation since the Last Glacial Maximum. Quaternary Science Reviews, 100, 1-9, doi:10.1016/j.quascirev.2014.06.025.

Bereiter, B., S. Eggleston, J. Schmitt, C. Nehrbass-Ahles, T. F. Stocker, H. Fischer, S. Kipfstuhl, and J. Chappellaz (2015), Revision of the EPICA Dome C CO2 record from 800 to 600 kyr before present, Geophysical Research Letters, 42, 542-549, doi:10.1002/2014GL061957

Berger, A. and M. F. Loutre (1991), Insolation values for the climate of the last 10 million years, Quaternary Sciences Review, 10(4), 297-317, doi: 10.1016/0277-3791(91)90033-Q

Bethke, I., C. Li, and K. H. Nisancioglu (2012), Can we use ice sheet reconstructions to constrain meltwater for deglacial simulations?, Paleoceanography, 27, PA2205,

doi:10.1029/2011PA002258.

Bindschadler, R. A., et al. (2013), Ice-sheet model sensitivities to environmental forcing and their use in projecting future sea level (the SeaRISE project). Journal of Glaciology, 59 (214), 195-224, doi:10.3189/2013JoG12J125.

Bintanja, R., G. van Oldenborgh, S. Drijfhout, B. Wouters, and C. Katsman (2013), Important role for ocean warming and increased ice-shelf melt in Antarctic sea-ice expansion. Nature Geoscience, 6 (4), 376-379, doi:10.1038/ngeo1767.

Bintanja, R., G. J. van Oldenborgh, and C. A. Katsman (2015), The effect of increased fresh water from Antarctic ice shelves on future trends in Antarctic sea ice. Annals of Glaciology, 56 (69), 120-126, doi:10.3189/2015AoG69A001.

Braconnot, P., S. P. Harrison, M. Kageyama, P. J. Bartlein, V. Masson-Delmotte, A. Abe-Ouchi, B. Otto-Bliesner, and Y. Zhao (2012), Evaluation of climate models using palaeoclimatic data. Nature Climate Change, 2 (6), 417-424, doi:10.1038/nclimate1456.

Braconnot, P., et al. (2007), Results of PMIP2 coupled simulations of the Mid-Holocene and Last Glacial Maximum Part 1: experiments and large-scale features. Climate of the Past, 3 (2), 261-277, doi:10.5194/cp-3-261-2007.

Bradley, S. L., M. Siddall, G. A. Milne, V. Masson-Delmotte and E. Wolff (2012), Where might we find evidence of a Last Interglacial West Antarctic Ice Sheet collapse in Antarctic ice core records?, Global and Planetary Change, 88-89, 64-75, doi:10.1016/j.gloplacha.2012.03.004.

Broecker, W. S. (1998), Paleocean circulation during the Last Deglaciation: A bipolar seesaw?, Paleoceanography, 13(2), 119-121, doi:10.1029/97PA03707.

Brown, N. and E. D. Galbraith (2016), Hosed vs. unhosed: interruptions of the Atlantic Meridional Overturning Circulation in a global coupled model, with and without freshwater forcing, Climate of the Past, 12, 1663-1679, doi:10.5194/cp-12-1663-2016.

Buizert, C., et al. (2014), Greenland temperature response to climate forcing during the last deglaciation, Science, 345(6201), 1177-1180, doi:10.1126/science.1254961.

Capron, E. et al. (2010), Millennial and sub-millennial scale climatic variations recorded in polar ice cores over the last glacial period, Climate of the Past, 6, 345-365, doi:10.5194/cp-6-345-2010.

Capron, E., A. Govin, E. J. Stone, V. Masson-Delmotte, S. Mulitza, B. Otto-Bliesner, T. L. Rasmussen, L. C. Sime, C. Waelbroeck and E. W. Wolff (2014), Temporal and spatial structure of multi-millennial temperature changes at high latitudes during the Last Interglacial, Quaternary Science Reviews, 103, 116-133, doi:10.1016/j.quascirev.2014.08.018.

Carlson, A. E. (2008), Why there was not a Younger Dryas-like event during the penultimate Deglaciation, Quaternary Science Reviews, 27, 882-887, doi:10.1016/j.quascirev.2008.02.004.

Carlson, A. E. and P. U. Clark (2012), Ice sheet sources of sea level rise and freshwater discharge during the last deglaciation, Review of Geophysics, 50, RG4007, 1-72, doi: 10.1029/2011RG000371.

Cheng, H., R. L. Edwards, W. S. Broecker, G. H. Denton, X. Kong, Y. Wang, R. Zhang and X. Wang (2009), Ice Age Terminations, Science, 326(5950), 248-252, doi:10.1126/science.1177840.

Church, J., et al. (2013), Sea Level Change In: Climate Change 2013: The Physical Science Basis. Contribution of Working Group I to the Fifth Assessment Report of the Intergovernmental Panel on Climate Change. Cambridge University Press, Cambridge, United Kingdom and New York, NY, USA.

Clark, P. U., et al. (2016), Consequences of twenty-first-century policy for multi-millennial climate and sea-level change. Nature Climate Change, 6, 360-369, doi:10.1038/nclimate2923.

Clark, P. U. and L. Tarasov (2014), Closing the sea level budget at the Last Glacial Maximum, PNAS, 111(45), 15861-15862, doi:10.1073/pnas.1418970111.

Clark, P. U., S. J. Marshall, G. K. C. Clarke, S. W. Hostetler, J. M. Licciardi and J. T. Teller (2001), Freshwater Forcing of Abrupt Climate Change During the Last Glaciation, Science, 293(5528), doi:10.1126/science.1062517.

Clark, P. U, N. G. Pisias, T. F. Stocker, and A. J. Weaver (2002), The role of the thermohaline circulation in abrupt climate change, Nature, 415, 863-869, doi:10.1038/415863a.

Conway H, B. L. Hall, D. H. Denton, A. M. Gades and E. D. Waddington (1999), Past and future grounding line retreat of the west Antarctic Ice Sheet, Science, 286(5438), 280-283, doi:10.1126/science.286.5438.280.

Cook, C. P., et al. (2013), Dynamic behavior of the East Antarctic ice sheet during Pliocene warmth. Nature Geoscience, 6 (6), 765-769, doi:10.1038/ngeo1889.

Cornford, S. L. et al. (2015), Century-scale simulations of the response of the West Antarctic Ice Sheet to a warming climate, the Cryosphere, 9, 1579-1600, doi:10.5194/tc-9-1579-2015.

Cuffey, K. and W. S. B. Paterson (2010), The Physics of Glaciers, 4th Edition, Elsevier, ISBN:978-0-123-69461-4.

de Boer, B., R. S. W. van de Wal, L. J. Lourens, R. Bintanja, and T. J. Reerink (2013), A

continuous simulation of global ice volume over the past 1 million years with 3-D ice sheet models. Climate Dynamics, 41, 1365-1384, doi:10.1007/s00382-012-1562-2.

de Boer, B., et al. (2015), Simulating the Antarctic ice sheet in the late-Pliocene warm period: PLISMIP-ANT, an ice-sheet model intercomparison project. The Cryosphere, 9 (3), 881-903, doi:10.5194/tc-9-881-2015.

de Rydt, J., P. R. Holland, P. Dutrieux and A. Jenkins (2014), Geometric and oceanographic controls on melting beneath Pine Island Glacier, Journal of Geophysical Research: Oceans, 119, 2420-2438, doi:10.1002/2013JC009513.

Deaney, E. L., S. Barker and T. van de Flierdt (2017), Timing and nature of AMOC recovery across Termination 2 and magnitude of deglacial CO2 change, Nature Communications, 8, doi:10.1038/ncomms14595.

Deconto, R. M., and D. Pollard (2016), Contribution of Antarctica to past and future sea-level rise. Nature, 531 (7596), 591-597, doi:10.1038/nature17145.

Depoorter, M. A., J. L. Bamber, J. A. Griggs, J. T. M. Lenaerts, S. R. M. Ligtenberg, M. R. van den Broeke, and G. Moholdt (2013), Calving fluxes and basal melt rates of Antarctic ice shelves. Nature, 502, 89-92, doi:10.1038/nature12567.

Dinniman, M. S., J. M. Klinck, L.-S. Bai, D. H. Bromwich, K. M. Hines, and D. M. Holland (2015), The Effect of Atmospheric Forcing Resolution on Delivery of Ocean Heat to the Antarctic Floating Ice Shelves. Journal of Climate, 28 (15), 6067-6085, doi:10.1175/JCLI-D-14-00374.1.

Dinniman, M. S., J.M. Klinck, and W. O. Smith (2011), A model study of Circumpolar Deep Water on the West Antarctic Peninsula and Ross Sea continental shelves. Deep Sea Research Part II: Topical Studies in Oceanography, 58, 1508-1523, doi:10.1016/j.dsr2.2010.11.013.

Dupont, T. K., and R. B. Alley (2005), Assessment of the importance of ice-shelf buttressing to ice-sheet flow. Geophysical Research Letters, 32, L04503, doi:10.1029/2004GL022024.

Dutton, A., and K. Lambeck (2012), Ice Volume and Sea Level during the Last Interglacial. Science, 337, 216-219, doi:10.1126/science.1205749.

Dutton, A., et al. (2015), Sea-level rise due to polar ice-sheet mass loss during past warm periods. Science, 349 (6244), doi:10.1126/science.aaa4019.

Favier, L., G. Durand, S. L. Cornford, G. H. Gudmundsson, O. Gagliardini, F. Gillet-Chaulet, T. Zwinger, A. J. Payne and A. M. Le Brocq (2014), Retreat of Pine Island Glacier controlled by marine ice-sheet instability, Nature Climate Change, 4, 117-121, doi:10.1038/nclimate2094.

Fogwill, C. J., S. J. Phipps, C. S. M. Turney, and N. R. Golledge (2015), Sensitivity of the Southern Ocean to enhanced regional Antarctic ice sheet meltwater input. Earth's Future, 3 (10), 317-329, doi:10.1002/2015EF000306.

Fretwell, P., et al. (2013), Bedmap2: improved ice bed, surface and thickness datasets for Antarctica. The Cryosphere, 7 (1), 375-393, doi:10.5194/tc-7-375-2013.

Gagliardini, O., G. Durand, T. Zwinger, R. C. A. Hindmarsh, and E. Le Meur (2010), Coupling of ice-shelf melting and buttressing is a key process in ice-sheets dynamics. Geophysical Research Letters, 37, 1-5, doi:10.1029/2010GL043334.

Galbraith, E. D., T. M. Merlis and J. B. Palter (2016), Destabilization of glacial climate by the radiative impact of Atlantic Meridional Overturning Circulation disruptions, Geophysic Research Letters, 43, 8214-8221, doi:10.1002/2016GL069846.

Galton-Fenzi, B. K., J. R. Hunter, R. Coleman, S. J. Marsland, and R. C. Warner (2012), Modeling the basal melting and marine ice accretion of the Amery Ice Shelf. Journal of Geophysical Research: Oceans, 117, C09031, doi:10.1029/2012JC008214.

Ganopolski, A. and S. Rahmstorf (2001), Rapid changes of glacial climate simulated in a coupled climate model, Nature, 409, 153-158, doi:10.1038/35051500.

Ganopolski, A. and D. M. Roche (2009), On the nature of lead-lag relationships during glacial-interglacial climate transitions, Quaternary Science Reviews, 28, 3361-3378, doi:10.1016/j.quascirev.2009.09.019.

Gersonde, R., X. Crosta, A. Abelmann, and L. Armand (2005), Sea-surface temperature and sea ice distribution of the Southern Ocean at the EPILOG Last Glacial Maximum - A circum-Antarctic view based on siliceous microfossil records. Quaternary Science Reviews, 24, 869-896, doi:10.1016/j.quascirev.2004.07.015.

Golledge, N. R., C. J. Fogwill, A. N. Mackintosh, and K. M. Buckley (2012), Dynamics of the last glacial maximum Antarctic ice-sheet and its response to ocean forcing. Proceedings of the National Academy of Sciences, 109, 16052-16056, doi:10.1073/pnas.1205385109.

Golledge, N. R., L. Manviel, L. Carter, C. J. Fogwill, M. H. England, G. Cortese, and R. H. Levy, (2014), Antarctic contribution to meltwater pulse 1A from reduced Southern Ocean overturning, Nature communications, 5, 1-10, doi:10.1038/ncomms6107.

Golledge, N. R., D. E. Kowalewski, T. R. Naish, R. H. Levy, C. J. Fogwill, and E. G. W. Gasson, (2015), The multi-millennial Antarctic commitment to future sea-level rise. Nature, 526, 421-425, doi:10.1038/nature15706.

Golledge, N. R., R. H. Levy, R. M. McKay and T. R. Naish (2017), East Antarctic ice sheet most vulnerable to Weddell Sea warming, Geophysical Research Letters, 44, doi:10.1002/2016GL072422.

Gong, Y., S. L. Cornford, and a. J. Payne (2014), Modelling the response of the Lambert Glacier-Amery Ice Shelf system, East Antarctica, to uncertain climate forcing over the 21st and 22nd centuries. The Cryosphere, 8, 1057-1068, doi:10.5194/tc-8-1057-2014.

Govin, A. et al. (2015), Sequence of events from the onset to the demise of the Last Interglacial: Evaluating strengths and limitations of chronologies used in climatic archives, Quaternary Science Reviews, 129, 1-36, doi:10.1016/j.quascirev.2015.09.018.

Gregoire, L. J., B. Otto-Bliesner, P. J. Valdes, and R. Ivanovic (2016), Abrupt Bølling warming and ice saddle collapse contributions to the Meltwater Pulse 1a rapid sea level rise, Geophys. Res. Lett., 43, 9130-9137, doi:10.1002/2016GL070356.

Greve, R. and H. Blatter (2010), Dynamics of Ice Sheet and Glaciers, Springer, ISBN: 978-3-642-03415-2.

Hasumi, H. (2006), CCSR Ocean ComponentModel (COCO) version 4.0. CCSR Report 25, Center for Climate System Research, University of Tokyo.

Hasumi, H., and S. Emori (2004), K-1 coupled model (MIROC) description, K-1 Tech. Rep.1, 34 pp. Center for Climate System Center Res., Univ. of Tokyo.

Hattermann, T., O. A. Nøst, J. M. Lilly, and L. H. Smedsrud (2012), Two years of oceanic observations below the Fimbul Ice Shelf, Antarctica. Geophysical Research Letters, 39, L12605, doi:10.1029/2012GL051012.

Hattermann, T., L. Smedsrud, O. A. Nøst, J. Lilly, and B. Galton-Fenzi (2014), Eddy-resolving simulations of the Fimbul Ice Shelf cavity circulation: Basal melting and exchange with open ocean. Ocean Modelling, (82), 28-44, doi:10.1016/j.ocemod.2014.07.004.

Hayes, C. T., A. Martinez-Garcia, A. P. Hasenfratz, S. L. Jaccard, D. A. Hodell, D. M. Sigman, G. H. Haug and R. F. Anderson (2014), A stagnation event in the deep South Atlantic during the last interglacial period, Science, 346(6216), 1514-1517, doi:10.1126/science.1256620.

He. F, J. D. Shakun, P. U. Clark, A. E. Carlson, Z. Liu, B. L. Otto-Bliesner, and J. E. Kutzbach (2013), Northern Hemisphere forcing of Southern Hemisphere climate during the last deglaciation, Nature, 494, 81-85, doi:10.1038/nature11822.

Hellmer, H. H. (2004), Impact of Antarctic ice shelf basal melting on sea ice and deep ocean properties. Geophysical Research Letters, 31, 1-4, doi:10.1029/2004GL019506.

Hellmer, H., S. Jacobs and A. Jenkins (1998). Oceanic erosion of a floating Antarctic glacier in the Amundsen Sea. Ocean, Ice, and Atmosphere: Interactions at the Antarctic Continental Margin, Antarctic Research Series, 75, 83-99, doi: doi:10.1029/AR075p0083.

Hellmer, H. H., F. Kauker, R. Timmermann, J. Determann, and J. Rae (2012), Twenty-first-century warming of a large Antarctic ice-shelf cavity by a redirected coastal current. Nature, 485, 225-228, doi:10.1038/nature11064.

Hellmer, H. H., and D. J. Olbers (1989), A two-dimensional model for the thermohaline circulation under an ice shelf. Antarctic Science, 1 (4), 325-336, doi:10.1017/S0954102089000490.

Hillenbrand, C-D. et al. (2017), West Antarctic Ice Sheet retreat driven by Holocene warm water incursions, Nature, 547, 43-48, doi:10.1038/nature22995.

Hoffman, J., P. U. Clark, A. C. Parnell and F. He (2017), Regional and global sea-surface temperatures during the last interglaciation, Science, 335, 276-279, doi:10.1126/science.aai8464

Holden, P. B., N. R. Edwards, E. W. Wolff, N. J. Land, J. S. Singarayer, P. J. Valdes and T. F. Stocker (2010), Interhemispheric coupling, theWest Antarctic Ice Sheet and warm Antarctic interglacials, Climate of the Past, 6, 431-443, doi:10.5194/cp-6-431-2010

Holland, D. M., and A. Jenkins (1999), Modeling Thermodynamic Ice-Ocean Interactions at the Base of an Ice Shelf. Journal of Physical Oceanography, 29, 1787-1800, doi:10.1175/1520-0485(1999)029<1787:MTIOIA>2.0.CO;2

Holland, D., and D. Holland (2015), On the rocks: The challenges of predicting sea level rise, Eos, 96, doi:10.1029/2015EO036667.

Holland, P. R., A. Jenkins, and D. M. Holland (2008), The response of Ice shelf basal melting to variations in ocean temperature. Journal of Climate, 21, 2558-2572, doi:10.1175/2007JCLI1909.1.

Holloway, M. D., L. C. Sime, J. S. Singarayer, J. C. Tindall, P. Bunch and P. J. Valdes (2016), Antarctic last interglacial isotope peak in response to sea ice retreat not ice-sheet collapse, Nature Communications, 7(12293), 1-9, doi:10.1038/ncomms12293.

Ivanovic, R. F., L. J. Gregoire, M. Kageyama, D. M. Roche, P. J. Valdes, A. Burke, R. Drummond, W. R. Peltier, and L. Tarasov (2016a), Transient climate simulations of the deglaciation 21-9 thousand years before present (version 1) - PMIP4 Core experiment design and boundary conditions, Geoscientific Model Developments, 9, 2563-2587, doi:10.5194/gmd-9-2563-2016.

Ivanovic, R. F., L. J. Gregoire, A. D. Wickert, P. J. Valdes, and A. Burke (2016b), Collapse of the North American ice saddle 14,500 years ago caused widespread cooling and reduced ocean overturning circulation, Geophysical Research Letters, 43, doi:10.1002/2016GL071849.

Jacobs, S. S., R. G. Fairbanks, and Y. Horibe (1985), Origin and evolution of water

masses near the Antarctic continental margin: evidence from H2 18O/H216 O ratios in seawater. Antarctica Research Series, 43, 59-85, doi: 10.1029/AR043p0059

Jacobs, S. S., H. H. Hellmer, and A. Jenkins (1996), Antarctic Ice Sheet melting in the southeast Pacific. Geophysical Research Letters, 23 (9), 957, doi:10.1029/96GL00723.

Jacobs, S. S., H. H. Helmer, C. S. M. Doake, A. Jenkins, and R. M. Frolich (1992), Melting of ice shelves and the mass balance of Antarctica. Journal of Glaciology, 38, 375-387, doi:10.3189/S0022143000002252.

Jacobs, S. S., A. Jenkins, C. F. Giulivi, and P. Dutrieux (2011), Stronger ocean circulation and increased melting under Pine Island Glacier ice shelf. Nature Geoscience, 4, 519-523, doi: 10.1038/ngeo1188.

Jenkins, A., and S. Jacobs (2008), Circulation and melting beneath George VI ice shelf, Antarctica. Journal of Geophysical Research: Oceans, 113, C04013, doi:10.1029/2007JC004449.

Johnson, J. S., M. J. Bentley, J. A. Smith, R. C. Finkel, D. H. Rood, K. Gohl, G. Balco, R. D. Larter and J. M. Schaefer (2014), Rapid Thinning of Pine Island Glacier in the Early Holocene, Science, 343, 999-1001, doi:10.1126/science.1247385.

Joughin, I., B. E. Smith and D. M. Holland (2010), Sensitivity of 21st century sea level to ocean-induced thinning of Pine Island Glacier, Antarctica, Geophysical Research Letters, 37, L20502, doi:10.1029/2010GL044819.

Joughin, I., B. E. Smith and B. Medley (2014), Marine Ice Sheet Collapse Potentially Under Way for the Thwaites Glacier Basin, West Antarctica, Science 344, 735-738, doi:10.1126/science.1249055.

Jouzel, J. et al. (2007), Orbital and Millennial Antarctic Climate Variability over the Past 800,000 Years, Science, 317, 793-796, doi:10.1126/science.1141038.

Kageyama, M. et al. (2013), Climatic impacts of fresh water hosing under Last Glacial Maximum conditions: a multi-model study, Climate of the Past, 9, 935-953, doi:10.5194/cp-9-935-2013.

Kawamura, K. et al. (2017), State dependence of climatic instability over the past 720,000 years from Antarctic ice cores and climate modeling, Science Advances, 3(2), doi:10.1126/sciadv.1600446.

Klockmann, M., U. Mikolajewicz and J. Marotzke (2016), The effect of greenhouse gas concentrations and ice sheets on the glacial AMOC in a coupled climate model, Climate of the Past, 12, 1829-1846, doi:10.5194/cp-12-1829-2016.

Knorr, G. and Lohmann, G. (2003), Southern Ocean origin for the resumption of Atlantic thermohaline circulation during deglaciation, Nature, 424, 532-536,

doi:10.1038/nature01855.

Knorr, G. and Lohmann, G. (2007), Rapid transitions in the Atlantic thermohaline circulation triggered by global warming and meltwater during the last deglaciation, Geochem. Geophy. Geosy., 8, Q12006, doi:10.1029/2007GC001604.

Kopp, R. E., F. J. Simons, J. X.Mitrovica, A. C.Maloof, and M. Oppenheimer (2009), Probabilistic assessment of sea level during the last interglacial stage. Nature, 462, 863-867, doi:10.1038/nature08686.

Krinner, G., O. Magand, I. Simmonds, C. Genthon and J. -L. Dufresne (2007), Simulated Antarctic precipitation and surface mass balance at the end of the twentieth and twenty-first centuries, Climate Dynamics, 28(2-3), 215-230, doi: 10.1007/s00382-006-0177-x.

Kusahara, K., and H. Hasumi (2013), Modeling Antarctic ice shelf responses to future climate changes and impacts on the ocean. Journal of Geophysical Research: Oceans, 118, 2454-2475, doi:10.1002/jgrc.20166.

Kusahara, K., T. Sato, A. Oka, T. Obase, R. Greve, A. Abe-Ouchi, and H. Hasumi (2015), Modelling the Antarctic marine cryosphere at the Last Glacial Maximum. Annals of Glaciology, 56(69), 425-435, doi:10.3189/2015AoG69A792.

Kusahara, K. (2016), Warming ocean erodes ice sheets. Nature Climate Change, 6(1), 22-23, doi:10.1038/nclimate2900.

Labeyrie, L. D., J. –C. Duplessy, J. Duprat, A. Juillet-Levlers, J. Moyes, E. Michel, N. Kallel, and N. J. Shackleton (1992), Changes in the vertical structure of the North Atlantic Ocean between glacial and modern times, Quaternary Science Reviews, 11(4), 401-413, doi:10.1016/0277-3791(92)90022-Z.

Levermann, A., P. U. Clark, B. Marzeion, G. A. Milne, D. Pollard, V. Radic and A. Robinson (2013), The multimillennial sea-level commitment of global warming, PNAS, 110(34), 13745-13750, doi:10.1073/pnas.1219414110.

Li, C., D. S. Battisti, D. P. Schrag and E. Tziperman (2005), Abrupt climate shifts in Greenland due to displacements of the sea ice edge, Geophysical Research Letters, 32, L19702, doi:10.1029/2005GL023492.

Lisiecki, L. E. and M. E. Raymo (2005), A Pliocene-Pleistocene stack of 57 globally distributed benthic δ18O records, Paleoceanography, 20, PA1003, doi:10.1029/2004PA001071.

Liu, Z. and Alexander, M. (2007), Atmospheric bridge, oceanic tunnel, and global climatic teleconnections, Reviews of Geophysics, 45, RC2005, 1-34, doi:10.1029/2005RG000172.

Liu, Z., et al. (2009), Transient simulation of last deglaciation with a new mechanism for Bølling-Allerød warming, Science, 325(5938), 310-314, doi:10.1126/science.1171041.

Locarnini, R. A. et al. (2013), World Ocean Atlas 2013, Volume 1: Temperature. S. Levitus, Ed., A. Mishonov Technical Ed.; NOAA Atlas NESDIS 73, 40 pp.

Losch, M., (2008), Modeling ice shelf cavities in a z coordinate ocean general circulation model. Journal of Geophysical Research: Oceans, 113, C08043, doi:10.1029/2007JC004368.

Loulergue, L., A. Schilt, R. Spahni, V. Masson-Delmotte, T. Blunier, B. Lemieux, J.-M. Barnola, D. Raynaud, T. F. Stocker, and J. Chappellaz (2008), Orbital and millennial-scale features of atmospheric CH4 over the past 800,000 years, Nature, 453(7193), 383-386, doi:10.1038/nature06950.

Loutre, M. F., T. Fichefet, H. Goosse, P. Huybrechts, H. Goelzer and E. Capron (2014), Factors controlling the last interglacial climate as simulated by LOVECLIM1.3, Climate of the Past, 10, 1541-1565, doi:10.5194/cp-10-1541-2014.

Lunt, D. J. et al. (2013), A multi-model assessment of last interglacial temperatures, Climate of the Past, 9, 699-717, doi:10.5194/cp-9-699-2013.

Manabe, S., K. Bryan, M. J. Spelman and K. Bryan (1991), Transient responses of a coupled ocean-atmosphere model to gradual changes of atmospheric CO2, part I: Annual mean response, Journal of Climate, 4(8), 785-818, doi: 10.1175/1520-0442(1991)004<0785:TROACO>2.0.CO;2.

Marcott, S. A. et al. (2014), Centennial-scale changes in the global carbon cycle during the last deglaciation, Nature, 514, 616-619, doi:10.1038/nature13799.

MARGO Project Members (2009), Constraints on the magnitude and patterns of ocean cooling at the Last Glacial Maximum. Nature Geoscience, 2, 127-132, doi:10.1038/ngeo411.

Marino, G., E. J. Rohling, L. Rodriguez-Sanz, K. M. Grant, D. Heslop, A. P. Roberts, J. D. Stanford and J. Yu (2015), Bipolar seesaw control on last interglacial sea level, Nature, 522, 197-201, doi:10.1038/nature14499.

Marson, J. M., L. Wainer, M. M. Mata and Z. Liu, (2014), The impacts of deglacial meltwater forcing on the South Atlantic Ocean deep circulation since the Last Glacial Maximum, Climate of the Past, 10, 1723-1734, doi:10.5194/cp-10-1723-2014.

Martrat, B., P. Jimenez-Amat, R. Zahn and J. O. Grimalt (2014), Similarities and dissimilarities between the last two deglaciations and interglaciations in the North Atlantic region, Quaternary Science Reviews, 99, 122-134, doi:10.1016/j.quascirev.2014.06.016.

Masson-Delmotte et al. (2013), Information from Paleoclimate Archives. In: Climate Change 2013: The Physical Science Basis. Contribution of Working Group I to the Fifth Assessment Report of the Intergovernmental Panel on Climate Change, Cambridge University Press, Cambridge, United Kingdom and New York, NY, USA.

McKay, R. M., P. J. Barrett, R. S. Levy, T. R. Naish, N. R. Golledge, and A. Payne (2016), Antarctic Cenozoic climate history from sedimentary records : ANDRILL and beyond. Philosophical Transactions of the Royal Society A, 374, doi:10.1098/rsta.2014.0301.

McManus, J. F., R. Francois, J.-M. Gherardi, L. D. Keigwin, and S. Brown-Leger (2004), Collapse and rapid resumption of Atlantic meridional circulation linked to deglacial climate changes, Nature, 428(6985), 834-837, doi:10.1038/nature02494.

Mellor, G. L., and L. Kantha (1989), An Ice-Ocean Coupled Model. Journal of Geophysical Research, 94 (89), 10937-10954, doi:10.1029/JC094iC08p10937

Mengel, M., J. Feldmann, and A. Levermann (2015), Linear sea-level response to abrupt ocean warming of major West Antarctic ice basin. Nature Climate Change, 6, 71-75, doi:10.1038/nclimate2808.

Mengel, M., and A. Levermann (2014), Ice plug prevents irreversible discharge from East Antarctica. Nature Climate Change, 4, 451-455, doi:10.1038/nclimate2226.

Menviel, L., A. Timmermann, O. E. Timm, and A. Mouchet (2011), Deconstructing the Last Glacial termination: The role of millennial and orbital-scale forcings. Quaternary Science Reviews, 30 (9-10), 1155-1172, doi:10.1016/j.quascirev.2011.02.005.

Mercer, J. H. (1968), Antarctic Ice and Sangamon Sea Level. Int. Assoc. Sci. Hydrol. Symp., 79 (139), 217-225.

Mignot, J., A. Ganopolski, and A. Levermann (2007), Atlantic Subsurface Temperatures: Response to a Shutdown of the Overturning Circulation and Consequences for Its Recovery, Journal of Climate, 20(19), 4884-4898, doi:10.1175/JCLI4280.1.

Miller, M. D., J. F. Adkins, D. Menemenlis, and M. P. Schodlok (2012), The role of ocean cooling in setting glacial southern source bottom water salinity. Paleoceanography, 27, 1-16, doi:10. 1029/2012PA002297.

Morales Maqueda, M. A., A. J. Willmott, and N. R. T. Biggs (2004), Polynya dynamics: A review of obsercations and modeling. Review of Geophysics, 42, RG1004.

Naish, T. et al. (2009), Obliquity-paced Pliocene West Antarctic ice sheet oscillations. Nature, 458, 322-328, doi:10.1038/nature07867.

Nakayama, Y., R. Timmermann, M. Schroder, and H. H. Hellmer (2014a), On the difficulty of modeling Circumpolar Deep Water intrusions onto the Amundsen Sea continental shelf. Ocean Modelling, 84, 26-34, doi:10.1016/j.ocemod.2014.09.007.

Nakayama, Y., R. Timmermann, C. B. Rodehacke, M. Schroder, and H. H. Hellmer (2014b), Model
ing the spreading of glacial melt water from the Amundsen and Bellingshausen Seas. Geophysical Research Letters, 41, 7942-7949, doi:10.1002/2014GL061600.

NEEM project members (2013), Eemian interglacial reconstructed from a Greenland folded ice core, Nature, 493, 489-493, doi:10.1038/nature11789

Nicholls, K. W., S. Osterhus, K. Makinson, T. Gammerlsrod and E. Fahrbach (2009), Ice-ocean processes over the continental shelf of the Southern Weddell Sea, Antarctica: a review, Review of Geophysics, 47, RG3003, doi:10.1029/2007RG000250

Nøst, O. A., M. Biuw, V. Tverberg, C. Lydersen, T. Hattermann, Q. Zhou, L. H. Smedsrud, and K. M. Kovacs (2011), Eddy overturning of the Antarctic Slope Front controls glacial melting in the Eastern Weddell Sea. Journal of Geophysical Research: Oceans, 116, C11 014, doi: 10.1029/2011JC006965.

Obase, T, A. Abe-Ouchi, K. Kusahara, H. Hasumi, R. Ohgaito (2017), Responses of basal melting of Antarctic ice shelves to the climatic forcing of the Last Glacial Maximum and CO2 doubling, Journal of Climate, 30(10), 3473-3497, doi:10.1175/JCLI-D-15.0908.1.

Obrochta, S. P., T. J. Crowley, J. E. T. Channell, D. A. hodell, P. A. Baker, A. Seki and Y. Yokoyama (2014), Climate variability and ice-sheet dynamics during the last three glaciations, Earth and Planetary Science Letters, 406, 198-212, doi:10.1016/j.epsl.2014.09.004.

Ohmura, A., M. Wild and L. Bengtsson (1996), A possible change in mass balance of Greenland and Antarctic Ice Sheets in the coming century, Journal of Climate, 9, 2124-2135, doi:10.1175/1520-0442(1996)009<2124:APCIMB>2.0.CO;2.

Oka, A., H. Hasumi and A. Abe-Ouchi (2012), The thermal threshold of the Atlantic meridional overturning circulation and its control by wind stress forcing during glacial climate, Geophysical Research Letters, 39, L09709, doi:10.1029/2012GL051421.

O'Leary, M. J., P. J. Hearty, W. G. Thompson, M. E. Raymo, J. X. Mitrovica and J. M. Webster (2013), Ice sheet collapse following a prolonged period of stable sea level during the last interglacial, Nature Geoscience, 6, 796-800, doi:10.1038/ngeo1890.

Otto-Bliesner, B. L. and E. C. Brady (2010), The sensitivity of the climate response to the magnitude and location of freshwater forcing: last glacial maximum experiments, Quaternary Science Reviews, 29, 56-73, doi:10.1016/j.quascirev.2009.07.004.

Otto-Bliesner, B. L., N. Rosenbloom, E. J. Stone, N. P. McKay, D. J. Lunt, E. C. Brady and J. T. Overpeck (2013), How warm was the last interglacial? New model-data comparisons, Philosophical Transactions of the Royal Society A, 371,20130097,doi:10.1098/rsta.2013.0097.

Parrenin, F. et al. (2007), 1-D-ice flow modelling at EPICA Dome C and Dome Fuji, East Antarctica. Climate of the Past, 3, 243-259, doi:10.5194/cp-3-243-2007.

Pauling, A. G., C. M. Bitz, I. J. Smith, and P. J. Langhorne (2016), The Response of the Southern Ocean and Antarctic Sea Ice to Freshwater from Ice Shelves in an Earth System Model. Journal of Climate, 29, 1655-1672, doi:10.1175/JCLI-D-15-0501.1.

Pedro, J. B, H. C. Bostock, C. M. Bitz, F. He, M. J. Vandergoes, E. J. Steig, B. M. Chase, C. E. Krause, S. O. Rasmussen, b. R. Markle, and G. Cortese (2016a), The spatial extent and dynamics of the Antarctic Cold Reversal, Nature Geoscience, 9, 51-56, doi:10.1038/NGEO2580.

Pedro, J. B., T. Martin, E. J. Steig, M. Jochum, W. Park and S. O. Rasmussen (2016b), Southern Ocean deep convection as a driver of Antarctic warming events, Geophysical Research Letters, 43, doi:10.1002/2016GL067861.

Peltier, W. R., D. F. Argus, and R. Drummond (2015), Space geodesy constrains ice age terminal deglaciation: The global ICE-6G-C(VM5a) model. Journal of Geophysical Research: Solid Earth, 120, 450-487, doi:10.1002/2014JB011176.

Peltier, W. R. and G. Vettoretti (2014), Dansgaard-Oeschger oscillations predicted in a comprehensive model of glacial climate: A “kicked” salt oscillator in the Atlantic, Geophysical Research Letters, 41, doi:10.1002/2014GL061413.

Peltier, W. R. (2004), Global Glacial Isostasy and the Surface of the Ice-Age Earth: The ICE-5G (VM2) Model and GRACE, Ann. Rev. Earth and Planet. Sci., 32, 111-149, doi:10.1146/annurev.earth.32.082503.144359.

Petty, A. A., D. L. Feltham, and P. R. Holland, 2013: Impact of Atmospheric Forcing on Antarctic Continental Shelf Water Masses. Journal of Physical Oceanography, 43, 920-940, doi:10.1175/JPO-D-12-0172.1.

Phipps, S. J., C. J. Fogwill, and C. S. M. Turney (2016), Impacts of marine instability across the East Antarctic Ice Sheet on Southern Ocean dynamics, The Cryosphere, 10, 2317-2328, doi:10.5194/tc-10-2317-2016.

Pittard, M. L., B. K. Galton-Fenzi, C. S. Watson and L. Roberts (2017), Future sea level change from Antarctica's Lambert-Amery glacial system, Geophysical Research Letters, 44, 7347-7355, doi:10.1002/2017GL073486.

Pollard, D. and R. M. DeConto (2009), Modelling West Antarctic ice sheet growth and collapse through the past five million years. Nature, 458, 329-332,

doi:10.1038/nature07809.

Pritchard, H., S. Ligtenberg, H. Fricker, D. Vaughan, M. van den Broeke, and L. Padman (2012), Antarctic ice-sheet loss driven by basal melting of ice shelves. Nature, 484 (7395), 502-505, doi:10.1038/nature10968.

Pritchard, H. D., R. J. Arthern, D. G. Vaughan, and L. A. Edwards (2009), Extensive dynamic thinning on the margins of the Greenland and Antarctic ice sheets. Nature, 461 (7266), 971-975, doi:10.1038/nature08471.

Rahmstorf, S., (2002), Ocean circulation and climate during the past 120,000 years, Nature, 419, 207-214, doi:10.1038/nature01090.

Rahmstorf, S., M. Crucifix, A. Ganopolski, H. Goosse, I. Kamenkovich, R. Knutti, G. Lohmann, R. Marsh, L. A. Mysak, Z. Wang, and A. J. Weaver (2005), Thermohaline circulation hysteresis: A model intercomparison, Geophysical Research Letters, 32(L23605), doi;10.1029/2005GL023655.

Raymo, M. E. and J. X. Mitrovica (2012), Collapse of polar ice sheets during the stage 11 interglacial, Nature, 483, 453-456, doi:10.1038/nature10891.

Reynolds, R. W., N. A. Rayner, T. M. Smith, D. C. Stokes, and W. Wang (2002), An improved in situ and satellite SST analysis for climate. Journal of Climate, 15, 1609-1625, doi:10.1175/1520-0442(2002)015<1609:AIISAS>2.0.CO;2.

Rignot, E., S. Jacobs, J. Mouginot, and B. Scheuchl (2013), Ice-shelf melting around Antarctica. Science, 341, 266-270, doi:10.1126/science.1235798.

Rignot, E., and S. S. Jacobs (2002), Rapid bottom melting widespread near Antarctic Ice Sheet grounding lines. Science, 296, 2020-2023, doi:10.1126/science.1070942.

Rignot, E., I. Velicogna, M. R. van den Broeke, A. Monaghan and J. T. M. Lenaerts (2011), Acceleration of the contribution of the Greenland and Antarctic ice sheets to sea level rise, Geophysical Research Letters, 38, L05503, doi:10.1029/2011GL046583.

Rintoul, S. R., A. Silvano, B. Pena-Molino, E. van Wijk, M. Rosenberg, J. S. Greenbaum and D. D. Blankenship (2016), Ocean heat drives rapid basal melt of the Totten Ice Shelf, Science Advances, 2, e1601610, doi:10.1126/sciadv.1601610.

Roberts, N. L., A. M. Piotrowski, J. F. McManus and L. D. Keigwin (2010), Synchronous Deglacial Overturning and Water Mass Source Changes, Science, 327(5961), 75-78, doi:10.1126/science.1178068.

Robinson, A., R. Calov and A. Ganopolski (2012), Multistability and critical thresholds of the Greenland ice sheet, Nature Climate Change, 2, 429-432, doi:10.1038/NCLIMATE1449.

Roche, D. M., A. P. Wiersma, and H. Renssen (2010), A systematic study of the impact of freshwater pulses with respect to different geographical locations, Climate Dynamics, 34(7-8), 997-1013, doi:10.1007/s00382-009-0578-8.

Roche, D. M., X. Crosta, and H. Renssen (2012), Evaluating Southern Ocean sea-ice for the Last Glacial Maximum and pre-industrial climates: PMIP-2 models and data evidence. Quaternary Science Reviews, 56, 99-106, doi:10.1016/j.quascirev.2012.09.020.

Rojas, M.,P. Moreno, M. Kageyama, M. Crucifix, C. Hewitt, A. Abe-Ouchi, R. Ohgaito, E.C. Brady, and P. Hope (2009), The Southern Westerlies during the last glacial maximum in PMIP2 simulations. Climate Dynamics, 32, 4, 525-548, doi:10.1007/s00382-008-0421-7.

Rosen, J. L., E. J. Brook, J. P. Severinghaus, T. Blunier, L. E. Mitchell, J. E. Lee, J. S. Edwards, and V. Gkinis (2014), An ice core record of near-synchronous global climate changes at the Bolling transition, Nature Geoscience, 7, 459-463, doi:10.1038/NGEO2147.

Roske, F. (2006), A global heat and freshwater forcing dataset for ocean models. Ocean Modeling, 11, 235-297, doi:10.1016/j.ocemod.2004.12.005.

Sato, T., and R. Greve (2012), Sensitivity experiments for the Antarctic ice sheet with varied sub-ice-shelf melting rates. Annals of Glaciology, 53 (60), 221-228, doi:10.3189/2012AoG60A042.

Schilt, A. et al. (2010), Atmospheric nitrous oxide during the last 140 000 years, Earth Planet. Sci. Lett., 300, 33-43, doi:10.1016/j.epsl.2010.09.027.

Schmittner, A. and E. D. Galbraith (2008), Glacial greenhouse-gas fluctuations controlled by ocean circulation changes, Nature, 456, 373-376, doi:10.1038/nature07531.

Schoof, C. (2006), A variational approach to ice stream flow. Journal of Fluid Mechanics, 556, 227, doi:10.1017/S0022112006009591.

Schoof, C. (2007), Ice sheet grounding line dynamics: Steady states, stability, and hysteresis. Journal of Geophysical Research: Earth Surface, 112, 1-19, doi:10.1029/2006JF000664.

Shakun, J. D., P. U. Clark, F. He, S. A. Marcott, A. C. Mix, Z. Liu, B. Otto-Bliesner, A. Schmittner, and E. Bard (2012), Global warming preceded by increasing carbon dioxide concentrations during the last deglaciation, Nature, 484, 49-54, doi:10.1038/nature10915

Shakun, J. D. and A. E. Carlson (2010), A global perspective on Last Glacial Maximum to Holocene climate change, Quaternary Science Reviews, 29, 1801-1816,

doi:10.1016/j.quascirev.2010.03.016.

Shepherd, A. et al. (2012), A Reconciled Estimate of Ice-Sheet Mass Balance, Science, 338(1183), doi:10.1126/science.1228102.

Sherriff-Tadano, S., A. Abe-Ouchi, M. Yoshimori, A. Oka and W. Chan (2017), Influence of glacial ice sheets on the Atlantic meridional overturning circulation through surface wind change, Climate Dynamics, 1-23, doi:10.1007/s00382-017-3780-0.

Smedsrud, L. H., A. Jenkins, D. M. Holland, and O. A. Nøst (2006), Modeling ocean processes below Fimbulisen, Antarctica. Journal of Geophysical Research: Oceans, 111, C01007, doi: 10.1029/2005JC002915.

Spence, P., S.M. Griffies, M. H. England, A.M. C. Hogg, O. A. Saenko, and N. C. Jourdain (2014), Rapid subsurface warming and circulation changes of Antarctic coastal waters by poleward shifting winds, Geophysical Research Letters, 41, 4601-4610, doi:10.1002/2014GL060613.

St-Laurent, P., J. M. Klinck, and M. S. Dinniman (2012), On the Role of Coastal Troughs in the Circulation of Warm Circumpolar Deep Water on Antarctic Shelves. Journal of Physical Oceanography, 43, 51-64, doi:10.1175/JPO-D-11-0237.1.

Steele, M., R. Morley, and W. Ermold (2001), PHC: A global ocean hydrography with a high quality Arctic Ocean, Journal of Climate, 14(9), 2079-2087, doi:10.1175/1520-0442(2001)014h2079:PAGOHWi2.0.CO;2.

Stocker, T. F. (1998), The Seesaw Effect, Science, 282, 61-62, doi:10.1126/science.282.5386.61.

Stocker, T. F. and S. J. Johnsen (2003), A minimum thermodynamic model for the bipolar seesaw, Paleoceanography, 18(4), 1087, doi:10.1029/2003PA000920.

Stone, E. J., E. Capron, D. J. Lunt, A. Payne, J. S. Singarayer, P. J. Valdes and E. W. Wolff (2016), Impact of meltwater on high-latitude early Last Interglacial climate, Climate of the Past, 12, 1919-1932, doi:10.5194/cp-12-1919-2016.

Stouffer, R. J. et al. (2006), Investigating the Causes of the Response of the Thermohaline Circulation to Past and Future Climate Changes, Journal of Climate, 19(8), 1365-1387, doi:10.1175/JCLI3689.1.

Stouffer, R. J., D. Seidov, and B. J. Haupt (2007), Climate response to external sources of freshwater: North Atlantic versus the Southern Ocean. Journal of Climate, 20, 436-448, doi: 10.1175/JCLI4015.1.

Suganuma, Y., H. Miura, A. Zondervan, and J. Okuno (2014) East Antarctic deglaciation and the link to global cooling during the Quaternary: Evidence from glacial geomorphology and 10Be surface exposure dating of the Sør Rondane Mountains,

Dronning Maud Land. Quaternary Science Reviews, 97, 102-120, doi:10.1016/j.quascirev.2014.05.007.

Sutter, J., P. Gierz, K. Grosfeld, M. Thoma, and G. Lohmann (2016), Ocean temperature thresholds for Last Interglacial West Antarctic Ice Sheet collapse. Geophysical Research Letters, 2675-2682, doi:10.1002/2016GL067818.

Swithinbank, C. W. (1988) Satellite Image Atlas of Glaciers of the World: Antarctica, U.S. Geological Survey Professinal Paper 1386-B.

Talbot, M. H. (1988), Oceanic environment of George VI ice shelf, Antarctic Peninsula. Annals of glaciology, 11, 161-164.

Tamura, T., K. I. Ohshima, and S. Nihashi (2008), Mapping of sea ice production for Antarctic coastal polynyas. Geophys. Res. Lett., 35, L07606, doi:10.1029/2007GL032903.

Tarasov, L., A. S. Dyke, R. M. Neal, and W. R. Peltier (2012), A data-calibrated distribution of deglacial chronologies for the North American ice complex from glaciological modeling, Earth Planet. Sci. Lett., 315-316, 30-40, doi:10.1016/j.epsl.2011.09.010.

Tarasov, L. and W. R. Peltier (2005), Arctic freshwater forcing of the Younger Dryas cold reversal, Nature, 435, 662-665, doi:10.1038/nature03617.

Taylor, K. E., R. J. Stouffer and G. A. Meehl (2012), A summary of the CMIP5 experiment design. Bull. Amer. Meteor. Soc., 93, 485-498, doi:10.1177/BAMS-D-11-00094.1.

Thoma, M., A. Jenkins, D. Holland, and S. Jacobs (2008), Modelling Circumpolar Deep Water intrusions on the Amundsen Sea continental shelf, Antarctica. Geophysical Research Letters, 35 (8), 2-7, doi:10.1029/2008GL034939.

Timmermann, R., and H. H. Hellmer (2013), Southern Ocean warming and increased ice shelf basal melting in the twenty-first and twenty-second centuries based on coupled ice-ocean finite element modelling. Ocean Dynamics, 63, 1011-1026, doi:10.1007/s10236-013-0642-0.

Timmermann, R., Q. Wang, and H. H. Hellmer (2012), Ice shelf basal melting in a global finiteelement sea ice-ice shelf - ocean model. Annals of Glaciology, 53 (60), 303-314, doi:10.3189/2012AoG60A156.

Turney, C. S. M., and R. T. Jones (2010), Does the Agulhas Current amplify global temperatures during super-interglacials?, Journal of Quaternary Science, 25(6), 839-843, doi:10.1002/jqs.1423.

Vaughan, D. G. et al. (2013): Observations: Cryosphere. In: Climate Change 2013: The

Physical Science Basis. Contribution of Working Group I to the Fifth Assessment Report of the Intergovernmental Panel on Climate Change, Cambridge University Press, Cambridge, United Kingdom and New York, NY, USA.

Velicogna, I. (2009), Increasing rates of ice mass loss from the Greenland and Antarctic ice sheets revealed by GRACE. Geophysical Research Letters, 36, 2-5, doi:10.1029/2009GL040222.

Veres, D. et al. (2012), The Antarctic ice core chronology (AICC2012): an optimized multi-parameter and multi-site dating approach for the last 120 thousand years, Climate of the Past, 9, 1733-1748, doi:10.5194/cp-9-1733-2013.

Vettoretti, G. and W. R. Peltier (2015), Interhemispheric air temperature phase relationships in the nonlinear Dansgaard-Oeschger oscillation, Geophysical Research Letters, 42, 1180-1189, doi:10.1002/2014GL062898.

WAIS Divide Project Members (2013), Onset of deglacial warming in West Antarctica driven by local orbital forcing, Nature, 500, 440-444, doi:10.1038/nature12376.

WAIS Divide Project Members (2015), Precise interpolar phasing of abrupt climate change during the last ice age, Nature, 520, 661-665, doi:10.1038/nature14401.

Walker, R. T., T. K. Dupont, B. R. Parizek, and R. B. Alley (2008), Effects of basal-melting distribution on the retreat of ice-shelf grounding lines. Geophysical Research Letters, 35, 1-5, doi:10.1029/2008GL034947.

Weaver, A. J., O. A. Saenko, P. U. Clark, and J. X. Mitrovica (2003), Meltwater Pulse 1A from Antarctica as a trigger of the Bølling-Allerød warm interval, Science, 299(5613), 1709-1713, doi:10.1126/science.1081002.

Weber, M. E. et al. (2014), Millennial-scale variability in Antarctic ice-sheet discharge during the last deglaciation, Nature, 510, 134-138, doi:10.1038/nature13397.

Weertman, J. (1974), Stability of the junction of an ice sheet and an ice shelf. Journal of Glaciology, 13 (67), 3-11, doi:10.3189/S0022143000023327.

Wild, M., P. Calanca, S. C. Scherrer and A. Ohmura (2003), Effects of polar ice sheets on global sea level in high-resolution greenhouse scenarios, Journal of Geophysical Research, Atmospheres, 108, D5, 4165, doi:10.1029/2002JD002451.

Whitworth, T., A. H. Orsi, S. J. Kim, and W. D. Nowlin Jr, (1998), Water masses and mixing near Antarctic Slope Front. Ocean, Ice, and Atmosphere: Interactions at the Antarctic Continental Margin, Antarctic Research Series, 75, 1-27, doi: 10.1029/AR075p0001

Williams, M. M., I. R. C. Warner, and W. F. Budd (1998), The effects of ocean warming on melting and ocean circulation under the Amery Ice Shelf, East Antarctica. Ocean, Ice,

and Atmosphere: Interactions at the Antarctic Continental Margin, Antarctic Research Series, 75, 75-80, doi:10.1029/AR075p0075.

Winkelmann, R., A. Levermann, A. Ridgwell and K. Caldeira (2015), Combustion of available fossil fuel resources sufficient to eliminate the Antarctic Ice Sheet, Science Advances, 1, e1500589, doi:10.1126/sciadv.1500589.

Yamamoto, A., M. Shigemitsu, A. Oka, K. Takahashi, R. Ohgaito, and Y. Yamanaka (2015), Global deep ocean oxygenation by enhanced ventilation in the Southern Ocean under long-term global warming. Global Biogeochemical Cycles, 29 (10), 1801-1815, doi:10.1002/2015GB005181.

Yamane, M., Y. Yokoyama, A. Abe-Ouchi, S. Obrochta, F. Saito, K. Moriwaki, and H. Matsuzaki (2015), Exposure age and ice-sheet model constraints on Pliocene East Antarctic ice sheet dynamics. Nature communications, 6, 7016, doi:10.1038/ncomms8016.

Yokoyama, Y. et al. (2016), Widespread collapse of the Ross Ice Shelf during the late Holocene, PNAS, 113(9), 2354-2359, doi:10.1073/pnas.1516908113.

Yoshimori, M., T. Yokohata, and A. Abe-Ouchi (2009), A comparison of climate feedback strength between CO2 doubling and LGM experiments. Journal of Climate, 22, 3374-3395, doi:10.1175/2009JCLI2801.1.

Zhang X., G. Knorr, G. Lohmann and S. Barker (2017), Abrupt North Atlantic circulation changes in response to gradual CO2 forcing in a glacial climate state, Nature Geoscience,10, 518-523, doi:10.1038/NGEO2974.

Zhang, X., G. Lohmann, G. Knorr, and C. Purcell (2014), Abrupt glacial climate shifts controlled by ice sheet changes, Nature, 512, 290-294, doi:10.1038/nature13592.

Appendix A: Additional experiments on meltwater

This chapter describes the settings and results of additional experiments, supporting deglaciation experiments of chapter 2.

Name	Insolation, Greenhouse gas	Ice sheet	Land-sea mask	Meltwater input	Duration [yr]
CTL_SHhose	PI	PI	PI	ANT 0.1Sv	500
CTL_NHhose	PI	PI	PI	NATL 0.1Sv	500
15ka_NHhose	15 ka	15 ka	15 ka	NATL 0.1Sv	500
LGM_NHhose	LGM	LGM	LGM	NATL 0.1Sv	500

Table A.1 List of MIROC experiments. The model is spun up with the boundary conditions of pre-industrial (PI), 15 ka and LGM, respectively. The meltwater was applied to North Atlantic or Antarctic Ocean for 500 years, respectively. ANT in the column of meltwater input indicates meltwater flux is uniformly applied to the Antarctic shelf seas (ocean depth shallower 1000 meters) of 65−90°S. CTL_NHhose, 15ka_NHhose, LGM_NHhose experiments are identical with the experiments that appears in Kawamura et al. (2017).

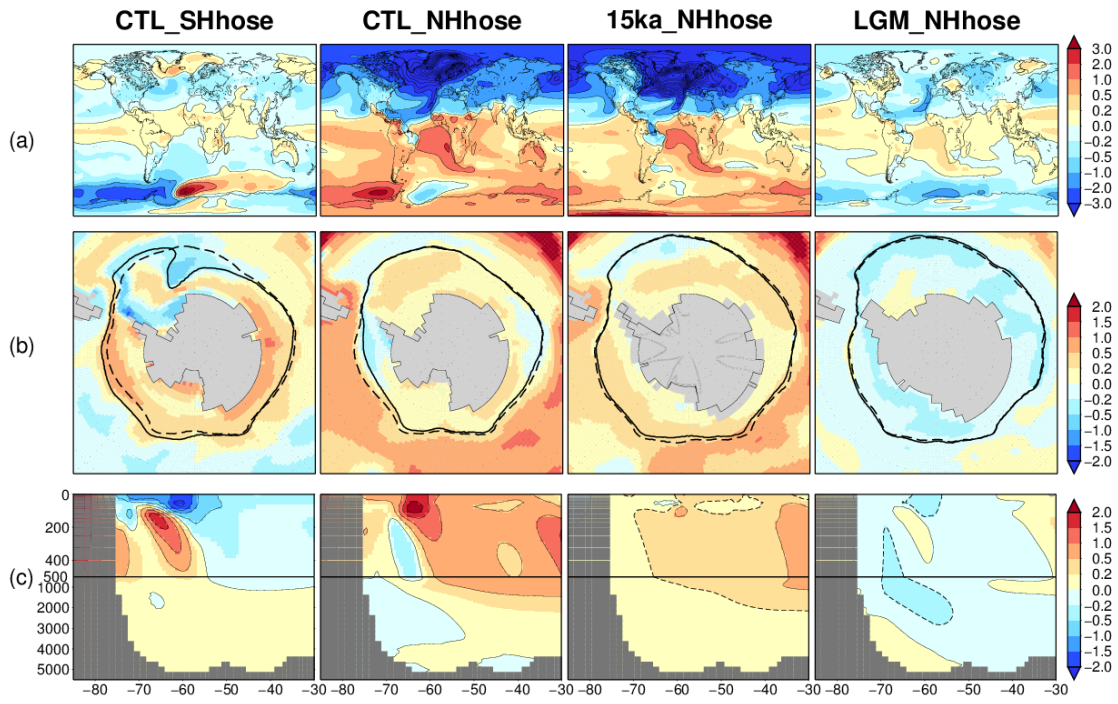

Fig. A.1 Results of the experiments indicated in Table A.1. (a) annual-mean surface air temperature change, (b) subsurface (200−800 m depth) ocean temperature change and sea ice edge in Austral winter: dashed (bold) lines indicates sea ice edge before (after) the meltwater input. (c) annual-mean ocean temperature change in the Southern Ocean (225−270°E).

Appendix B: Additional experiments on deglaciation

This chapter describes the settings and results of additional experiments on deglaciation, supporting Chapter 2. The T1_14kaice and T2_15kaGEO experiment investigated the impact of ice sheet and coastline to the recovery of AMOC, respectively. The T1_16kaPIAIS experiment investigated the impact on Antarctic ice sheet on recovery of the AMOC. The T2_13kaPIAIS experiment investigated the impact of Antarctic ice sheet to the extent of sea ice in the Southern Hemisphere. The PI_LGMice and the PI (Pre-industrial) experiment investigated the impacts of Antarctic ice sheet on Antarctic surface air temperature.

Name	Insolation, Greenhouse gas	Ice sheet	Land-sea mask	Meltwater input	duration
T1-like (reference)	21−11 ka	LGM	LGM	~0.06 Sv	21−11 ka
T1_14kaice	same	Ice6g,14 ka	LGM	same	14−13 ka
T2_15kaGEO	same	LGM	15 ka	same as T2-like	16−14.5 ka
T1_16kaPIAIS	same	(*1)	LGM	same	16−14.5 ka
T2_13kaPIAIS	same	(*1)	LGM	same as T2-like	13−12 ka
T2_13kaPIGEO	same	PI	PI	same as T2-like	13−12ka
PI_LGMice	PI	LGM	LGM	no	(*2)
PI	PI	PI	PI	no	(*2)

Table B.1 List of additional deglaciation experiments. “same” indicates that the setting is same as T1-like experiment. (*1): The prescribed ice sheet is that of present-day in the Southern Hemisphere but LGM in the Northern Hemisphere. (*2): initialized with T1D experiment of Fig. 2.7 at 11ka, and 2000-year integrations were conducted. The ice sheet and land-sea mask is indicated in Figs. 2.19 and Fig. B.6.

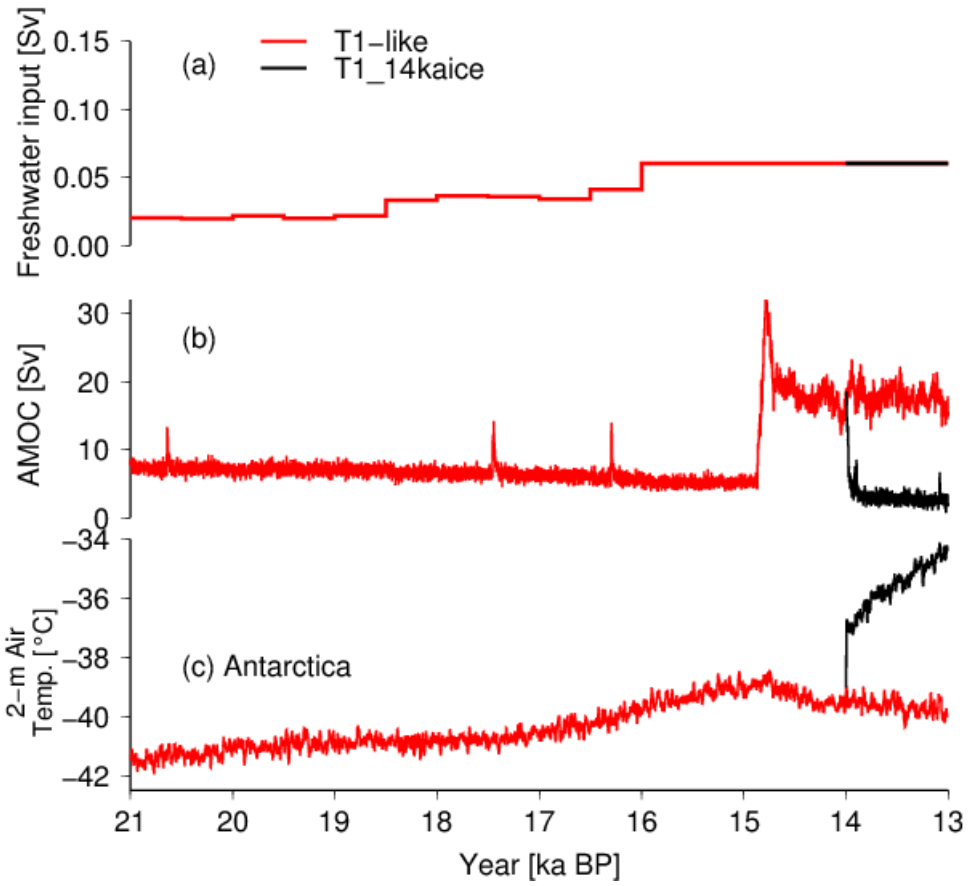

Fig. B.1 Experimental design and result for the T1_14kaice experiment are compared to the T1-like expeirment. (a) freshwater input in the North Atlantic, (b) simulated AMOC streamfunction, (c) simulated annual-mean 2-m air temperature at dome Fuji, Antarctica.

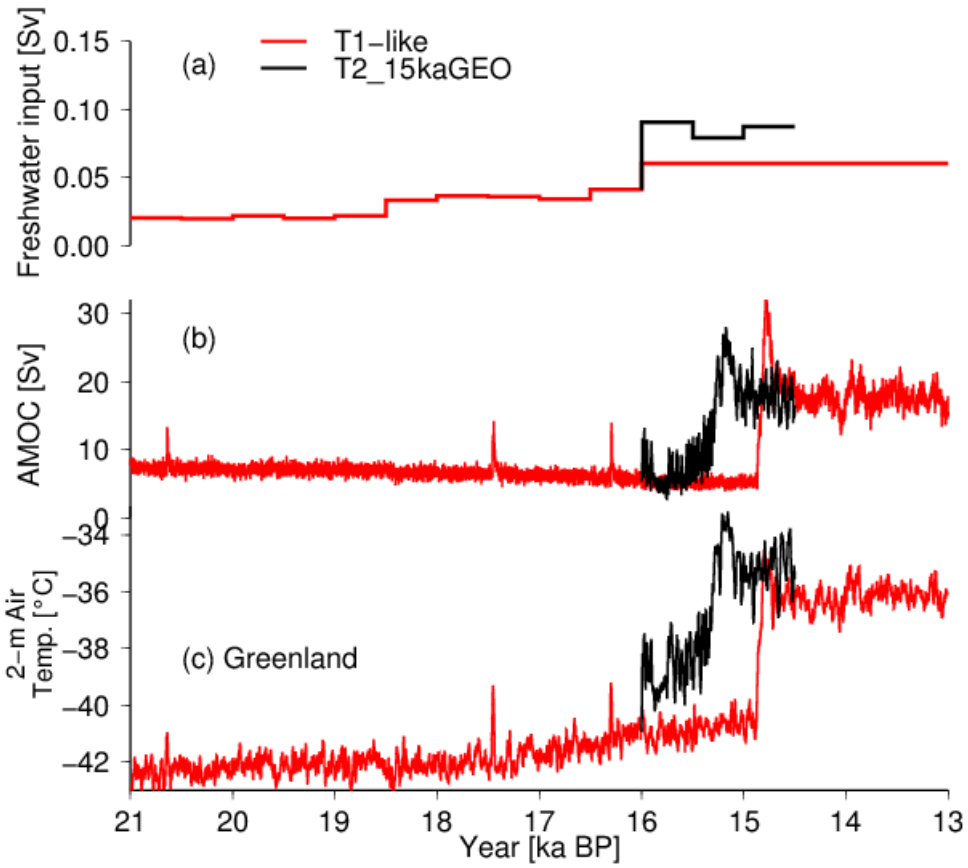

Fig. B.2 Experimental design and result for the T2_15kaGEO experiment are compared to the T1-like expeirment. (a) freshwater input in the North Atlantic, (b) simulated AMOC streamfunction, (c) simulated annual-mean 2-m air temperature on Greenland (average for three deep ice core locations of GISP2, NGIP and NEEM)

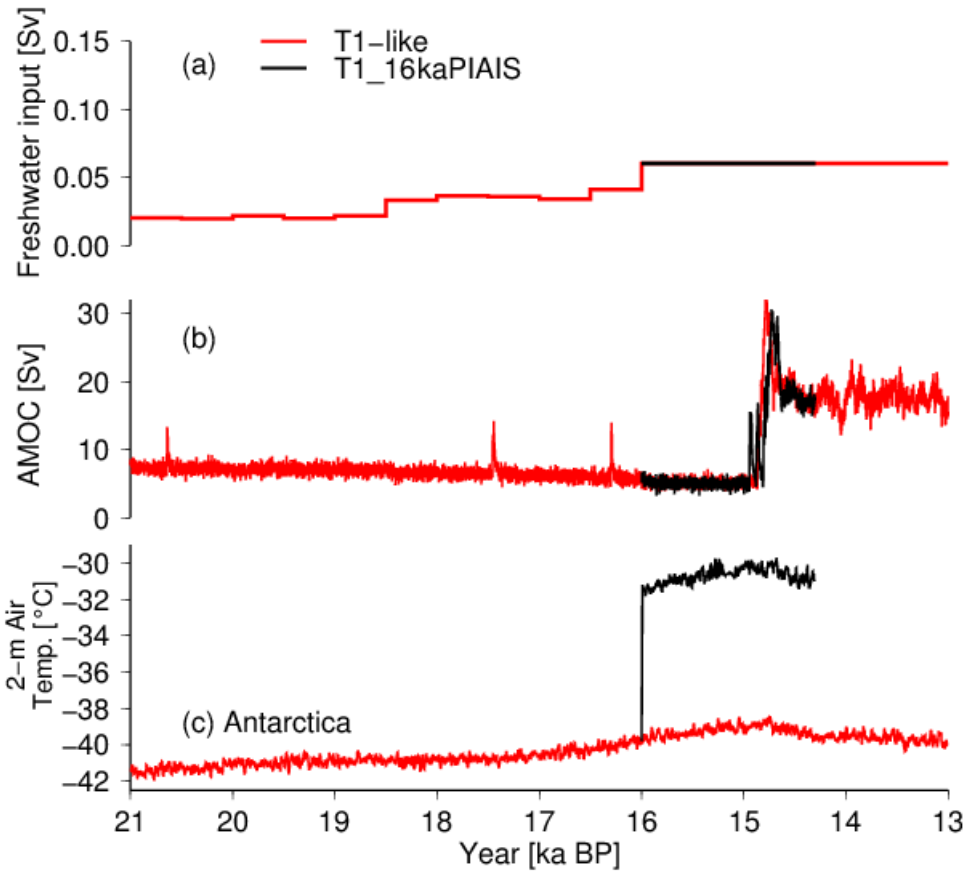

Fig. B.3 Experimental design and result for the T1_16kaPIAIS experiment are compared to the T1-like expeirment. (a) freshwater input in the North Atlantic, (b) simulated AMOC streamfunction, (c) simulated annual-mean 2-m air temperature at dome Fuji, Antarctica.

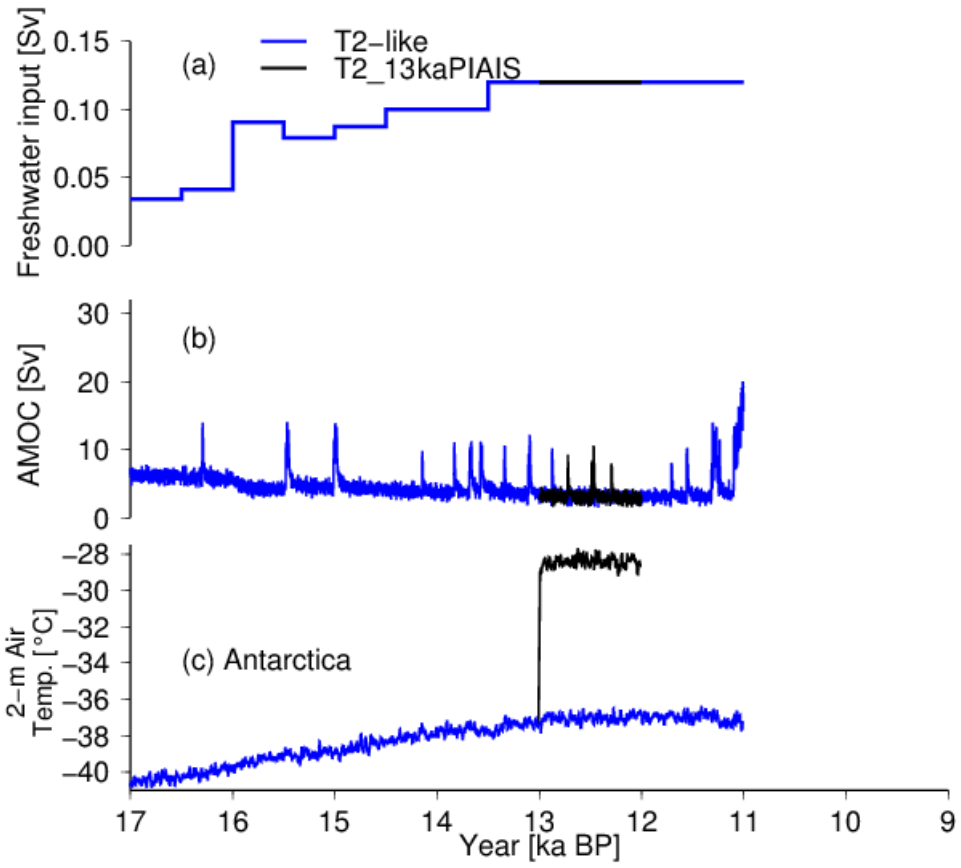

Fig. B.4 Experimental design and result for the T2_13kaPIAIS experiment are compared to the T2-like expeirment. (a) freshwater input in the North Atlantic, (b) simulated AMOC streamfunction, (c) simulated annual-mean 2-m air temperature at dome Fuji, Antarctica.

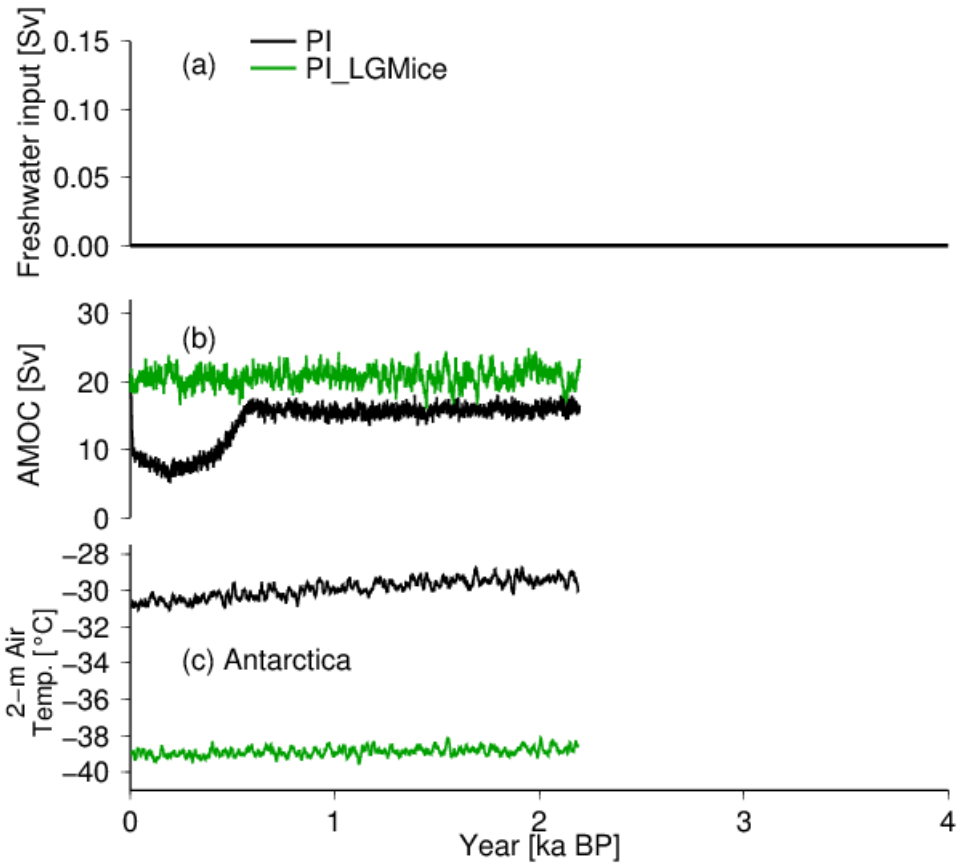

Fig. B.5 Experimental design and result for the PI and PI_LGMice experiment are compared to the T2-like expeirment. (a) freshwater input in the North Atlantic, (b) simulated AMOC streamfunction, (c) simulated annual-mean 2-m air temperature at dome Fuji, Antarctica.

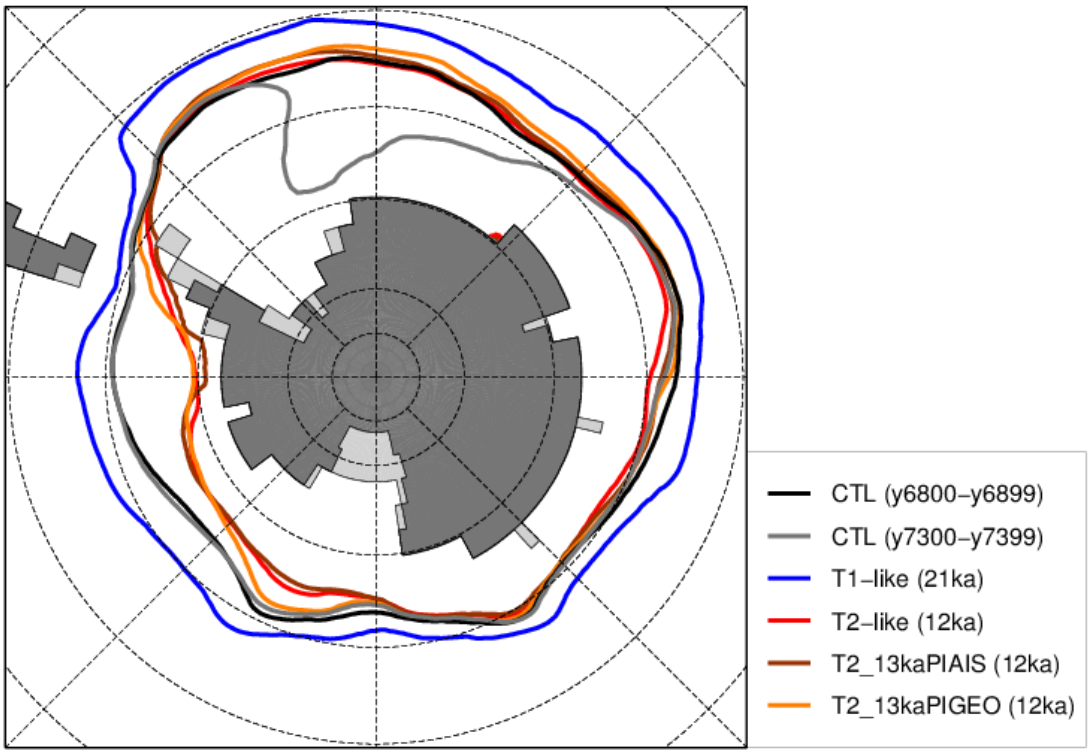

Fig. B.6 Results of the additional experiments. Winter sea ice extents (sea ice concentration > 0.15) in the Antarctic regions from the T2_13kaPIAIS and T2_13kaPIGEO experiment at 12 ka (brown) is compared with T1-like experiment at 21 ka (blue), T2-like experiment at 12 ka (red), as well as CTL, present-day experiment (black and gray lines). As the CTL experiment exhibits a multi-millennial variability in the Southern Ocean, the two 100-year climatology for year 6800−6899 and 7300−7399 (Fig. B.7) are presented in the figure. The dark gray and the light gray area indicate geometry of the Pre-Industrial and the LGM, respectively.

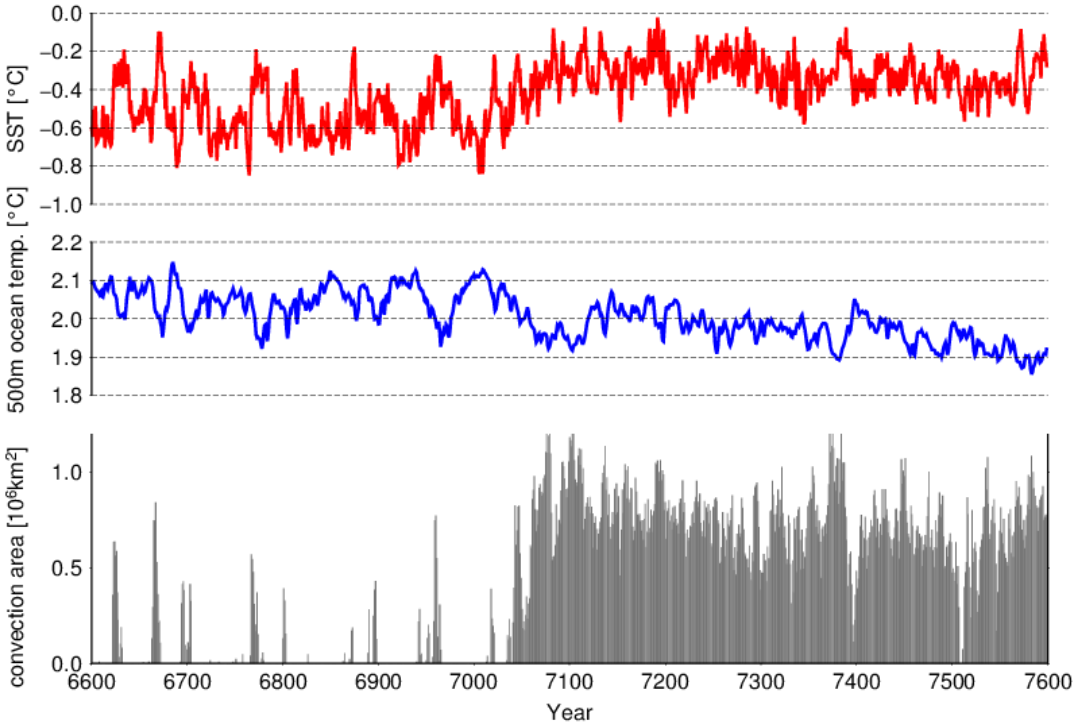

Fig. B.7 Analysis of the CTL (present-day) experiment, indicating that there is a multi-millennial variability in the Southern Ocean. The time series of sea surface temperature and subsurface ocean temperature (500 meter depth) in the Antarctic region (60−90°S), and the area of deep convection (winter mixed layer depth > 2000 m) in the Southern Ocean are displayed. The mixed layer depth is defined by the depth where density anomaly is less than 0.03 g/cm^3 compared to the sea surface.

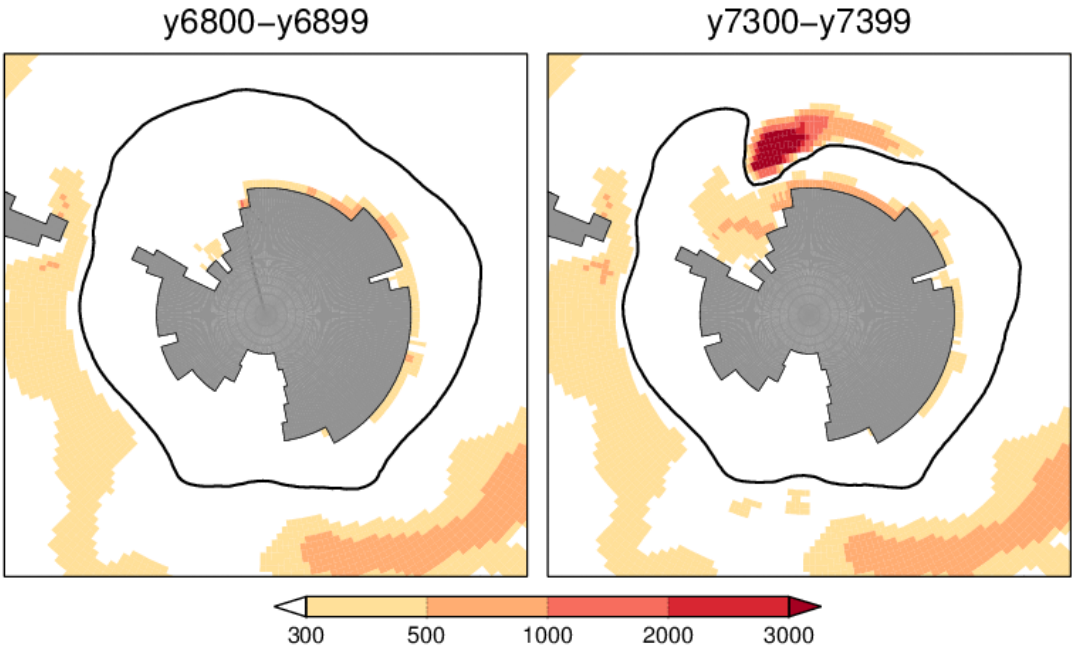

Fig. B.8 Analysis of the CTL (present-day) experiment. Bold lines indicate winter sea ice edge (sea ice concentration > 0.15). The color indicates mixed layer depth during Austral winter [m], defined by the depth where density anomaly is less than 0.03 g/cm^3 compared to the sea surface. The times of climatology correspond to that of Fig. B.7.

Appendix C: Role of bathymetry of Antarctic continental shelves and Antarctic glacial meltwater on basal melting rate

This chapter describes the experiments and results of modifying the bathymetry of Antarctic continental shelves and Antarctic glacial meltwater. The impacts on basal melting rate of Antarctic ice shelves and the intrusion of warm water onto continental shelves and are investigated using a regional ocean model used in Chapter 3.

C.1 bathymetry of Antarctic continental shelf

In the TOPO-A experiment, the depth of Antarctic continental shelf (including ice shelf cavities) is deepened by 400 meters from the present-day (TOPO-A). In the TOPO-B experiment, the depth of the entire Antarctic continental shelf (excluding ice shelf cavities) is set to 600 meters. The results are summarized in Fig. C1. The deepening of whole Antarctic continental shelf leads to a promoted intrusion of warm water onto continental shelves (a, c, d), but did not in Pine Island Glacier (b), where cold and saline water persisted near ice shelves. In contrast, if the continental shelf was flat (nevertheless shallower than the CTL), the warm water intruded onto continental shelves and approached near Pine Island Glacier. These results suggest the topography of Antarctic continental shelves affects the intrusion of warm water by two ways: (1) the deeper of continental shelf break promotes warm water to easily intrude onto the continental shelves (2) the deepened area of the continental shelves (depression) maintains cold and saline water, which prevents the intrusion of warm water onto the continental shelves. The result also suggests the representation in the Amundsen Sea continental shelf might have contributed to the model bias of a weaker warm water intrusion onto the continental shelves and smaller basal melt rate of ice shelves.

C.2 Antarctic Glacial meltwater

In this experiment, meltwater input of 0.1 Sv was applied to the Antarctic continental shelves (same as CTL_SHhose experiment of appendix A). The model was integrated for 40 years to reach quasi steady states, and climatology of the last 20-year was analyzed. As shown in Fig. C2, the stratifications in the Antarctic shelf seas were strengthened, and warm water intruded onto the continental shelves of the Pine Island Glacier and other ice shelves (Fig. C2).

The responses of the Antarctic Ocean were compared to the experiment of MIROC, with the same input of Antarctic meltwater input (experiment of CTL_SHhose in Appendix A). The ocean model exhibits a larger response of ocean temperature in the Antarctic shelf seas, but the response of sea ice and subsurface ocean temperature in the Southern Ocean were small compared to the MIROC AOGCM experiment (Fig. C3). The larger response in the Antarctic shelf seas likely came from the reproducibility of the Antarctic shelf seas of the respective CTL experiment, in that the cold water was absent in the MIROC AOGCM (Fig. 3.A1). The smaller response of Antarctic sea ice and subsurface ocean temperature likely came from the lack of atmosphere-ocean interaction in the COCO experiment, in that the sea surface atmospheric climatology is fixed to the present-day. These results indicate that the meltwater input to the Antarctic Ocean due to melting of ice shelves or ice sheets act as a positive feedback of melting Antarctic ice shelves, and the interaction between the atmosphere and the ocean could amplify the responses.

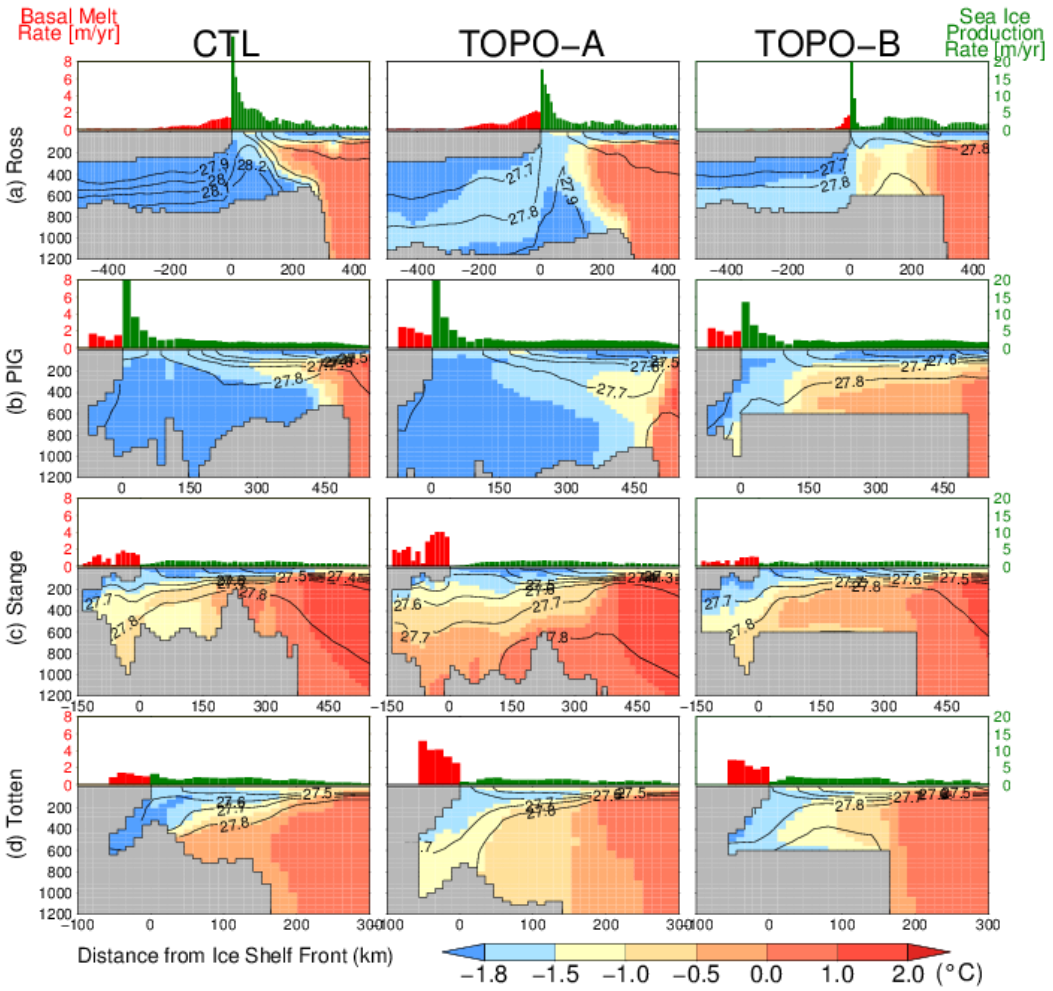

Fig. C1. Result of the experiments modifying bedrock topography of Antarctica. The ocean transects for 4 representative ice shelves are displayed in this figure. The lines denote the neutral density of seawater, and the colors denote the ocean temperature. Basal melt rate (red bars above ice shelves) and sea ice production rate (green bars above open ocean) are displayed in the upper panels. The vertical axis denotes ocean depth and the horizontal axis denotes the distance from the ice shelf front.

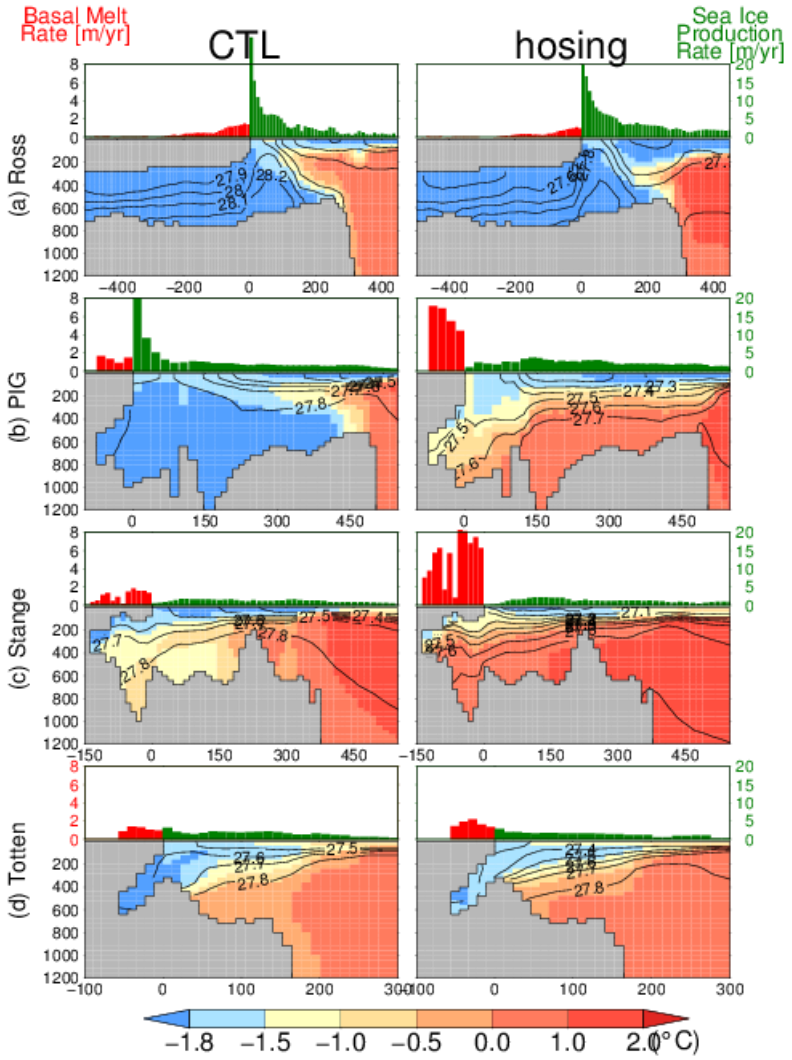

Fig. C2. Result of the experiments applying a glacial meltwater flux of 0.1 Sv to Antarctic Ocean. The ocean transects for 4 representative ice shelves are displayed in this figure. The lines denote the neutral density of seawater, and the colors denote the ocean temperature. Basal melt rate (red bars above ice shelves) and sea ice production rate (green bars above open ocean) are displayed in the upper panels. The vertical axis denotes ocean depth and the horizontal axis denotes the distance from the ice shelf front.

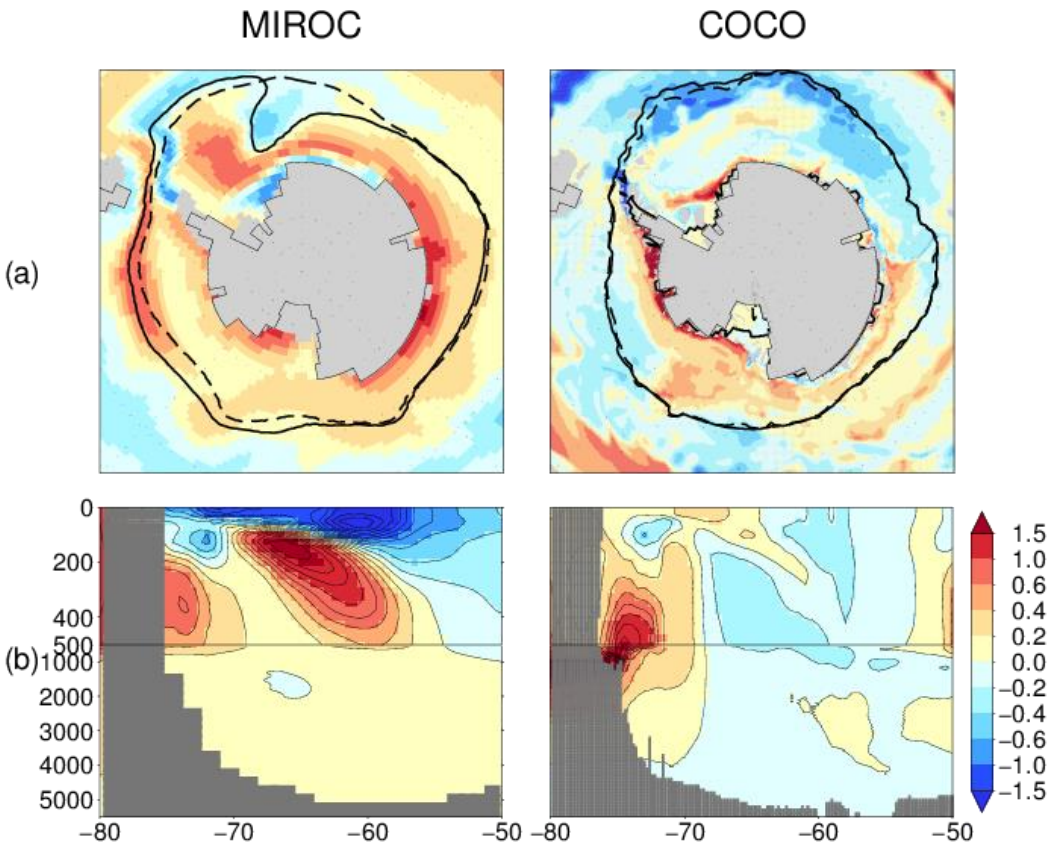

Fig. C3. Result of the experiments applying a glacial meltwater flux of 0.1 Sv to Antarctic Ocean. (Left) MIROC AOGCM experiment (same as CTL_SHhose of Appendix A). (Right) COCO experiment (present chapter). (a) Subsurface (500 m depth) ocean temperature change and sea ice edge in Austral winter: dashed (bold) lines indicates sea ice edge before (after) the meltwater input. (b) annual-mean ocean temperature change in the West Antarctica (225−270°E).

Appendix D: Responses of ice sheet to basal melt rate change

This chapter describes numerical model experiments to investigate the responses of ice sheet to change in basal melt rate using a two-dimensional ice sheet model.

D.1 model description

An ice sheet model IcIES2 (Saito, unpublished) was used in this chapter. The model calculates the flow of isothermal ice (without thermodynamics) along the flow-line (zonally integrated) with the shallow-ice approximation for the grounded ice sheet and the shallow-shelf approximation for the floating ice shelf. The movement of grounding line is parameterized with the ice flux at the grounding line following Schoof (2007).

D.2 experimental design and results

The responses and stabilities of ice sheet were investigated under three different bedrock topographies: an idealized geometry from MISMIP2d (Pattyn et al. 2013) and transects of the Shirase Glacier catchment (experiment S) and Wilkes Land ice sheet (experiment W) (Fig. D.1). The Horizontal resolution of the ice sheet model was set to 10 km. The ice was isothermal, and the rate factor of the ice was equivalent to −0.35 °C. Accumulation is assumed to 0.1 m/yr all over the domain. Basal mass balance was assumed to be constant over ice shelves, and basal mass balance at the grounding line was prescribed based on floating area of the grid at the grounding line, as Feldmann et al. (2015). The model was initialized with the present-day ice thickness and spun up for 50,000 years with basal mass balance of 0. The steady-states of ice sheets were acquired by conducting 50,000-year simulation under constant basal mass balances. The results indicate there is hysteresis in the equilibrium shape of ice sheet due to the bedrock topography, without climate-atmosphere interactions. Also, the threshold of the significant retreatment of ice sheet depends on the bedrock topography.

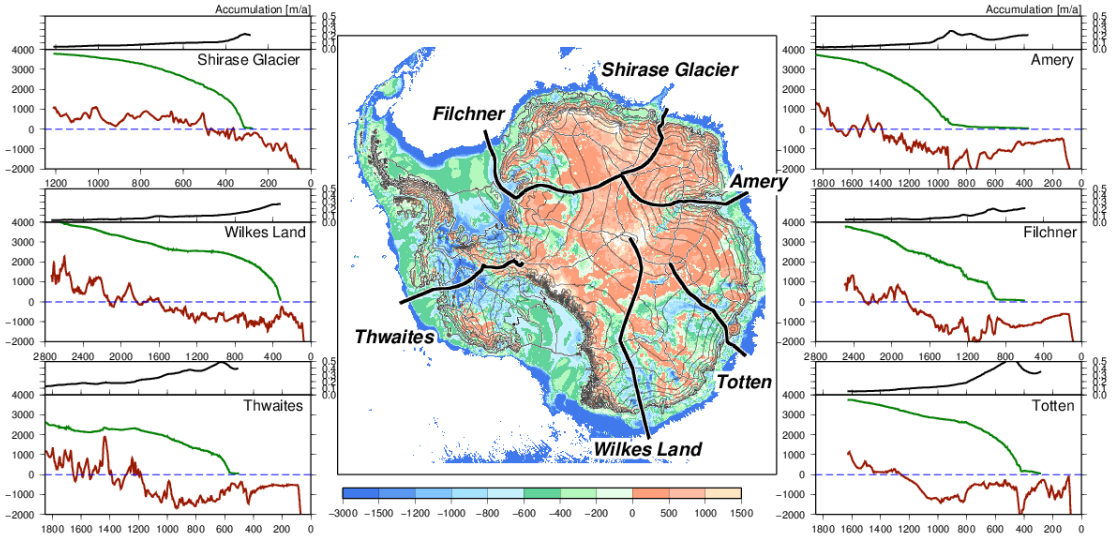

Fig. D.1 Observed bedrock topography (brown lines), surface elevation (green lines) and accumulation rate (black lines). The bedrock topography and surface elevation are from BEDMAP2 (Fretwell et al. 2013), and accumulation rate is from ALBMAP (Le Brocq et al. 2010). The locations of transects are indicated by the bold lines in the middle panel. The bedrock topography from the Shirase Glacier, the Wilkes Land are used in this chapter.

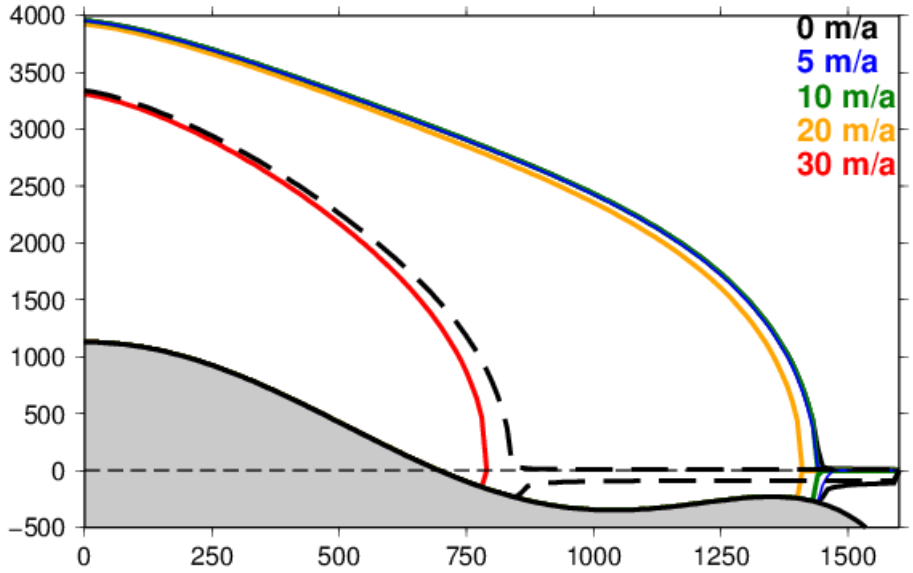

Fig. D.2 Results of the idealized topography experiment. Bold lines indicate steady-state initialized with large ice sheet, and dashed lines indicate initialized with small ice sheet.

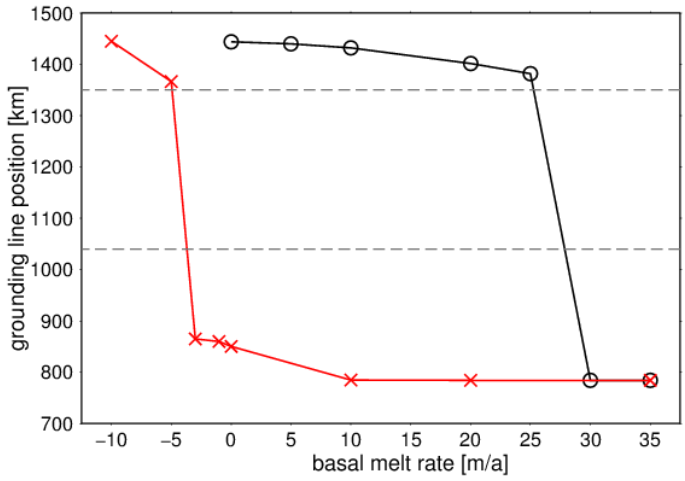

Fig. D.3 Hysteresis diagram on the position of grounding line against basal melt rate of ice shelves for the idealized topography. Circles denote steady states when the model is initialized with the large ice sheet (basal melt rate of 0), and crosses denote steady states when the model is initialized with the small ice sheet (basal melt rate of 35 m/yr in this case). Positive values of basal melt rate indicate melting. The horizontal dashed lines indicates the positions of the depression and rises in the bedrock topography.

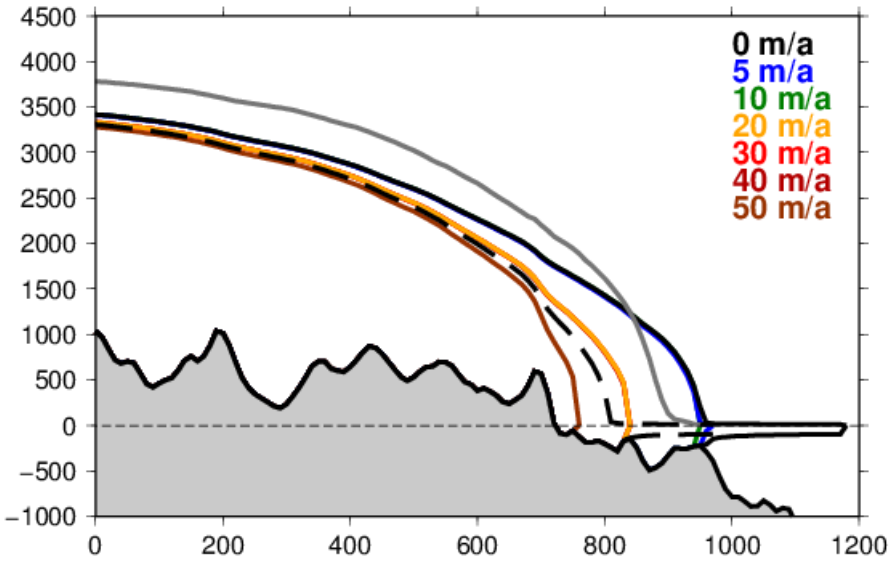

Fig. D.4 Results of the experiment S (Shirase Glacier). Bold lines indicate steady-state initialized with large ice sheet, and dashed lines indicate initialized with small ice sheet. The grey line indicates surface elevation of the present-day (BEDMAP2).

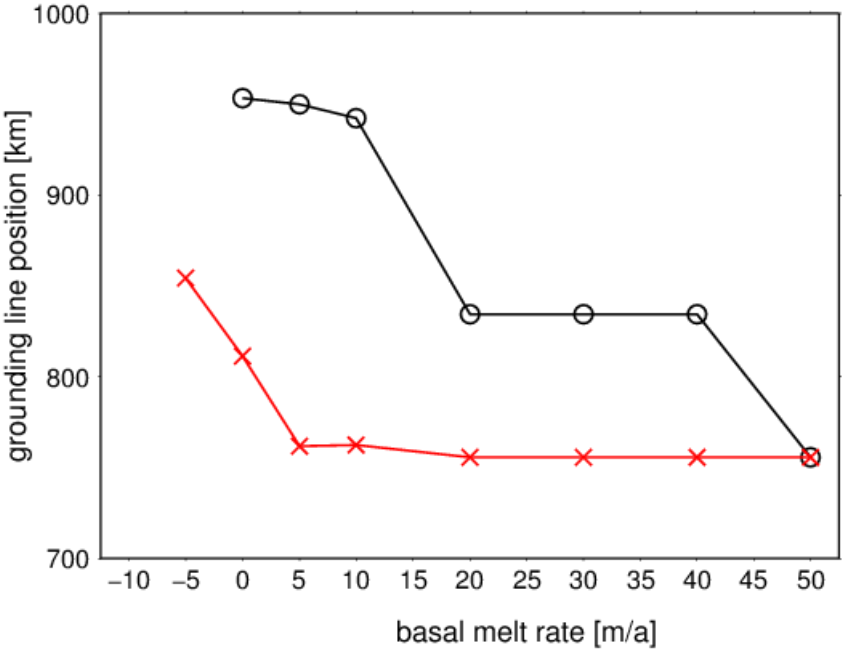

Fig. D.5 same as Fig. D.3, but for the experiment S.

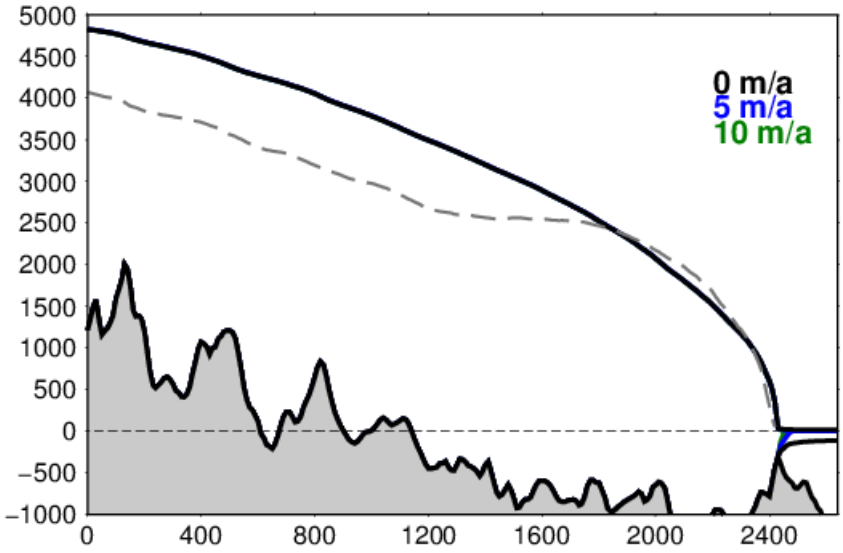

Fig. D.6 Results of the experiment W (Wilkes Land ice sheet). Steady-state ice sheets. The steady-states were not acquired in case basal melt rate was higher than 15 m/a because of numerical instabilities during the retreatment of the grounding line.

References

Schoof, C. (2007), Ice sheet grounding line dynamics: Steady states, stability, and hysteresis. Journal of Geophysical Research: Earth Surface, 112, 1-19, doi:10.1029/2006JF000664.

Feldmann, J. and Levermann, A (2015), Interaction of marine ice-sheet instabilities in two drainage basins: simple scaling of geometry and transition time. The Cryosphere, 9, 631-645, doi:10.5194/tc-9-631-2015.

Fretwell, P., et al. (2013), Bedmap2: improved ice bed, surface and thickness datasets for Antarctica. The Cryosphere, 7 (1), 375-393, doi:10.5194/tc-7-375-2013.

Kawamura, K. et al. (2017), State dependence of climatic instability over the past 720,000 years from Antarctic ice cores and climate modeling, Science Advances, 3(2), doi:10.1126/sciadv.1600446.

Le Brocq, A. M., A. J. Payne and A. Vieli (2010), An improved Antarctic dataset for high resolution numerical ice sheet models (ALBMAP v1), Earth System Science Data, 2, 247−260, doi:10.5194/essd-2-247-2010.

Pattyn, F. et al. (2013), Grounding-line migration in plan-view marine ice-sheet models: results of the ice2sea MISMIP3d intercomparison, 59 (215), 410−422, doi:10.3189/2013JoG12J129.